Universitetet
i Stavanger

FACULTY OF SCIENCE AND TECHNOLOGY

MASTER'S THESIS

Study programme/specialisation:	Spring semester, 2018
Natural Gas & Drilling technology	Open
Authors: Thomas Løklingholm Charlotte Andreassen	.... (signature of authors)

Internal supervisor: Dimitrios.G.Pavlou

External supervisor: Kjell Einar Ellingsen(Equinor ASA)

Title of master's thesis:

Material behavior of perforated and non-perforated simply supported steel plates in air and water, subjected to impact loads.

Credits(ECTS): 30

Keywords:	Number of pages: 145
Impact energy, Subsea, CAP-X, Material behavior	+ supplemental material/other: 3
	Stavanger 11/06/2018

----------This page is left blank intentionally----------

Universitetet i Stavanger

equinor

Master Thesis

University of Stavanger

Spring 2018

Material behavior of perforated and non-perforated simply supported steel plates in air and water, subjected to impact loads.

By

Thomas Løklingholm & Charlotte Andreassen.

Abstract

Due to challenging economic times, industries such as oil and gas face the need of moving from customized, time-consuming, and costly solutions, to more standardized technologies, to reduce costs and maintain high profits. In line with this, the Norwegian oil and gas company Statoil (now Equinor) has developed Cap-X, a revolutionary integrated template structure technology for erecting installations on the seabed. However, to enter the market, Cap-X needs to meet the NORSOK standards and requirements, developed by the Norwegian petroleum industry.

This thesis contributes towards such verification, by studying the impact of applied load to the Cap-X technology. It addresses how applied load varies between a perforated plate, such as the surface of Cap-X, and a solid plate, both in water and air, for material within its elastic region. The findings of this study indicate that the perforated plate has a consistent reduction in impact strain, in water and air for the same impact energy. This is perhaps also indicative of NORSOK design criteria being too conservative, as effect of perforations and geometries play important part on strain produced by any given impact energy. However, due to relatively small difference between air and water compared uncertainties in the measurements, this difference cannot be accurately quantified. In addition, as the impact energy being conservatively calculated, that actual difference between strain in water versus air is most likely larger than documented. Based on the results and conclusion made in this paper, further investigation on this topic would be strongly encouraged to accurately determine the reduction in dynamic strain when submerging a perforated plate in water.

Acknowledgement

The study in this Master's thesis has been prepared and performed at the University of Stavanger, Department of Petroleum Engineering at the Faculty of Science and Technology. The study, and thus the topic of this master's thesis was proposed by the Subsea Technology and Operation at Statoil ASA in Stavanger.

There have been a lot of contributors in the process of this Master´s thesis, and much of the work would not have reached the current degree of completion without the support and help of a number of resources. First of all, we want to thank our supervisor, Professor Dimitrios Pavlou. Thank you for agreeing to guide us through the thesis despite already having a packed agenda. We are very grateful for your support and for you sharing your knowledge with us.

We would also like to thank our external supervisor at Statoil, Kjell Einar Ellingsen for always being available, guiding and supporting us throughout our work on this master's thesis. Further, we would like to extend a special thanks to Senior Engineer, Ahmad Yaaseen Amith, at the University of Stavanger. Thank you for the effort you put into teaching us how to prepare and install strain gauges, and for making all the various devices needed for the test available.

Furthermore, we would like to thank the laboratory personnel at the University of Stavanger for their support and for training us in the various tools and machinery we have used, and for their guidance prior to and throughout the experiments. We are also grateful for the help from Martin Bae when our experimental devices did not give us adequate data. Lastly, we would like to thank Åsmund Sveinsvoll for great discussions and practical help prior to and during the experiments.

Stavanger, 1st of June 2018.

Personal Acknowledgement – Charlotte Andreassen

My time as a student has come to an end. An unforgettable era filled with learning, new acquaintances and countless good memories is now over. This Master's thesis has therefore been extremely important to me, precisely because it symbolizes the end of an important chapter in my life. However, I would not be where I am today without all the great people around me.

I would therefore like to take this opportunity to thank some of those who have helped to make my studies possible. Thank you to my grandparents, parents and siblings, who have only been a phone call away when things have been extra tough or when my longing for home became too great.

Mum and Dad, thank you for helping to shape me into the person I am and for always having faith in me, particularly during times when I lacked faith in myself.

An extra big thank you also goes to Uncle Mathias, who pointed me in the direction of these studies and who has been an important support throughout the entire study period.

Thanks to my fellow students in Bergen, Brazil, Australia and Copenhagen. A special thanks to Anne Lene and Hedda, it has been a pleasure getting to know you – a friendship that will last a lifetime.

Thomas, thank you for putting up with me as a collaborative partner. Sofie and Alvilde, without you the thesis would not have had the same quality. Kristoffer, thank you for all the practical assistance in the simulation work.

Last but not least, a big thank you to my partner Rasmus. Thank you for your genuine interest in my studies, for good discussions and input. Thank you for keeping me going when I was struggling to stand upright.

It is with mixed emotions that I now draw a close to this era of my life. I am so incredibly grateful for everything I have learned and for all the people I have met during the course of my studies. Just think, now I can finally call myself a graduate civil engineer!

Stavanger, 1st of June 2018.

Table of Contents

Abbreviations

GPE: Gravitational Potential Energy

KE: Kinetic Energy

LHS: Left hand side

RHS: Right hand side

VLFS: Very large floating structures

1 Introduction

1.1 Background

In recent years, costs associated with the subsea industry have increased considerably. The industry has been characterized by high profit margins, which has allowed high-cost customized solutions. However, challenging economic times have impacted on industries such as oil and gas in recent years, and there is a necessity for proactive change and adaptation. A new approach with creative thinking is needed in the industry, and necessary priorities must be made.

The company Equinor, formerly named Statoil, is the largest oil and gas operator in Norway, and among the largest offshore operators worldwide. In this study the company will be referred to as Statoil, as our collaboration was initiated before the rebranding.

To cope with the need of change, Statoil has already initiated a variety of measures to reduce costs. The aim is to move from customized, time-consuming and costly solutions, to more standardized solutions, as a way of reducing costs and improving efficiency. An example is the development of Cap-X, which is a simplified and standardized subsea concept based on suction anchor technology for erecting installations on the seabed.

Cap-X is a revolutionary new technology. The suction anchor is made of steel and serves as a foundation, while both the skirt and cap solutions are made of fiberglass, which provides a solid, simple and low-cost structure (Andersen, 2016). The protective cover of the Cap-X has perforations on the horizontal surface.

As for all new technologies, Cap-X must meet a set of standards and requirements in order to be released to the market. NORSOK standards are developed by the Norwegian petroleum industry to ensure safety, value adding and cost-efficient industry. NORSOK has strict requirements related to applied load and new technologies, such as Cap-X, have to cope with these requirements. This lead us to the research question of this study.

1.2 Research Question

As Cap-X has a completely new design, it is reasonable to assume that the strict restrictions to applied load given in NORSOK do not entirely apply to this new design. To conduct research, we strive to find out if it is possible to quantify how Cap-X performs to applied load in water versus how it performs in air. Furthermore, we aim to find out how the strength of a structure with perforations differ from a structure without perforations, and whether this can be quantified. This brings us to the key questions of this paper:

1. *Will a cushioning effect arise when the perforated material is submerged in water, resulting in reduced maximum strain associated with impact loading?*
2. *If so, to which degree and why does this effect occur?*

To answer the research questions, two impact tests was performed. The tests are carried out both in air and water, on two types of test objects; a solid pate and a perforated plate. The plates are tested with various loads, and the loads are dropped from different heights. In addition, simulations of the material behavior are carried out in a simulation program called Solidworks. The results from the tests are then compared to the simulation. The goal of this comparison is to illustrate how the strain is distributed in the material, and how much energy has been absorbed by the steel plates. If it turns out that the material behaves differently in solid compared to perforated materials, the aim to determine the difference in percentage or as a factor, in order to reduce the material thickness and in turn reduce the costs per unit.

1.3 Project Organization

The study consists of nine chapters. *Chapter 1* comprehend the introduction to the paper. In this section the aim of the study is explained, and the research questions are pointed out. In addition, the workload distribution between the authors of this paper is explained. *Chapter 2* consists of the preparatory work of the study. Before getting the results, a lot of trial and error was made. This led to a high workload during the whole semester. In this chapter, the aim is to reveal the whole process of this study by explaining the iterative work that was done. In *Chapter 3* relevant theory for this study is elaborated.

This includes theory about Cap-X technology, NORSOK standards, force of impact and measuring equipment. *Chapter 4* concerns the simulations performed in Solidworks, theory behind the simulations and observations regarding the results are given. In *chapter 5*, the experimental setups are explained in detail, with diagrams that includes all the parameters involved. Most importantly, the procedure for each experiment type, in both air and water, is explained with respect to data sampling, proctor use, temperature, water depth etc. In *chapter 6* a presentation of the results is made, with tables and graph. Observations regarding the results are given, but no comparison is made in this chapter. However, the chapter focus on center mounted strain gauge. *Chapter 7* includes comparison and evaluation of the results for solid and perforated plate, with respect to correlations discovered, data variation, experimental uncertainty, and general observations pertaining to the measurements conducted. *Chapter 8* Is the final argumentation regarding the thesis objective regarding the findings from *chapter 6* and *chapter 7* is concluded. The final chapter, *chapter 9,* consist of recommendations and suggestions to future work within this field.

1.4 Workload Distribution

Starting up in February, the workload of this Master's thesis has been fairly distributed from February and June. It has been a time-consuming process, and retrospectively, we are pleased to have worked continuously throughout the semester. Writing this paper, we have experienced that the process of writing a Master's thesis has been a great deal of trial and error.

The workload distribution between the authors has been based on several factors. First and foremost, we distributed our work with respect to our set of skills. Secondly, we distributed some work with regards to our personal preferences. Thomas Løklingholm has been responsible for the majority of the analytical and theoretical work with respect to NORSOK. In addition, he has been responsible for the force of impact and energy balance, selection and design of steel plates, apparatus and experimental setup, present results from the impact tests and the discussion around the results gained. Charlotte Andreassen, on the other hand, initially established the dialogue with Statoil, and held the contact with the company throughout the process.

She made sure there was a good collaboration with the company from beginning to end. Further, she has been in charge of the organization, planning and structuring of the Master's thesis. On a technical level, Charlotte has been responsible for the work performed in the Solidworks software for impact loading simulations. In addition, she has been responsible for writing the abstract, introduction and acknowledgement sections of the paper, as well as preparatory work, Cap-X and strain gauge theory, measuring- and data processing equipment.

The overall workload has been fairly distributed between the two of us. Our working methods and personal strengths varies, which we have seen as a strength in our collaboration. We believe that we have managed to involve each other in each other's work, and by using our different personal strengths, we improved the overall quality of the work. Consequently, the project would not have been of the same quality without the collaboration between the two of us. We are pleased with having worked dedicatedly throughout the process, and of the goals we have accomplished working on this thesis together.

2 Preparatory Work

In this chapter, the work performed previous to the execution of the tests will be explained. It should be noticed that a lot of work and time was put into the preparatory work. Mainly, this consisted of determining and getting access to test equipment and adjusting software configurations. This preparatory work was done in an iterative manner, building several test setups and improving them along the way.

During our engineering studies, we have been introduced to a variety of well-known and used test methods. In collaboration with professors at the university, deciding which test methods to use in our study was relatively straight forward. We decided to run two different tests, with the need of two different instrument setups. The equipment and test methods will be discussed in *chapter 5.2* and *chapter 5.4* respectively. However, finding the right equipment has been a challenging and time-consuming process. For the purpose of this study, there was no adequate test equipment available at our university. Consequently, we had to design and build our own instruments. This work included planning, drafting and getting materials and parts to the setups. This also included a lot of trial and error, leading to the final test setup.

Further, we were on a relatively tight budget, thus we mainly had to use materials and parts available at the university to build the test setup. Due to a limited selection of materials, we had to think creatively when designing the setups.

Even though building the test setups was an iterative process, the test results implied that our instrument setup was not stable enough. This led to a change in the construction of the setup, changing from pipette stand to frame with clamps, pulley and nylon rope. The difference between the first and second setup is shown in *Figure 2* and *3*.

After changing the test setup, once again results indicated unstable records. This lead to a significant change in the test setup; the configuration of software needed to be adjusted. As for the change in equipment, changing the software configuration deferred further work with our study and resulted in a second run of all the tests. Retrospectively, a more thorough testing of the first software configuration before performing the tests would have been preferable.

To summarize, designing and building suitable test setups was a significant part of the preparatory work, and was a challenging and time-consuming process.

2.1 Unused Theory: Very Large Floating Structures

During the initial planning phase of the project the theory that was available was believed could be adjusted to account for different fluid medium. The theoretical equation in question was based on very large floating structures (VLFS) behavior when subjected to pulse loads (Dimitrious.G.Pavlou, 2011).

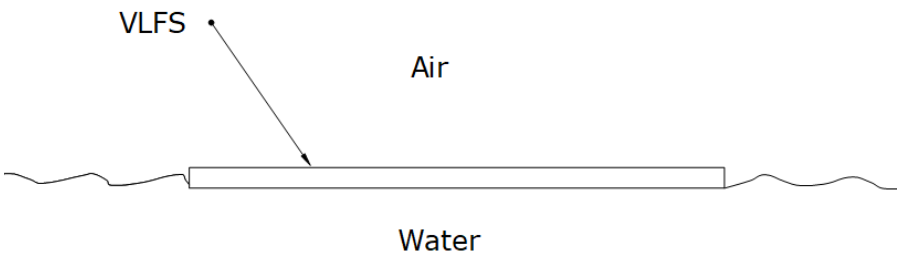

Figure 1: Illustration of material (e.g. steel plate) floating on water.

It proved to be more difficult than initially believed, since showing illustrations of analytical values for completely different scenario other than a simply supported steel plate would not be beneficial to the thesis. This was despite having the Mathematica script for the analytical solution for an infinite plate which is placed in Appendix A.

2.2 Constructing the Test Setups

As presented in the introduction, one of the main research question of this master thesis is finding out to which degree a construction is affected by its perforation, and how it is affected. In order to do this, impact tests were performed. This is done to observe the mechanics in the material, calculate the amount of energy being absorbed and measure the deflection in the material when it is exposed to an impact load.

It was decided to perform two types of tests, with different setups: *Proctor* and *ball drop method*. Both test types will be elaborated upon in the upcoming sub chapters.

2.2.1 Test type 1: Proctor

After brainstorming and discussing with engineers and professors at the university, we decided to use a *proctor* to apply load on the steel plates. A proctor is known as a standardized tool commonly used to perform for soil compaction tests, also referred to as modified proctor compaction test (Day, 2001). Using the proctor, the goal was to recreate an impact equivalent to a pulse load.

In order to do this, the proctor needs to be suspended above the surface of the steel plate. The weight is than let down from a given height and hits the plate. Because of the construction, the weight rebounds, which in turn creates a pulse/accidental load.

Considering the limited access to equipment at the university, an attempt was initially made to use pipette stand with clamps to position the proctor above the steel plate. The pipette stand setup is shown in *Figure 2*. However, this setup turned out to be somewhat unstable. To achieve more satisfying test results, every measure had to be consistent and performed under identical conditions. Consequently, a more stable test equipment had to be designed.

Figure 2: The pipette stand setup.

After iterative processes of sketches and discussions, a more suitable setup was reached. The final solution is shown in *Figure 3*.

Figure 3: Final solution test type 1 – Proctor.

This solution includes a frame with clamps to keep the proctor directly over the steel plate as well as a pulley with a nylon rope to keep the proctor vertically stable above the steel plate and unload the clamps. To construct this setup, we had to cut the frame in the right lengths and weld it together. Holes with internal screw threads in two of the sides as well as bars with external screw threads were made. They should function as extensions for the clamps. To increase the stability, we made legs and put weights on the frame. Using this setup, it was easier to centralize and keep the proctor stable above the steel plate. As a result, the measurements could be carried out in a more consistent manner and were able to compare the results.

2.2.2 Test type 2: Ball Drop Method

The second test type is ball drop method, which consists of a PVC pipe and a steel ball. This setup was less time consuming to construct, compared to the first test type. In this setup the applied load was a steel ball. The ball was dropped from a specific height through a PVC pipe installed over the test objects. The PVC pipe was purchased by the construction technology department at the university. In this case, the ball should come to rest on the test object after the impact, not rebound. Spotlights were installed to enhance the quality of the video. Figure 4 illustrates the setup used to execute the tests in the water tank.

Figure 4: Test type 2 – Ball drop method.

2.2.3 iPhone and Measuring Board

We had to find a way to measure the rebound height of the proctor after colliding with the steel plate. We considered multiple ways to do this. Firstly, we explored the possibilities of using photocells. However, this turned out to be too complicated to implement to measure the rebound height. Secondly, we explored the possibilities of using the camera normally used in the university laboratory. In order to do this, we were in need of a light-bridge, which should send signals to the camera. This required programming in Matlab, which was too time-consuming and advanced to implement.

Lastly, the possibility of using the iPhone camera was examined. The iPhone camera has a slow-motion function and relative high frequency (pictures per second) to measure the rebound height of the weight. Consequently, it was decided to use an iPhone camera installed on a stand. In addition, we put up a measuring board marked with millimeters behind the test object, as shown in *Figure 5*.

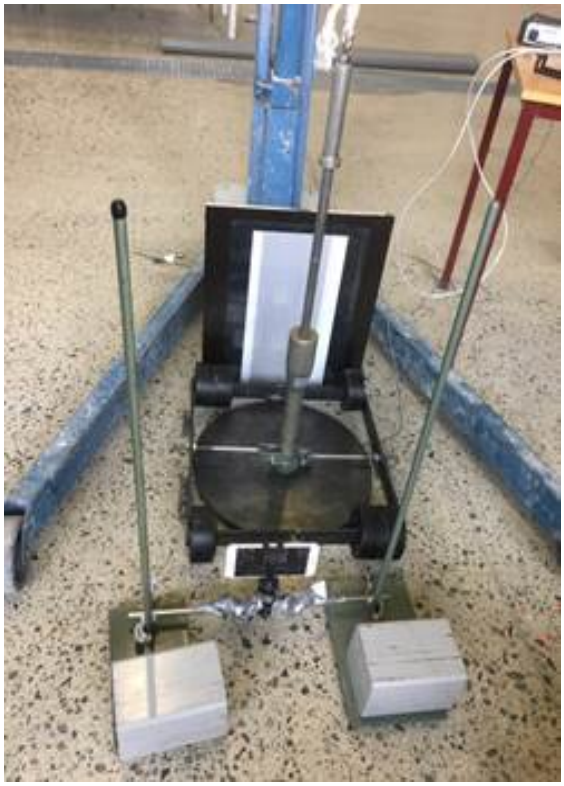

Figure 5: iPhone installed on stand and measuring board.

2.2.4 Water Tank

The water tank was built according to a set of requirements. First, the water tank had to be waterproof. Plywood plates coated with phenolic film was used. In addition to silicone sealant for all the seams to make it waterproof. Secondly, to being able to take video recordings of the solder when hitting the plate, the water tank had to be either fully or partly transparent. It was also decided to build one of the walls from SAN plastic, which is a transparent and waterproof material. We milled out grooves in the plates of plywood in order for the Plexiglas to fit in and used a decent amount of sealant in the seams. The measuring plate was glued inside the water tank with the same silicone sealant. Here, we used a thin layer of sealant, to prevent the measuring plate from becoming uneven. The water tank is displayed in *Figure 6* below.

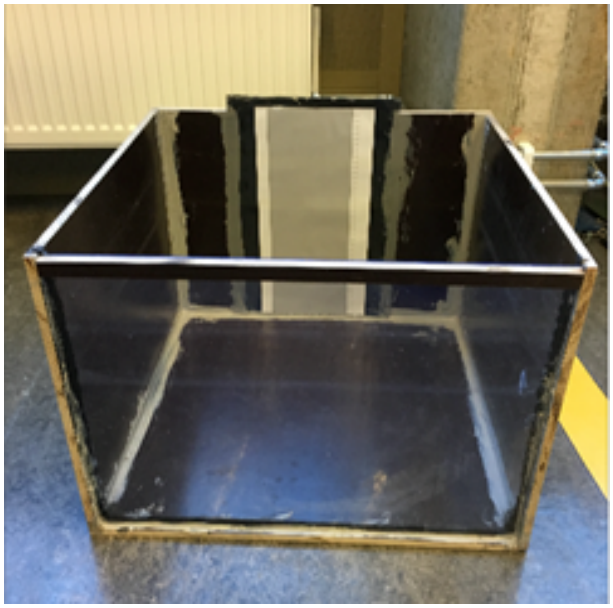

Figure 6: The water tank used in the study

2.2.5 Steel Plates

In order to find out to which degree a construction is affected by its perforations, and how it is affected, circular steel plates were chosen as test objects. Initially, we planned to make the steel plates from steel available at the university. This steel turned out to be rusty, and not of the right size. In addition, there were no suitable equipment for cutting the steel of these dimensions. As a consequence, order for two circular steel plates was made, one solid and one perforated, from Svenskt Stål AB (SSAB) in Stavanger. *Figure 7* below shows both the solid (left) and perforated (right) plate. The selection and design of steel plates will be elaborated upon in *chapter 3.3*.

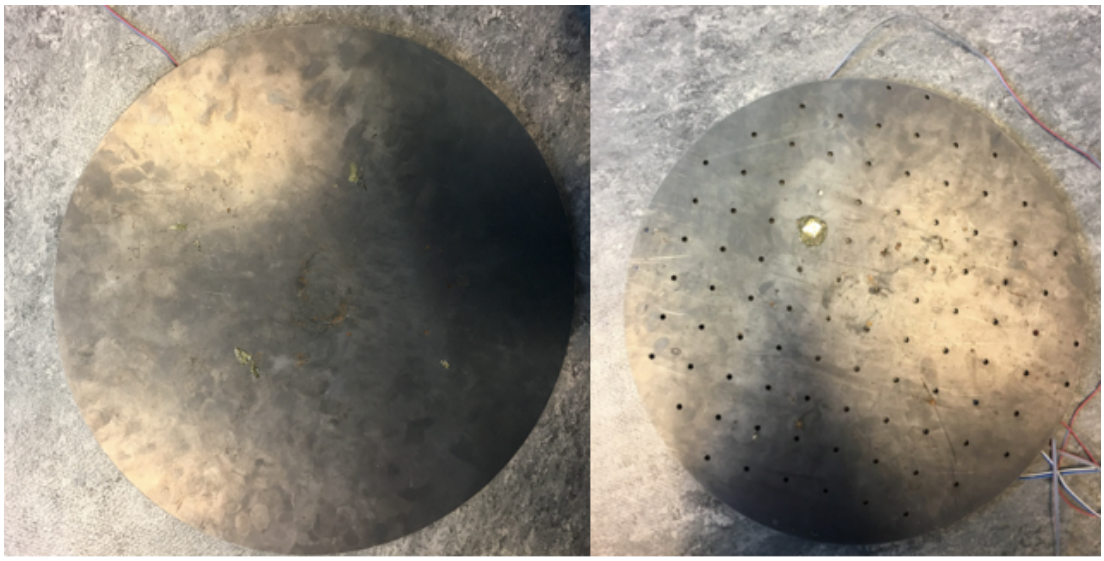

Figure 7: Solid steel plate (left) and perforated steel plate (right)

2.2.6 Measuring- and Data Processing Equipment

In the interest of determining whether a cushioning effect arise when the perforated material is associated with an impact load, strain gauges were mounted on the test specimens in order to detect the amount of strain along the material. Additionally, some data acquisition and recording equipment is needed to be able to amplify, interpret, analyze and display the measurements performed by the strain gauges. This subchapter will review the different configurations examined, leading to the final measuring- and data processing equipment used in the experiments of this thesis.

During the preparatory work, a great variety of different configurations of the measuring- and data processing equipment. Initially started off with a configuration consisting of active strain gauge on test specimen, dummy strain gauge on dummy steel, Spider8 amplifier, Catman 4.5, and a 15-pin VGA, which is compatible with Spider8. This equipment is widely used at UiS, as well as in several previous master studies similar to this study.

After performing several tests with these configurations, realizing the results to be incorrect. The variation in the measurements were not desirable, and the results were much lower than what was theoretically calculated in advance. In dialogue with plurality professors, with good experience in this measuring equipment, we found that the frequency of the measurements was likely to be too low.

Catman 4.5 has a maximum limit of measurements at a frequency of 9600 Hz, while Catman 4.5 and Spider8 together, the limit was only 4500 Hz. As a result, decision to install a new equipment capable of taking measurements with a higher frequency was made. Finally landing on QuantumX, SCM SG-120 adapter and upgraded to Catman 5.2 software, which can do measurement up to 19.2 kHz. Also, because of the equipment we had to switch the adapter, as the old adapter type was not compatible with the new amplifier (QuantumX). Here, we had to learn the solder configuration for the new SCM SG-120 adapter, followed by soldering of the wires to this new adapter.

To summarize, we tried two different configurations of the measuring- and data processing equipment where the last one was used in the final experiment of this thesis. Both arrangements are illustrated as a sequence in *Figure 8* and *Figure 9* below.

2.2.6.1 First Configuration

The first configuration consisted of active strain gauge on test specimen, dummy strain gauge on dummy steel, Spider8 amplifier, VGA 15-pin adapter, and Catman 4.5 software.

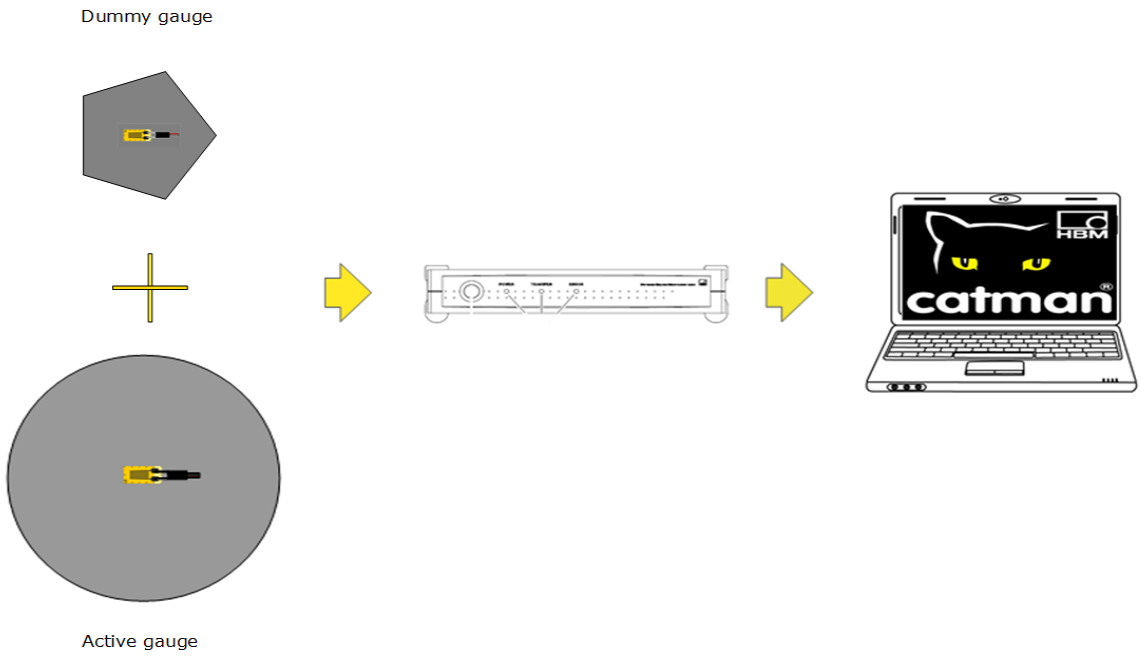

Figure 8: First configuration.

2.2.6.2 Second Configuration

The second and final configuration consists of active strain gauge on test specimen, QuantumX amplifier, SCM SG-120 adapter, and Catman 5.2 software. It should be noticed that the dummy strain gauge is removed for this configuration. This is because the circuit for this configuration does not require any more elements to fulfill the requirements of a full bridge circuit.

Figure 9: Second and final configuration.

2.3 Installation of Strain Gauge

A perfectly functioning measuring point is not only dependent on the strain gauge itself. Consequently, the accuracy of the results is highly dependent of a thorough preparation of the application surface, careful bonding, correct connection, in addition to a protective coating (HBM, u.d.). With that in mind, we were constantly in close dialogue with both professors at the university, as well as professionals from HBM, the supplier of the strain gauges used in this study.

We were given a video, released by HBM, that explained step by step how to install the strain gauges. Both methods and materials used in the preparation and application of the strain gauges, are reliable and suitable for the purpose of this thesis (HBM, u.d.). The focus in this paper is based around the strain produced at the center of the plate, as this is the region that is expected to experiences the highest amount of strain since this is the point of impact. With this in mind, one strain gauge was installed at the center of the solid plate. However, the perforated plate was mounted with a total of six strain gauges in order to determine strain variation from the center. All the following sub chapters applies to both the first as well as the final configuration of the measuring equipment, except for *2.3.4 Coupling of cables*. Two methods were used in order to couple the cables to the adapters - one for the first configuration, and another for the second configuration.

2.3.1 Surface Preparation

The surface of the steel plates has to be prepared and cleaned before installing the strain gauges. The steel plates have been heat rolled under production. Thus, an oxide scale has been formed on the surface. This had to be rubbed down where the strain gauges should be installed. Thereafter, we wanted to make a smooth surface, in order to install the strain gauges using glue. We strived to make a cleaned surface, without rust, fat and other contaminants. We did this in three main steps. Firstly, we used a coarse sandpaper on the installation area. Secondly, we used a fine sandpaper on the installation area and thirdly, the measuring point was cleaned using a cleaning agent called RMS1, which is a mixture of acetone and isopropanol (HBM, u.d.).

2.3.2 Bonding Procedure

As mentioned previously, one strain gauge was installed on the solid plate, whereas six strain gauges were installed on the performed plate. For the solid plate, the maximum strain will be measured at the point of impact.

Therefore, the strain gauge is installed exactly on the center of the solid plate. For the perforated plate, it was mounted a total of six strain gauges to determine strain variation from the center and around the holes.

The strain gauges are glued to the underside of the steel plates with an extremely quick-drying superglue called Z70, which harden by applying pressure (HBM, u.d.). We faced challenges using the glue, as the glue would not harden. After several attempts, we contacted HMB, in order to find out what could have gone wrong in the process. We discussed the procedure with HMB, who also thought it was strange that the glue would not harden. However, we concluded that the Z70 is relatively sensitive to low humidity and low temperatures. During the period we tried to glue the strain gauges, there were low temperatures, as well as low humidity (Yr measured minimum temperature to -11 degrees and humidity below 30% (YR, 2018)). HMB also emphasized the importance of using a minimal amount of Z70. Consequently, we had to heat the plates so that they got an approximate temperature of 20 degrees before we could install the strain gauges. In addition, we used a minimal amount of Z70. After implementing these measures, the glue hardened properly.

The following steps for the gluing process were performed, according to the instructions given by HBM:

1. A tweezer was used to remove the strain gauge from the package, to avoid finger marks, grease, etc. from the fingers.
2. A heat resistant polyimide tape was attached to the strain gauge (HBM, u.d.). Then, the strain gauge attached to the tape was placed on the measurement point, with the solder pads facing upwards.
3. The polyimide tape was used to lift the strain gauge from the steel plate while the Z70 glue was put at the measurement point, as shown in *Figure 10*.

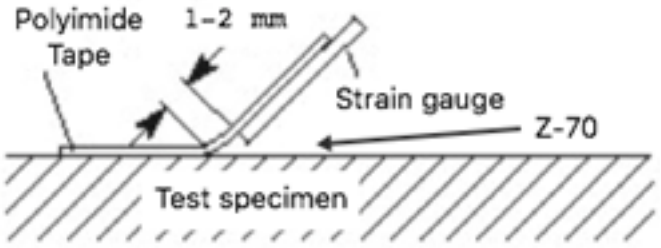

Figure 10: Strain gauge bonding procedure.

The Z70 was immediately spread out as a thin layer with a Teflon-strip. Here, it was important that no pressure was applied, so that the Z70 did not begin to harden. Then, the strain gauge was bent down using a Teflon separating foil with even pressure from the thumb, for about two minutes. The pressure had to be constant until the glue was hardened. Finally, the polyimide tape was removed with a tweezer.

2.3.3 Inspection

After the assembling, the strain gauges were carefully inspected. It was checked for loose edges, bubbles or cavities underneath the strain gauges. We also used a multimeter to measure the resistance of the strain gauge, which should be 120 ohms when mounted correctly. This part of the procedure was important, as the strain gauges had to be replaced if deviations were found.

2.3.4 Coupling of Cables

Two methods were used in coupling the cables - one for the first configuration, and another for the second. Both the methods are explained in the following sub chapters.

2.3.4.1 Coupling of Cables - First Configuration

The first configuration had a more complicated coupling than the second configuration. There are three wires from each gauge (one active and one dummy), 2 grey wires and 1 red per gauge. These wires are connected to a 15-pin port, as illustrated in *Figure 11*. The wires have to be carefully mounted in specific pinholes of the port, depending on the function of the specific gauge. The 15-pin port adapter is then connected to Spider8 amplifier.

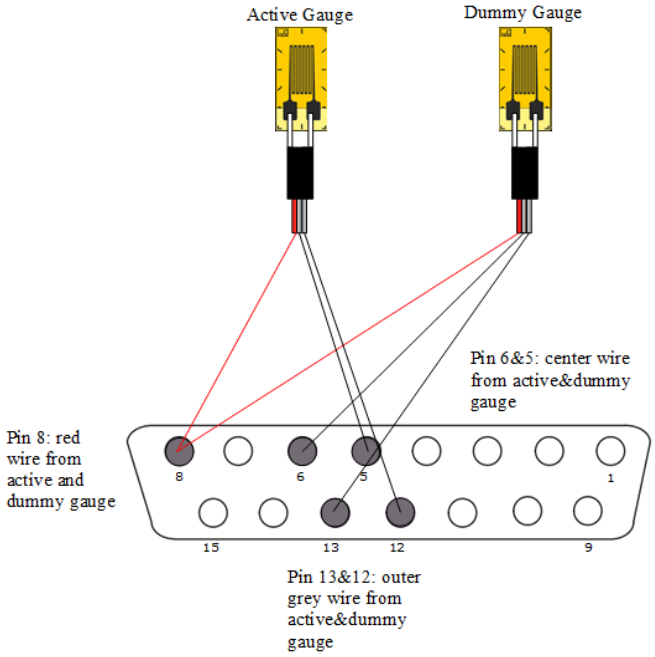

Figure 11: Active and Dummy strain gauge wires mounted to the 15-pin port adapter.

2.3.4.2 Coupling of Cables - Final Configuration

In the second and final configuration, the cables from the gauge were soldered directly on the electronics inside the adapter. There are three wires from each gauge, 2 grey wires and 1 red per gauge. These wires are connected to a SCM SG-120 adapter, as illustrated in *Figure 12*. The SCM SG-120 adapter is then connected to Quantum-X amplifier.

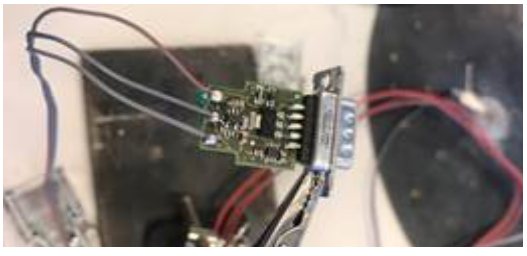

Figure 12: Strain gauge wires mounted to the SCM SG-120 adapter.

2.3.5 Completion of Strain Gauge Installation

After gluing the strain gauge, connecting to adapter by soldering wires and checking the resistance with a multimeter, the strain gauge was covered with SG250, a single-component cover material, to protect the strain gauge installation. The product is solvent free and harden in contact with air at room temperature (HBM, u.d.). Further, the cables near the strain gauge were tightened to the plate with X60, a two-component superglue, to avoid tension in the cables. This product also hardens in contact with air at room temperature (HBM, u.d.). Lastly, the area around the strain gauge was covered with ABM75, putty covered with an aluminum foil. This material, in combination with the SG250, will ensure water retention stretching, and achieve an optimal measurement point protection for the tests to be performed immersed in water (HBM, u.d.). *Figure 13* is an illustration of a mounted strain gauge.

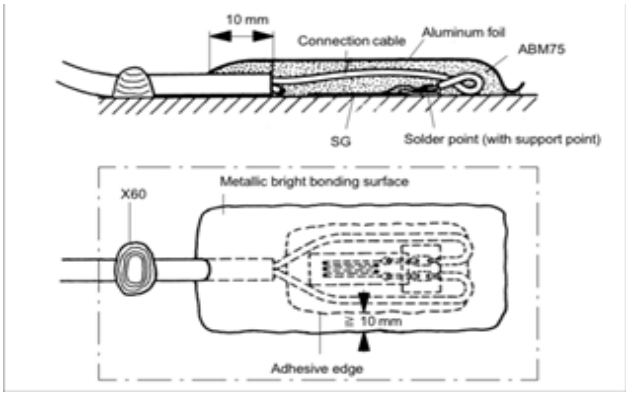

Figure 13: Mounted strain gauge with SG250, ABM75 and X60 (HBM, 2018).

Figure 14 show the mounted strain gauge both for the solid (left) and perforated plate (right). At this stage only ABM75 is missing to make the strain gauges waterproof.

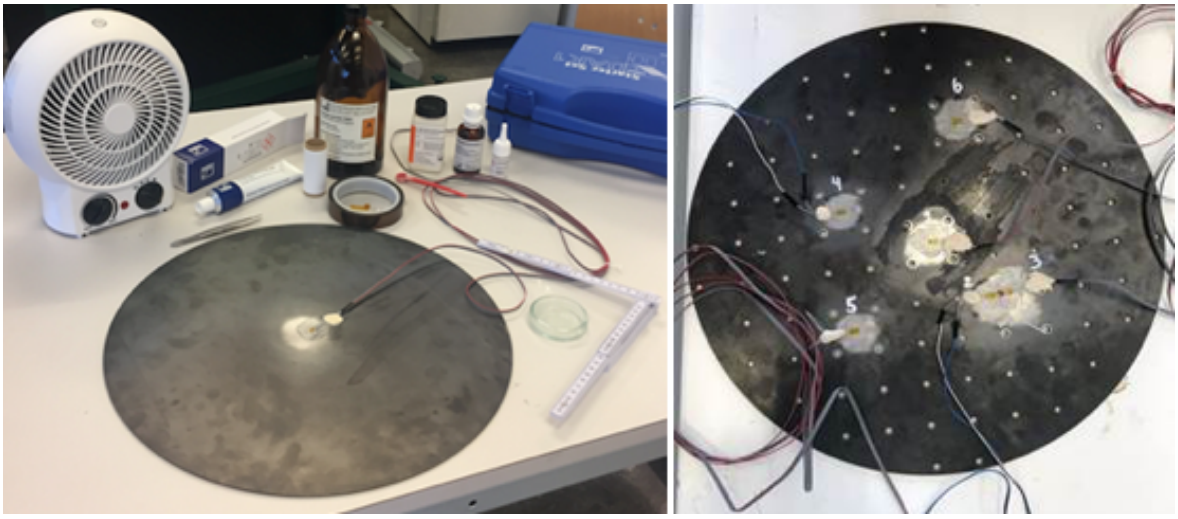

Figure 14: Mounted strain gauge on solid (left) and perforated (right) plate.

3 Background Theory

In this chapter, theory relevant to this study is presented. Firstly, by elaborating on the Cap-X Technology and the NORSOK and IOS standards, which forms the basis of this study. Secondly, the physics, force of impact and the energy balance used for analysis and discussion in this paper. Lastly, the measuring equipment used in this study will be elaborated upon, in light of the Wheatstone theory.

3.1 Cap-X Technology

In recent years, the costs associated with the subsea industry have increased considerably. The industry has long been characterized by high profit margins, which has enabled it to allow high-cost customized solutions. However, challenging economic times, which have impacted on industries such as oil and gas in recent times, call for proactive change and adaptation. A fresh approach and creative thinking are needed in the industry, and the necessary priorities and focus must be ensured.

Statoil has already initiated a variety of measures. Among other things, they want to move from customized, time-consuming and costly solutions to standard solutions as a way of reducing costs and improving efficiency.

Developed by Statoil, Cap-X is a revolutionary new subsea concept based on simplification and standardization. The technology is based on the company's experience from previous drilling campaign in the Barents Sea, with well-proven and new elements being combined into a new technology. Development of the technology started in 2013 and the original aim was to increase profitability in potential resources in the Barents Sea (Statoil, 2016). In recent times, however, it has become clear that the technology also has further potential elsewhere on the Norwegian continental shelf (Andersen, 2016).

As already mentioned, the concept is based on simplification and standardization, with the idea that Cap-X should function as a standard platform. This platform will encompass a larger part of the supplier industry and give more suppliers the opportunity to place their technologies in the standard solution. The subsea market is opening up to more and new suppliers by ensuring that the major players do not have a monopoly on the seabed, whilst giving smaller niche companies the opportunity to gain direct access to the market (Ellingsen, 2017). In addition, the technology's main component can be produced in a shorter timeframe, and there is the potential for localised production (Statoil, 2016).

The subsea concept is based on suction anchor technology for erecting installations on the seabed. The suction anchor is made of steel and serves as a foundation, while both the skirt and cap solutions are made of fiberglass, which provides a solid, simple and low-cost structure (Andersen, 2016). Both the single and dual Cap-X are illustrated below.

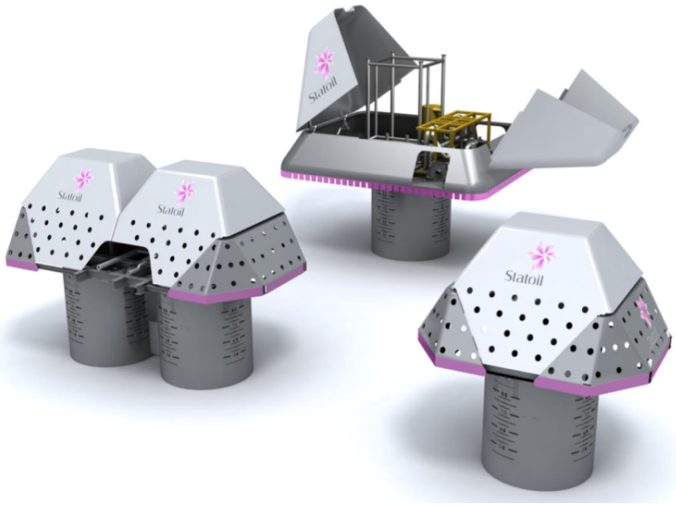

Figure 15: Dual Cap-X (left), Open Dual Cap-X (back), Single Cap-X (right), (Ellingesen, 2016).

Cap-X has numerous benefits. First and foremost, the new subsea solution is one quarter the size of earlier subsea frames, making it easier to handle and considerably reducing production costs. *Figure 16* below shows an example of a single subsea frame (Left), compared to a single Cap-X construction (Right).

Figure 16: Single Subsea Frame (left), Single Cap-X (right) (Ellingesen, 2016).

The biggest cost savings, however, are not in production; the main advantage is that this solution can be installed and operated by simpler vessels, which will reduce the number of rig days as well as marine installation costs. In addition to Cap-X being smaller, it is also more flexible and can hold more equipment than traditional solutions (Ellingsen, 2017).

It seems that Statoil is following the maxim of Albert Einstein among others, which is 'Make things as simple as possible, but not simpler.' (Einstein, u.d.). Meaning that simplicity should be a key goal and unnecessary complexity should be avoided. For the Cap-X technology, it is precisely this simplicity that is the core feature, and Statoil's endeavors here will bring it one step closer to a 'plug and play' solution on the seabed (Statoil, 2016).

3.1.1 Protective Cover

As mentioned initially, we will study the protective cover for Cap-X. The protective cover we have used as our basis is illustrated below in *Figure 17*.

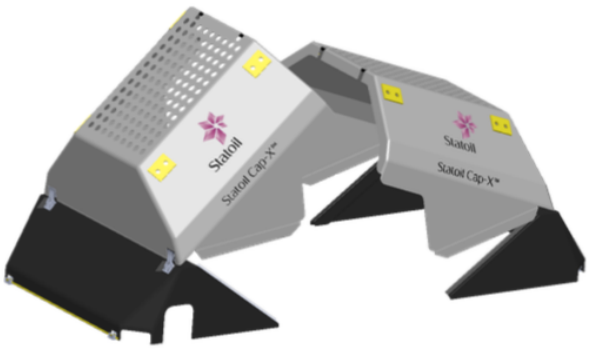

Figure 17: Dual GRP Cap-X cover.

Objective is to study the impact of perforations in the material. It was therefore chosen to simplify the test object by solely examining the top horizontal surface of the protective cover. The theoretical part in *chapter 3.3* will explain how the test object is designed and optimized, in order to achieve the best test results.

3.2 NORSOK standard and ISO 13628-1:2005 Dropped Objects

Refers to datasheet in appendix F from NORSOK standard, highlighting common loads for fish trawling and dropped objects. For dropped load, the impact energy for design purposes ranges from 5kJ to 50kJ. The calculation being based on point loads with object ranging from 100-700 mm respectively, as displayed in *table 1*. Impact energy in this case being the kinetic energy the object has before impact and subsequently delivers to the structure.

Table 1: Dropped objects parameters for multi-well structures.

Impact energy	Impact area	Object diameter
5 kJ	Point Load	100 mm
50 kJ	Point Load	700 mm

Since the NORSOK standard base their design on impact energies, means that ranges of masses and velocities must be accounted for. For any given level of impact, energy can be fulfilled by using either as small mass with significant velocity or small velocity with corresponding large mass. It is also important to note the behavior of impact energy of dropped objects as the energy is linearly dependent on mass, whilst exponentially dependent on velocity. This means that velocities become exceedingly large for small masses as shown in *Figure 18*.

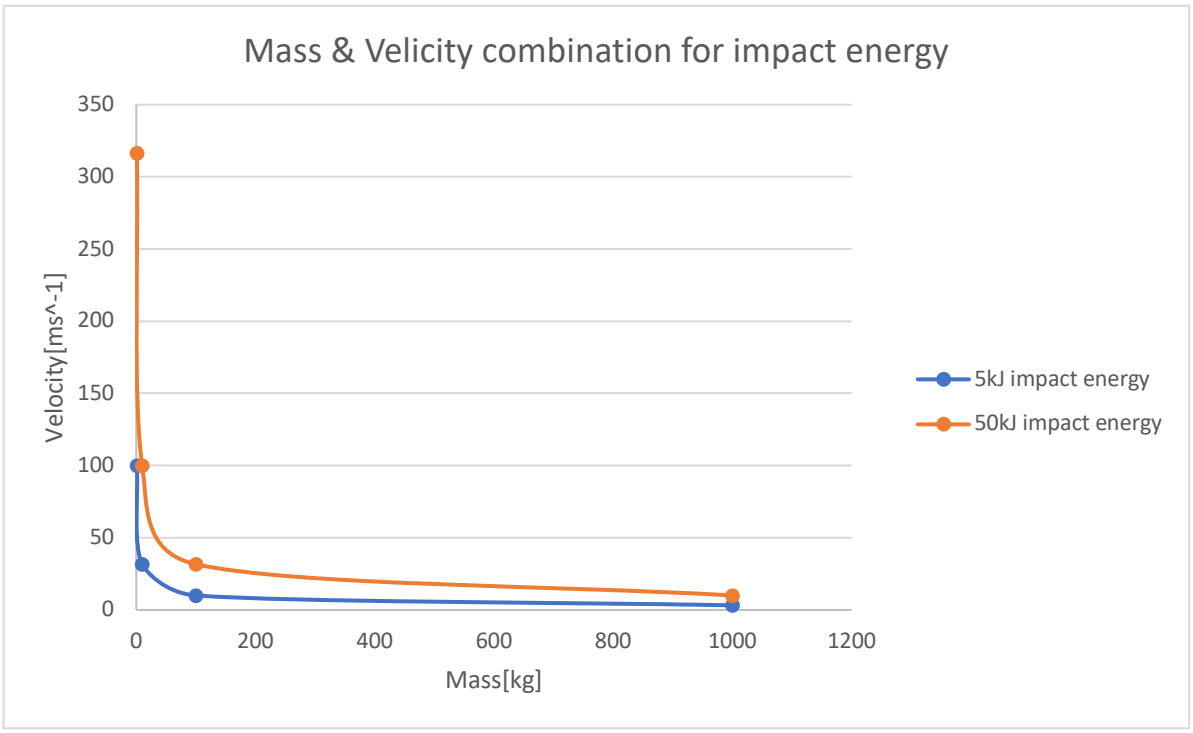

Figure 18: Mass & velocity relationship for impact energy of dropped objects.

As an example, a mass of 1 kg aiming to achieve an impact energy of 50 kJ needs a velocity of 316 ms^{-1}, which is close to the speed of sound. However, the terminal velocity for dropped objects (based on steel spheres) in saline water is much lower. Consequently, such a scenario is highly unrealistic to occur for dropped objects in water. Terminal velocity for any object can be determined using *Equation 1*.

$$v_t = \sqrt{\frac{2g(m - \rho_l V)}{\rho_l A C_d}} \qquad \textit{Equation 1}$$

Where the values for the drag coefficient "C_d" is approximated as 0.5 for spherical object at turbulent conditions. "A" is the cross-section surface area for the sphere in the direction motion,"V" being the volume displaced by the mass "m" in question. The NORSOK values for impact energies from 5-50 kJ the terminal velocity is approximately 10 $ms^{-1}$for the mid-range masses.

A representation of the expected masses and expected velocities can be calculated based on constant drag"C_d" coefficient of 0.5 for a sphere is represented in *Figure 19*.

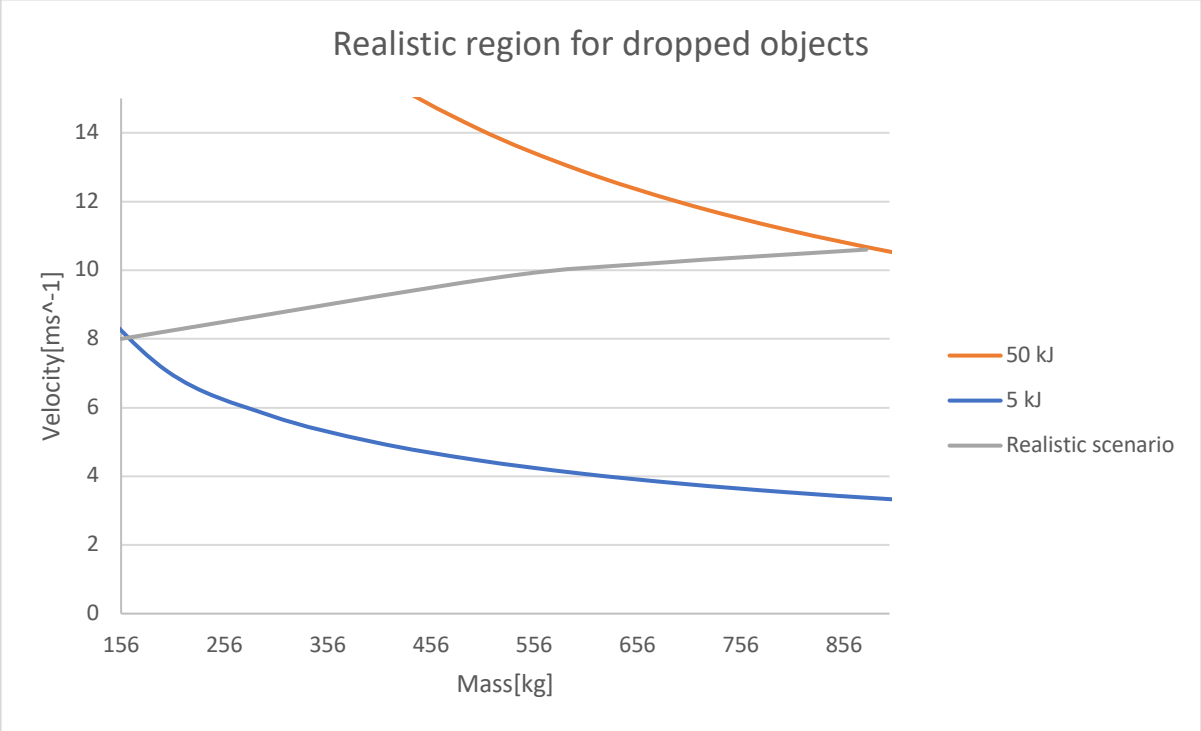

Figure 19: Range of mass & velocity combinations based on steel spheres.

This means that for impact-based calculations for steel spheres for terminal velocity calculations, the corresponding mass and velocity for 5kJ is 156 kg and 8 ms^{-1} for diameter of 0.338 m. For 50kJ it is 878 kg and 10.6 ms^{-1} with a diameter of 0.598 m. Size of the steel sphere therefore must exceed 337 mm to have achieve impact energy of 5 kJ, and 598 mm for 50 kJ.

The NORSOK standard serves as a reference in this paper with regards to scale of impact for dropped object. The experiments conducted in this study have an impact energy range between 14 - 19.6 J, which correspond to a scale difference of 255 to 3500. Consequently, the velocity ranges between 1-9 ms^{-1} in the experiments. Thus, it is more important to look at the nature of the impacts which can indicate what type of strain rates to expect in the field.

3.3 Selection & Design of Plates Used for Impact Loading Experiment

This segment will deal the with the initial process of selecting dimension parameters for circular steel plates. It will highlight the different approaches and calculations which resulted in the final dimensions for steel plate illustrated in *Figure 20*. In addition to the main challenges involved with regards to approximating dynamic impact.

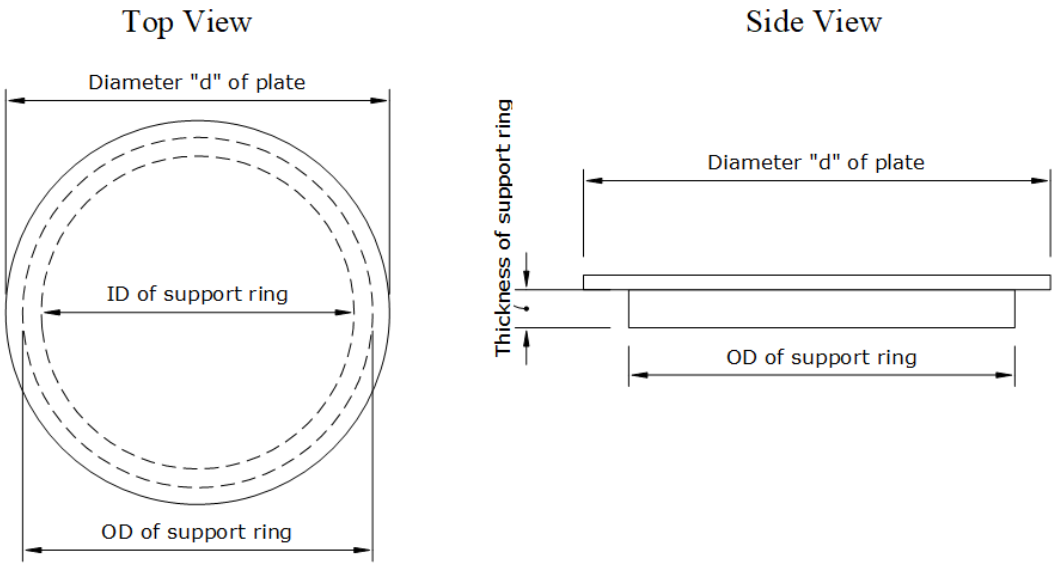

Figure 20: Overview of the plate/s and support ring.

When starting out with the initial outline for how to conduct the experiments, the discussion regarding the geometry and type of supports was evaluated. The first reason was due to suggestion made by councilor with regards to available analytical solutions for circular plates. Secondly, for a solid circular plate the center orientation of the strain gauge does not matter due to axisymmetric behavior of a circular plate. This also meant that for measurement purposes, only a single strain gauge would be required. It was therefore not that rectangular or square shaped was not viable, it was more that the circular plate was more of an attractive option at the time.

Last component of pre-design was the material selection. As previously mentioned, GRP is the material used for the protection covers in CAP-X technology. The reason for not selecting GRP was due to the limitations of the analytical equations, used for these composite materials, being much more complex than well-defined materials such as steel and aluminum.

When considering the design criteria based on static forces using mechanical equations. The main constant used for the design process was the mass dropped on the plate, which was based on the modified proctor device where the mass and height are 4.8 kg and 30cm use in the experiments. This was used as a maximum impact for the design, as any alterations to the test with regards to the dropped mass would have to have a combination of mass and height, resulting in a lower Gravitational Potential Energy (GPE). Using this max GPE from the proctor the first design route was to select a diameter “D” and desired deflection “e” and subsequently calculate the thickness “t”. Design parameters being illustrated in *Figure 21.*

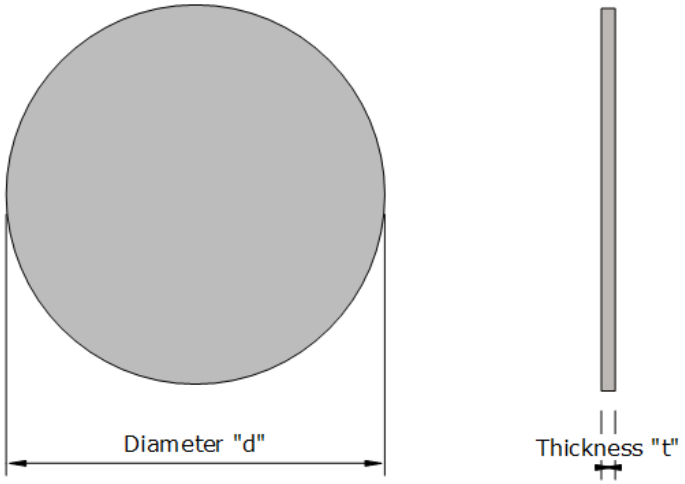

Figure 21: Key parameters for dimensioning the steel plates.

The strain "ε" would then be calculated to check how close this strain was to yield strength of steel, where the selected yield strength was based on the yield strength of the material Domex 355 MC E. Deflection of the simply supported plate is illustrated in *Figure 22*

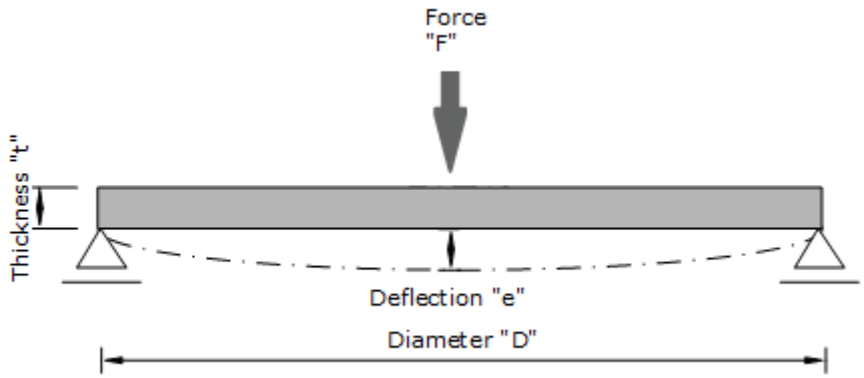

Figure 22: Deflection of simply supported circular plate highlighting key design parameters thickness, diameter and load(force).

Equation 2 gives the deflection of a simply supported plate subjected to a point load at center. This formula is achieved by assuming $\frac{1}{2}Fe = mgh$ and combining it with empirical formulae for normal stress "σ"

$$e(\mathrm{t}) = \frac{2mgh}{\varepsilon E t^2}\left((1+v)\left(0.485\log\left(\frac{D}{2t}\right)+0.52\right)+0.48\right) \qquad \textit{Equation 2}$$

The equation for the thickness is then based on *equation 3*.

$$t = \sqrt[3]{\frac{6(3+v)(1-v^2)D^2mgh}{16\pi E(e(t))^2}} \qquad \textit{Equation 3}$$

When the specific strain was selected all parameters for equation # was known such that deflection e(t) could be calculated. The solution for a given diameter and thickness can then be achieved through the relationship iterative process until LHS = RHS.

Though there are no issues with the calculations approach, the problem is related to not using dimensions for the steel plate as design parameters. If geometric dimensions are not used as independent variables one does not have control over the resulting weight of the of steel plate. Knowing the weight of the plate is very important as it is very easy to get steel plates with mass exceeding 50 kg (plate with D=1m with t=1cm has a mass of 62 kg).

Taking an alternate approach to dimensioning of the steel plate by using selected thickness "t" and diameter "d" using *equations 4* and *5* (Woinowsky-Krieger, 1959).

$$e(\max) = \frac{3(3+v)(1-v^2)D^2F}{16\pi Et^3} \qquad \textit{Equation 4}$$

Main differences for the second approach is that deflection "e" is an output and the fact that load/force is calculated based on mechanics where the kinetic energy from the mass being dropped is used to estimate the velocity "V", which is then used to calculate the force required to stop the mass. The important assumption is that all the energy from the mass is absorbed on impact, as the mass is not bouncing upon collision. Equation can be written as follows:

$$e(\max) = \frac{V^2 m}{2F} \qquad \textit{Equation 5}$$

The method of calculation applied was to iterate using *equation 4* and *equation 5* until they give the same value. Results from these calculations however show that center deflection is expected to be 7.94 mm for the 36 mm diameter, 3mm thick plate, when subjected to impact from 4.8kg dropped from 30cm.

Next step is to calculate the strain produced from such a deflection, by using tensile stress function given in *equation 6:*

$$\sigma(\max) = \frac{F}{t^2}((1+v)\left(0.485\log\left(\frac{D}{2t}\right)+0.52\right)+0.48) \qquad \textit{Equation 6}$$

Which by correlation $\sigma = E\varepsilon$ can be rewritten as

$$\varepsilon = \frac{F}{Et^2}((1+v)\left(0.485\log\left(\frac{D}{2t}\right)+0.52\right)+0.48) \qquad \textit{Equation 7}$$

Final step is then to calculate to produced strain based on the force of impact. This approach sees the use of strain based on the yield strain of steel, which in this case is estimated using the yield strength of steel. Mass dropped from the proctor should ideally produce no more strain on the plate equivalent to 90% of the yield strain, to remain within the elastic region. This was desirable for the tests to be repeatable. the Structural steel was used initially for the yield strength (250 MPa) as it has a one of the lowest of all steel types available, this was to avoid under dimensioning the plates.

For the calculation mentioned however, strain produced is 5921.76 µm/m which is an exceedingly large value 4.8 kg dropped from 30cm. The yield strain for both structural steel and Domex 355 are 1196 µm/m and 1698 µm/m respectively. This highlights the issue regarding dimensioning based on dynamic impacts as strain calculated are unrealistic when using static formulas. Reason being that the force on impact is assumed constant in the previous calculations. This force is quickly reduced as the mass is decelerated. This relationship can be illustrated by equation $F(t) = F_d(t) + F_s$ and displayed in *Figure 23* (Dimitrios.G.Pavlou, 2018), highlights the total load "$F(t)$" into dynamic "$F_d(t)$" and static load "F_s".

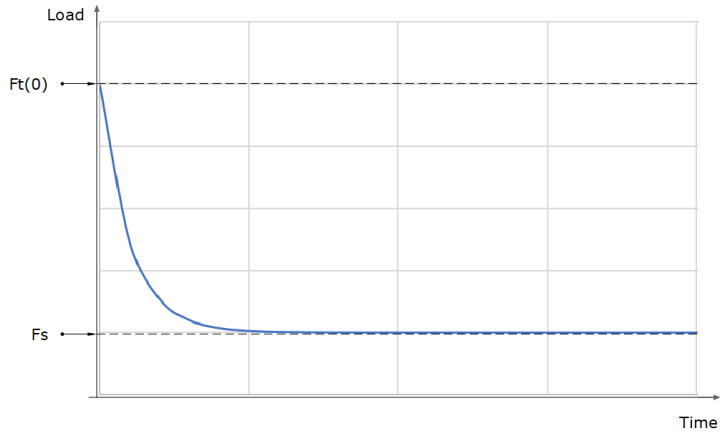

Figure 23: Dynamic load behavior during impact loading with mass resting on center after collision.

Lastly, even with an accurate representation for the load behavior, it is not possible to use static formulas to approximate dynamic behavior of the steel plate. This is because the lack of a dynamic component in these equations, that does not take into consideration the time it takes to reach a certain deflection when subjected to a given load. Overall, the complexity with regards to dynamic is what prevents a straightforward approach with regards to estimating plate using an analytical approach.

The selection of the plate dimensions was decided to be 40 cm for plate with a support ring with ID of 36 cm. Mass of the plate being 2.955 kg and support rim weighing in at 1.550 kg, displayed in *Figure 24.*

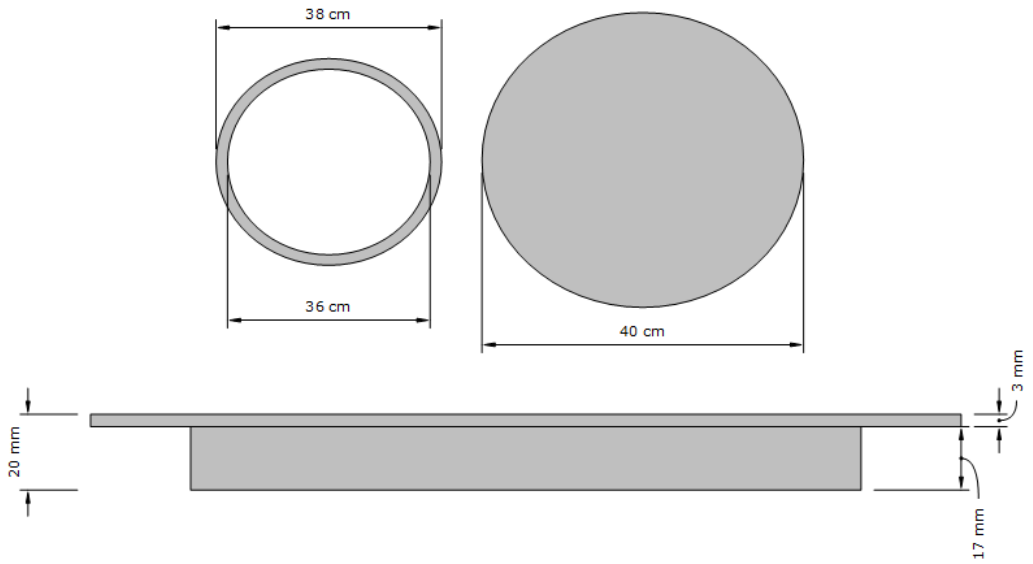

Figure 24: Final dimensions and parameters for plate and support ring.

3.3.1 Perforation Optimization & Selection

One of the major goal of this paper is to determine cushioning effect of having perforated plates, when subjected to impact loads. Therefore, designing the layout of the perforated surface is of great importance, with parameters such as hole diameters and their respective horizontal "x" and vertical separation "y" from each other. *Figure 25* serves to demonstrate the density of perforation per square unit area, to get overview of the number of perforations as well as the percentage of empty area for the given grid. Selection of perforated area was also greatly influenced by the number of holes required in total, as exceedingly large quantities of perforation would require and exorbitant amount of time to produce by hand. The combination of hole sizes and "x1 & x2" and "y1 & y2" separations could also be used to yield a large variety of perforated surfaces.

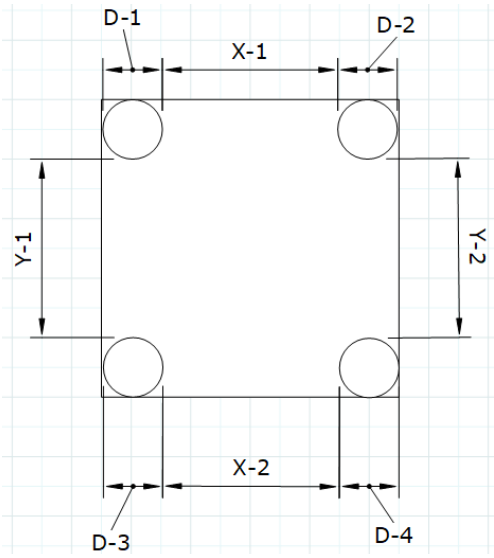

Figure 25: Diagram highlighting the perforated grid area.

Using the limitation imposed on the design, a perforation grid was selected. The selected perforations used for the perforated plates as shown in *Figure 26*, was a grid with 4x4 cm ($6cm^2$) with 5mm perforated holes in the corners resulting in a symmetrical biaxial grid. Percentage of empty area of 4.9% for each small grid. However, the plate itself consisting of a total of 97 perforations (0.5 cm diameter), making the total empty area 1.5%. Since the thickness of the perforated plate is the same as the solid plate this means that weight is also 1.5% less. As a result, the perforated plate has a weight 2911 kg, being 44.325 g lighter than the solid plate.

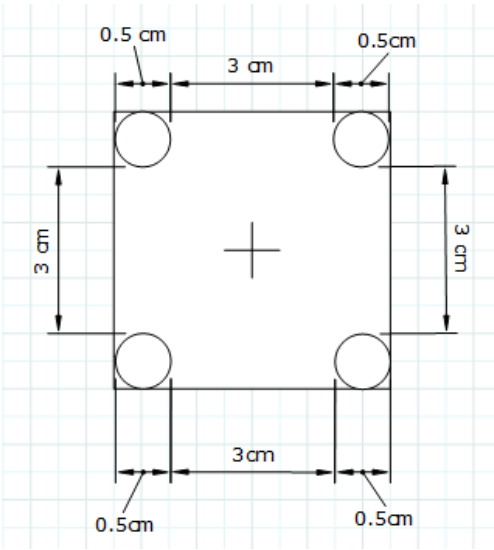

Figure 26: Final perforation design.

The design for the protection are yet to be finalized but the most current design is as shown in *Figure 27*. Perforations on the top section of the cover are 100mm in diameter and the thickness of the cover is 30-40 mm thick. Perforated top section as shown has a very large percentage of empty area, relative to 1.5% used in experiments in this paper. It is therefore clear that the perforated area top section of the CAP-X covers is considerably more perforated than the plates used for the experiment. The hypothesis is that the selection of perforation pattern is something that has a very profound effect on the cushioning/damping effect associated with impact loading, as this will be shown and discussed in later chapters.

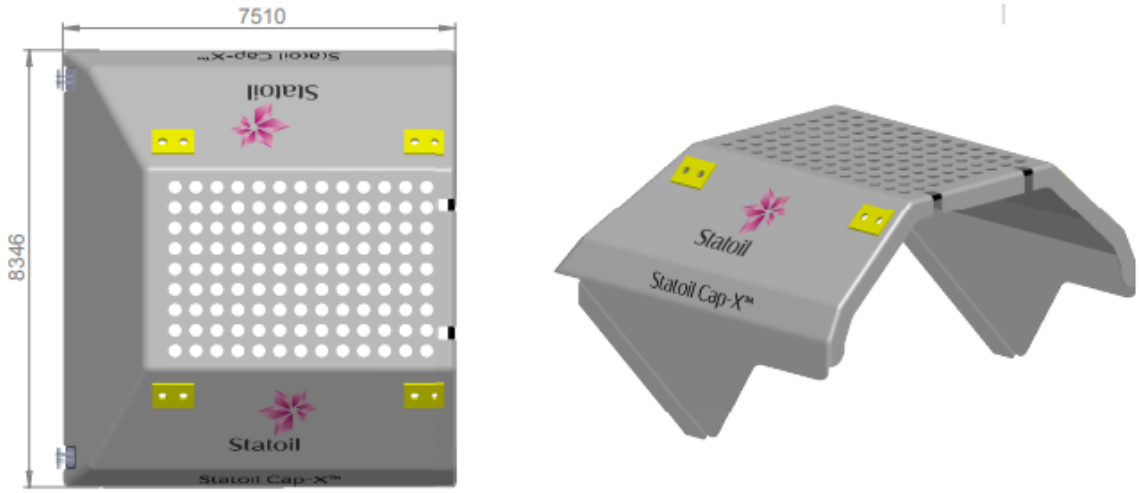

Figure 27: Design of GRP protection cover for CAP-X technology (Anon., 14.12.2016)

3.4 Force of Impact & Energy Balance

When conducting the measurements with both proctor and ball drop method, a observation were made with regards to the amount of bounce that occurred, especially true for measurements done in air. The Impact energy, being the amount of kinetic energy the mass (dropped object) has before impact, that it has gained from gravitational potential energy. Impact energy will be used to determine the behavior of the impact loading measurements conducted in air and water, to determine differences between them. This section will lay the foundation for how the impacts are evaluated and the corresponding assumptions.

First, by looking at an object that impacts a surface when dropped from a certain height. If the ball bounces back to the same specific height, then this would mean that all the energy was transferred to the plate and then back to the ball, with no loss in the exchange.

Energy balance can be written as follows, with energy of the mass "E_m" and plate "E_p" and the loss of energy "E_L"

$$E_m = mgh = E_P + E_L \qquad \textit{Equation 8}$$

$$E_m = mgh = \frac{1}{2}mv^2 \qquad \textit{Equation 9}$$

The *equations 8 & 9* indicates the amount of energy transferred between each bounce, and due to the nature of the experiments conducted this amount will vary slightly from each measurement. The major assumption made is that energy loss is negligible, and energy is only transferred between the plate and the mass. Loss of energy being the amount of energy that is lost to friction, sound, frame etc that is not pertaining to the plate and mass. For the tests conducted on submerged plates the case is different as the mass is subjected to a large amount of drag when entering & traveling through water. In this scenario, the option to estimate the estimate velocity using slow motion footage, or by mechanics formulas. The reason why the velocity was determined by calculations, rather than slow motion footage, will be explained further in *chapter 7*.

The second reason why measurement bounce height is important is that it indicates the amount of force that the plate is subjected to. This is due to the rate of range of momentum that the mass is undergoing, explained by Newton's 2nd law of motion. The height of bounce is therefore directly correlated to the amount of load applied to the plate and should hopefully be observable in the results. Impact force due to momentum change is illustrated in *Figure 28.*

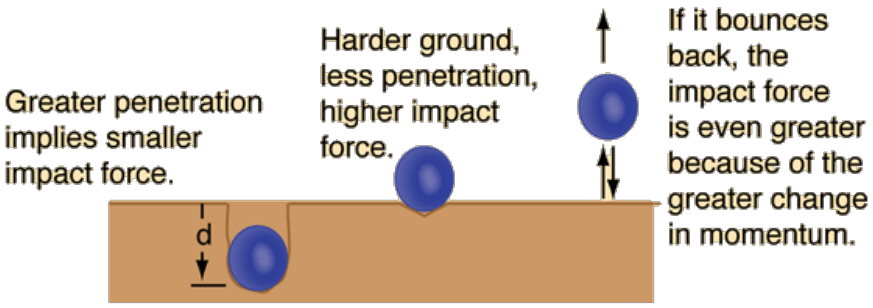

Figure 28: Force of impact due to different changes in momentum (Anon., 2009).

Determining the velocity using classical mechanics, combined with fluid mechanics, it is possible to approximate impact energy before impact. This is important, because otherwise determining the different impact load responses with regards to air and water would be futile. Velocity is determined based on simple force balance for a sphere, and cylinder (proctor). Where this velocity can then be used to determine the impact energy of the object

Force balance equations used to describe the velocity can be written first as:

$$F_{net} = F_{gravity} - F_{Bouyancy} - F_{Drag} \qquad \textit{Equation 9}$$

Then by adding the individual force functions for gravity, buoyancy and drag results in:

$$F_{net} = mg - \rho_f g V_d - \frac{1}{2}\rho_f A C_d {v_n}^2 \qquad \textit{Equation 10}$$

The assumptions being that force of gravity, fluid density and Drag coefficient "C_d"are all constant during the calculation. Method of calculations is based on iteration process for which is based around number of steps to complete, where steps define the distance the object has travelled through the fluid in question (e.g. air or water). For each step the net force calculated is used to estimate the change in velocity using *equation 12.*

$${v_{n+1}}^2 - {v_n}^2 = 2ad_n \qquad \textit{Equation 11}$$

$$v_{n+1} = \sqrt{{v_n}^2 + 2ad_n} \qquad \textit{Equation 12}$$

When the velocity of the object at distance "d" is calculated, it can be used to calculate the impact energy to equivalate the impact loading response. This is done in order to make fair comparison between air and water tests.

$$Impact\ Energy = \frac{1}{2}mv^2 \qquad \textit{Equation 13}$$

Equations 9,10,12 and *13* can then be implemented into any software such as Excel, Matlab, Mathematica etc. Software used in this paper for this type of iteration was Excel, as equations are neither complex nor numerous.

The distance of each step was selected to be in the order of magnitude of 0.1 cm for the measurements, which meant that velocity calculations was done 300 times for a distance of 30 cm However, it is important to note that for small velocities, the number of iterations selected causes insignificant variation in impact energy calculated.

The only limitation with this method is that drag coefficient is approximated. This meant that calculations approach affects the calculated values accuracy. For example, if the impact energy is smaller than, which can be achieved by selecting larger than expected drag coefficient to be used, or other conservative measures. In detail explanation of calculation approximation is shown in the discussion chapter.

Drag coefficients used for these equations are based on turbulent region collected from general fluid dynamics book (Çengel, 2006).

3.5 Review of Plate Theory - Analytical Solutions

Analytical solutions have always given the most accurate answers when compared to any numerical solution and should be applied for any situation if possible. The complexity involved in the dynamics of a simply supported plate, meant that the initial plan to rely heavily on analytical solutions was not viable, as no analytical solutions for a simply supported perforated plates exist. The analytical solutions that could be found was only applicable the solid steel plate. For the impact test on a freely supported plate, the two modeling scenarios that occurs is the plate remaining on its supports, and the plate being lifted of its supports freely vibrating in the air, as shown in *Figure 29*.

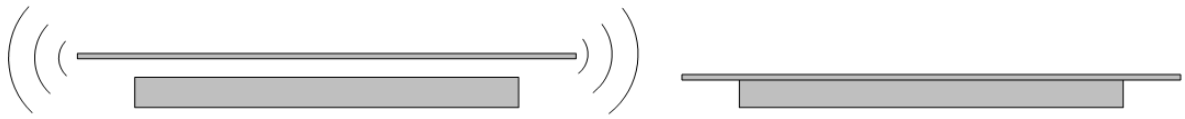

Figure 29: Two possible scenarios occurring during impact loading tests for a simply supported plate.

The reason why no analytical solution is displayed in this paper is because only one real solution was discovered for circular solid steel plates. This solution was also only valid for modal solutions and is highlighted in Kar F. Graff's book titled "Wave motion in elastic solids". There are also references to Dohrenwend et al 1945 (DohrenWend, 1944)who did studies on impact behavior by striking steel beams with a sledgehammer and calculating approximate results.

3.6 Measuring Equipment

As described previously in the thesis, to be able to detect the amount of stretch along the material being tested, strain gauges are mounted on the test specimen. In this sub-chapter the theory behind the strain gauge are being described.

3.6.1 Strain Gauge

Strain is defined as the ratio of the change in length to the initial unstressed reference length. A strain gauge is an element that senses this change and converts strain into an electrical signal (OMEGA, u.d.).

Since 1940, the bonded resistance strain gauge has been the most powerful single tool in the field of experimental stress analysis (R.L Hannah, 1992). During the existence of the strain gauge, a large variety of designs has been introduced, to suit the various demands that arise due to different material types, type of strain being measured, environmental conditions and desired strain sensitivity (Hoffmann, 1973-1978).

The configuration of the strain gauges is commonly divided in three types; *quarter-*, *half-* and *full-bridge. The configuration type* is determined by the number of active elements in the Wheatstone bridge (National Instruments, 2016). The Wheatstone bridge will be further elaborated on in the next section.

3.6.2 The Wheatstone Theory

The theory describing the bridge circuit for the measurement of electrical resistances, is known as *the Wheatstone theory,* carried out by the English physicist Sir Charles Wheatstone (Hoffmann, 1973-1978). The main purpose of the theory is to compare unknown resistance with well-defined resistance (Wheatstone, 1843).

The Wheatstone bridge is configured by combining four resistors, as shown in *Figure 30* below. Initially $R1 = R2 = R3 = R4$, leading to zero output.

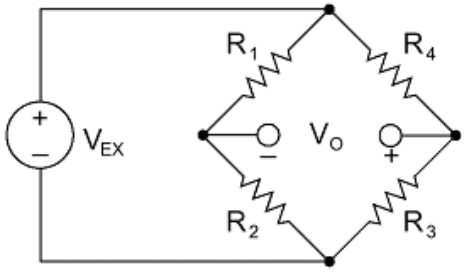

Figure 30: Wheatstone Bridge.

In the experiment being described in this thesis, one resistor is replaced with a strain gauge attached to the test object. This strain gauge will then act as an active quarter-bridge, while the remaining three resistors are fixed resistors incorporated in the SCM-SG120 adapter, which work as passive elements. This configuration is illustrated in the electrical circuit in *Figure 31* below.

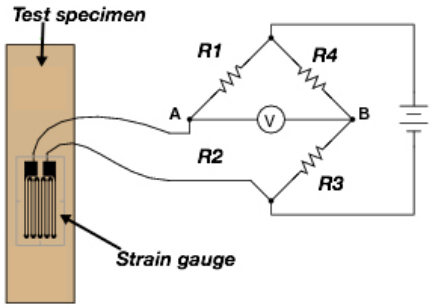

Figure 31: Active quarter-bridge (left) together with internal, passive completion network (right).

When a force is applied to the test object, the specimen will either be stretched or compressed, if the impact is large enough. The geometrical alternation leads to a change in the resistance of the gauge, which again leads to an electrical output signal. The relationship between the relative change of the resistance and the strain experienced by the strain gauge is described by *Equation 14* (Hoffmann, 1973-1978):

$$\frac{\Delta R}{R_o} = k * \varepsilon \qquad \textit{Equation 14}$$

Referring to *Equation 14*, the factor k is known as the gauge factor, ε is the strain and $\frac{\Delta R}{R_o}$ is the relative change in resistance. In accordance with the manufacturer´s recommendation for this type of strain gauge, a gauge factor of 2 was chosen.

4 Solidworks Simulation

Solidworks is a 3D-CAD-software, which means it is a '*Computer Aided Design*' tool. The software was founded in 1993, first released in 1995 (Bethany, 2017), and have grown and gained a lot of functionalities throughout its 23 years as a modeling software for users worldwide. In addition to 3D-modeling capabilities and enhancements, it has evolved into also being a Computer aided engineering tool (CAE). This means that it can also perform structural analysis of the modeled 3D-parts, by inding failure and weak points of the specific parts of interest (Bethany, 2017).

To provide a framework of what to expect when conducting the experimental tests, Solidwork Simulation is used to model and simulate the steel plates. This also gives a point of reference with respect to later analyses of the results. The simulations are performed to analyze the stress and strain distribution together with the deflection in theory, of both solid and perforated plates. Additionally, a Cap-X GRP cover under impact load has been modelled and simulated.

4.1 Theory

In this chapter the theory related material and simulations utilized in this paper is elaborated upon.

4.1.1 Mechanics of Materials

The theory of mechanics of materials, also known as the strength of materials, is concerned with the behavior of solid objects subjected to forces. When a load is applied to a material, it will induce an internal force called stress. Furthermore, the stress causes a deformation of the material, called strain (Hibbeler, 2010).

The study of stress and strains developed in a material, when applied to a load, gives insights about the load capacity of that component. This can be simulated in Solidworks. The user implements inputs such as geometry of the member, its constraints, together with the dynamic load applied to the test object. The Solidworks software then simulates various outputs, such as the state of both stress and strain at any point, in addition to the deflection within the material.

The simulated values may then be compared to the given material properties of the test object, such as its material *yield strength* and *ultimate strength*. These properties refer to different points on the engineering stress-strain curve, illustrated in *Figure 32*.

The material yield strength refers to the point at the curve where the material goes from elastic deformation (i.e. deformations that will not be permanent upon removal of the load) to plastic deformation (i.e. deformations that will result in permanent deformation upon removal of the load). The ultimate strength of the material refers to the maximum stress attained in the stress-strain diagram. If the material is loaded beyond its yield strength, both stress and strain within the material increases until the specimen goes into failure (Agonafir, 2015). In addition, the *deflection* describes the magnitude to which the test object is displaced, when subjected to an applied load.

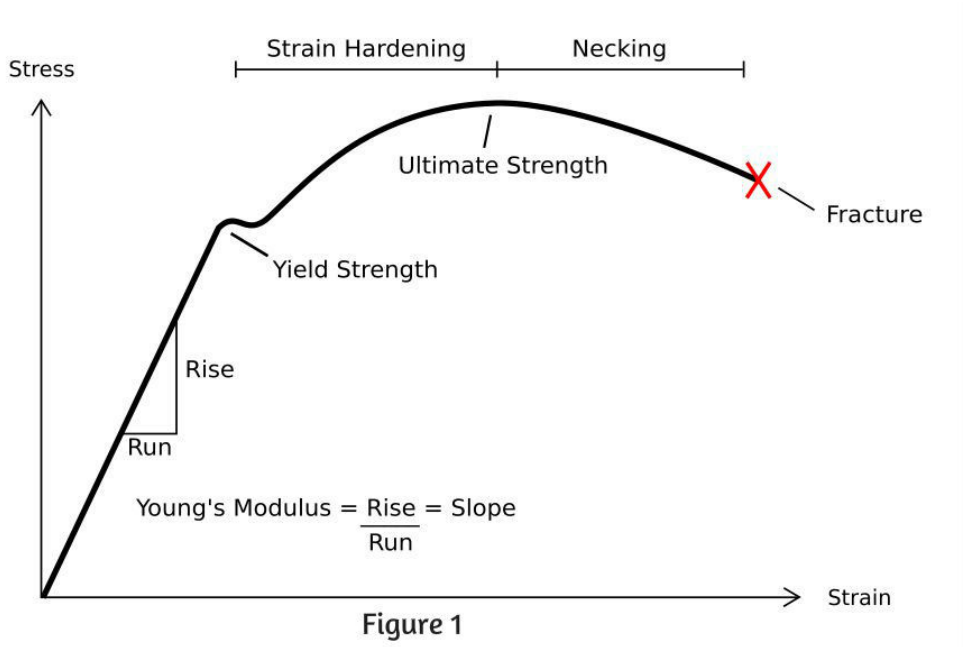

Figure 32: Stress-Strain diagram (Figari, 2015).

As mentioned previously in the paper, the tests performed in this thesis is within the elastic range of the material, due to unwanted plastic deformation.

4.1.2 Von-Mises Failure Criterion

Von Mises stress is a value used to determine if a material will yield, i.e. go into plastic deformation. It is mostly used for ductile materials, such as metals. The von Mises yield criterion has been used as one of the most reliable failure criteria for engineering materials for decades (Gambhir, 2009). The theorem states that if the Von Mises stress of a specific material, experienced when subjected to a load, is less than the yield strength of the same material, the material is safe and will not go into plastic deformation (SimScale, u.d.). Consequently, if the von Mises stress is less than the yield stress of the material, the material will not undergo a plastic deformation.

The von Mises stress is based on the combination of the three principal stresses; axial stress, radial stress, and hoop stress, in addition to the shear stress caused by torque (Agonafir, 2015). If there is no torque applied to the object, the shear stress term "τ" is not included equation. The von Mises stress is given by:

$$\sigma_{VM} = \sqrt{\frac{1}{2}((\sigma_\theta - \sigma_r)^2 + (\sigma_r - \sigma_a)^2 + (\sigma_a - \sigma_\theta)^2) + 3\tau^2} \qquad \textit{Equation 15}$$

Solidworks determines the von Mises stress, based on the equation above, for the implemented material properties and loading scenario. Subsequently, this value can be compared to the yield strength of the material to determine whether the material will undergo plastic deformation or stay in the elastic region. This comparison is very important regards to the fact that plastic deformation of the test objects used in the experiments of this thesis are unwanted.

4.1.3 FEA – Finite Element Analysis

Solidworks is based on the Finite Element Analysis (FEA). FEA is a term describing virtual method of solving engineering problems like stress-distribution, structural or performance issues within a loaded material (SIEMENS, u.d.). The Finite Element approach is a numerical technique within the mathematics used to model and solve problems, ranging from very easy to very complex, described by a set of partial differential equations. The term *finite* is used to emphasize the fact that the elements are not infinitely small, but relatively small in comparison to the overall size of the model (Kurowski, 2015).

The FEA-based analysis tool simulates by solving huge matrices, representing different points. Those points are called nodes, which again forms the shape of the chosen design (Cârstea, u.d.). The finite elements are connected to these nodes and forms the mesh of the element, in addition to containing material- and structural properties of the model (SIEMENS, u.d.).

4.1.4 Elements and Mesh

As mentioned above, the finite elements are connected to the nodes and forms the mesh of the structure. In other words, the mesh is a buildup of the elements. Both the order of elements and the density of the mesh may vary. Regions that experience high changes in stress usually requires a higher mesh density compared to the once experiencing little or no stress variation (SIEMENS, u.d.). The number of elements that can be implemented by the operator depends on the wanted fineness of the mesh, the size of the model and the required accuracy of the results. The creation of the finite elements within Solidworks, is commonly called meshing (Kurowski, 2015).

When it comes to the order for the elements, second order tetrahedral has been used for the simulations being described in the thesis. This type of element can either be presented as first order "draft quality", or second order "high-quality" (Kurowski, 2015). The high-quality element was chosen for these simulations.

Tetrahedral second order elements consist of 10 nodes; one node in each corner in addition to mid-side nodes, this is illustrated in *Figure 33*. This element has 3 degrees of freedom (DOF) for each node, which means that one element has 30 DOF in total (Kurowski, 2015). According to (Kurowski, 2015), the degrees of freedom is described as follows; "The degrees of freedom (DOF) of a node in a finite element mesh define the ability of the node to perform translation and rotation", where each DOF constitutes as an unknown (Kurowski, 2015).

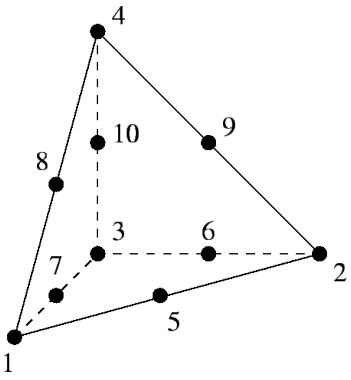

Figure 33: Tetrahedral Second Order Elements (MIT, 2014).

4.1.5 Split-line Feature

Split-line features can be added, to define specific areas of interest on the 3D model. In some occasions the split-line is used to specify an area where we want to increase the resolution of the results. A reasonable use of split-lines can for instance be around holes, bends or thigh corners, where we know that the stress gradient increase.

These lines do not add any structural properties to the 3D-model.

4.2 Simulation of the Steel Plates

To create a simulation that is comparable to the practical test scenario, two plates with the same material- and structural properties as well as geometry, are used as experimental plates.

Firstly, the material properties, loads and restraints are defined. Secondly, the mathematical model is split into relatively small and simply shaped finite elements, using discretization, commonly referred to as meshing. Geometry, loads and restraints are all discretized and applied to the nodes of the finite element mesh (Kurowski, 2015). Finally, the FEA model is solved using a numerical solver within Solidworks Simulation, and color contour figures are obtained. The procedure described is illustrated in *Figure 34*.

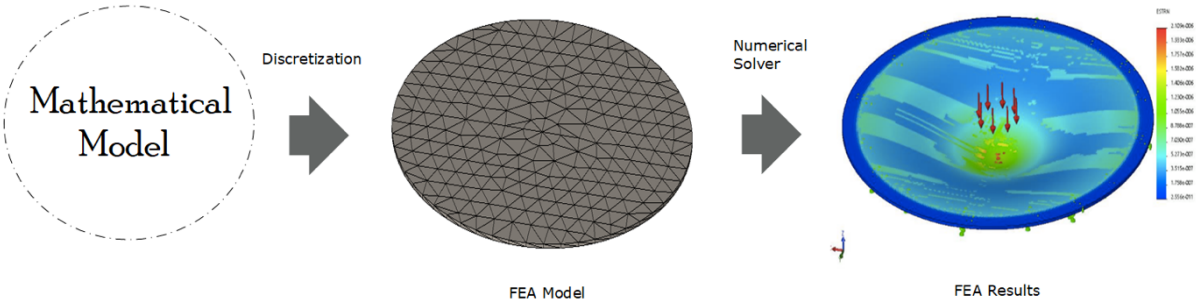

Figure 34: Solidworks procedure of building the finite element model.

4.2.1 Material

The experimental plates, both solid and perforated, are made from hot rolled steel. To obtain accurate simulation results, hot rolled steel was chosen as the material used in Solidworks as well. The material is selected from a default material library in Solidworks. Furthermore, a set of parameters given by the producer of the physical steel plates are being manually implemented.

Table 2 shows the material properties for hot rolled steel, provided by the supplier. *Table 3* represents the parameters used in the simulation. The parameters marked with green in *Table 2*, were implemented from the supplier into the material settings in Solidworks, *Table 3*. While the parameters marked in red in *Table 3*, were not provided from the producer. Consequently, they were left with the default parameters from the hot rolled material in Solidworks, as shown in *Table 3*. The parameters which not marked in *Table 2*, are not used in the simulations.

Table 2: Material properties from supplier.

	Abbreviation	***Value***	***Unit***
Modulus of elasticity	E	208 000	MPa
Poisson's ratio	υ	0.285±0.005	1
Shear modulus	G, μ	83±2	GPa
Density	ρ	7850±20	Kg/m^3
Linear expansion coefficient	α	$12 \cdot 10^{-6}$	1/K
Thermal Conductivity	λ	45±2	W/Km
Specific heat	C_p	470±20	J/kgK
Thermal diffusivity		$= \lambda / (\rho * C_p)$ $=1.22\ 10^{-5}$	m^2/s
Resistivity		0.2 - 0.3	µΩm
Tensile Strength		500	$\frac{N}{mm^2}$
Yield Strength		355	$\frac{N}{mm^2}$

	Value	*Unit*
Modulus of elasticity	2080000	$\frac{N}{mm^2}$
Poisson's Ratio	0.285	N/A
Shear Modulus	83000	$\frac{N}{mm^2}$
Mass Density	7850	$\frac{kg}{m^3}$
Tensile Strength	325	$\frac{N}{mm^2}$
Compressive Strength	-	$\frac{N}{mm^2}$
Yield Strength	205	$\frac{N}{mm^2}$
Thermal Expansion Coefficient	1.22e005	/K
Thermal Conductivity	45	$\frac{W}{m * K}$
Specific Heat	470	$\frac{J}{kg * K}$
Material Damping Ratio	-	N/A

Table 3: Material Properties Solidworks.

4.2.2 The Proctor

To keep the simulation time at a reasonable level, the proctor was simplified. However, all important parameters, such as contact area and weight of the proctor is implemented identical to the proctor used in the experiments. The area is set to $5.0\ cm$ and the weight $4.8\ kg$. The simplified proctor is shown in *Figure 35*.

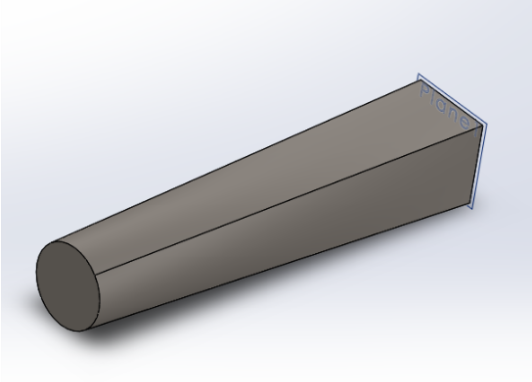

Figure 35: Simplified Proctor.

In *Figure 36*, two green arrows are shown on top of the proctor. These arrows indicate that the proctor is locked in x and y direction, just able to move downwards in z-direction.

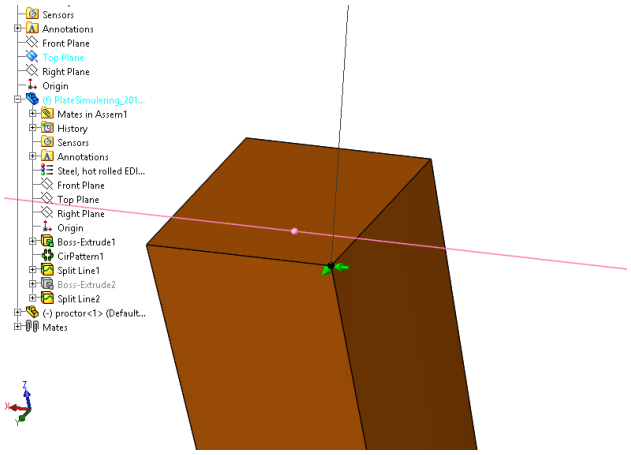

Figure 36: Green arrows locking proctor in x and y direction.

4.2.3 The Dynamic Load

The proctor is initially at rest, lifted 15 cm and 30 cm above the plates. While at rest, the proctor has no kinetic energy, however it has potential energy mgh. When the mass is released from a specific height, the potential energy is converted into kinetic energy (Paul A. Tipler, 2008). By the origin in conservation of energy, and assuming no friction, the relation between potential and kinetic energy for the proctor is shown in equation 16 below:

$$\frac{1}{2}mv^2 = mgh \qquad \textit{Equation 16}$$

Where m is the mass, v is the velocity, g is the gravitational constant and h is the height above the plate.

Equation 17 express the velocity of the proctor:

$$v = \sqrt{2gh} = \sqrt{2 * 9{,}81 * h} \qquad \textit{Equation 17}$$

By using *equation 17*, the velocity for the two different heights is found to be:

$$\text{For } h = 15cm, v = 1{,}71\frac{m}{s}$$

$$\text{For } h = 30cm, v = 2{,}42\frac{m}{s}$$

These velocities are implemented as inputs for the dynamic load, for both perforated and solid steel plate.

4.2.4 Constraints

In the experiments performed in the laboratory, a metal ring is used for the plates to rest on. In Solidworks, a small piece of the ring is defined as a fixed geometry with split-lines, to implement that the ring is a part of the simulation. A fixed geometry means no rotation nor translation for this area. The rest of the ring will be freely supported, as for the experiment scenario in the laboratory. The constraints are illustrated in *Figure 37* below.

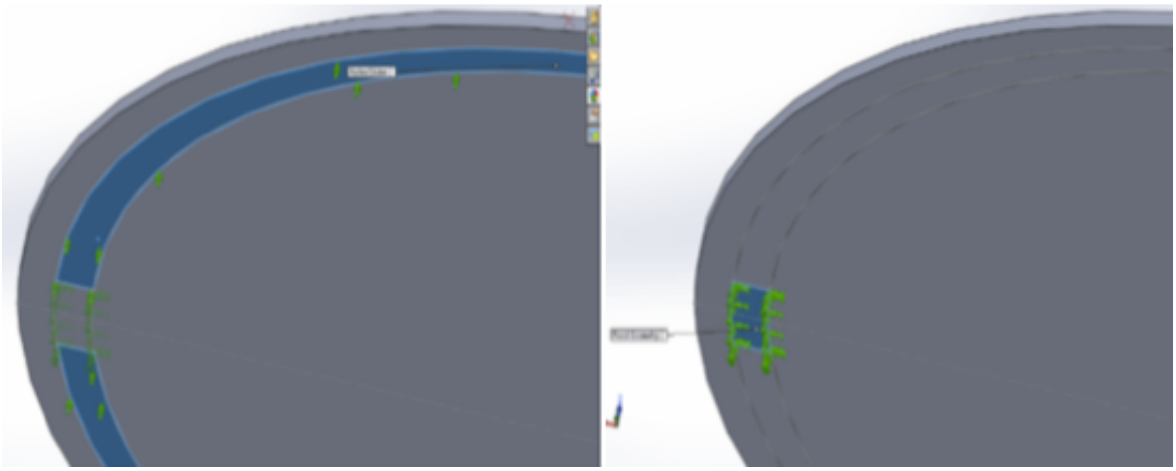

Figure 37: Fixed Geometry feature.

Another restriction is to implement "*no penetration*" of the impact load. This is done to ensure that the proctor collides with the plate, i.e. no penetration through the test object. This restriction is illustrated in *Figure 38* below.

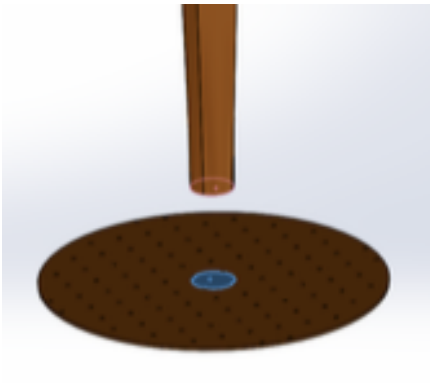

Figure 38: No penetration feature.

It should be noted that the restrictions presented applies to both solid and perforated plate for the simulations performed.

4.2.5 Meshing

The mesh is set to 12 mm for the solid plate and 9 mm for the perforated plate. Since the geometry is relatively simple and the load comparatively small, the chosen meshes are likely to provide sufficient results. We have chosen different mesh for the solid and the perforated plate, since there will be stress concentrations around the holes. This in turn, requires a finer mesh to be detected. Although the mesh itself only differs with 3 mm, the number of elements for 12 mm mesh (the solid plate) is exceeding 7690 elements, while the number of elements for 9 mm mesh (the perforated plate) is exceeding 26840 elements. This constitutes a difference of approximately 19 000 elements. Meshes for the solid and the perforated steel plate are illustrated in *Figure 39* and *Figure 40* respectively.

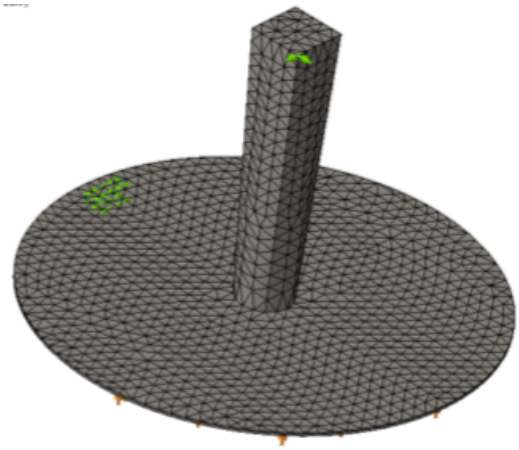

Figure 39: 12mm mesh solid steel plate.

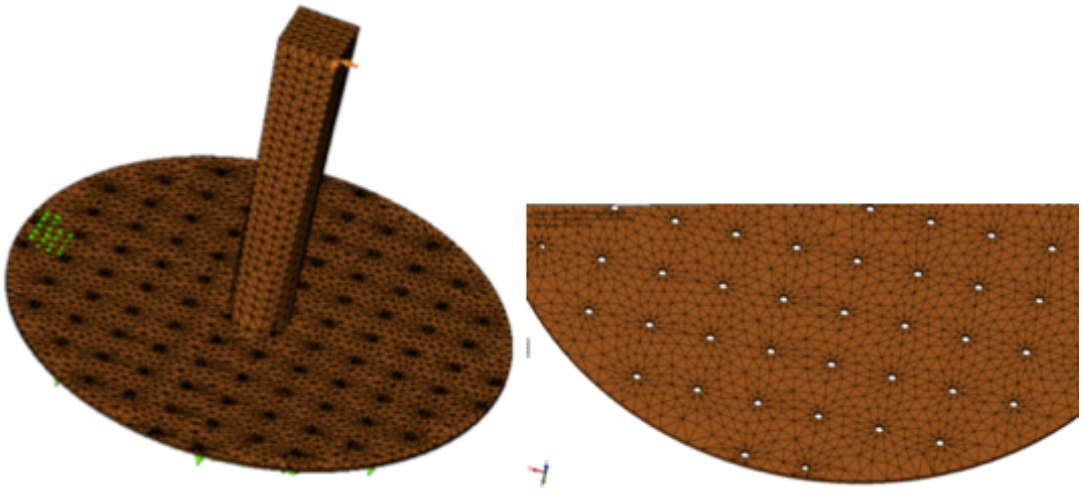

Figure 40: 9mm mesh perforated steel plate.

Even though the plate models used in the simulations described are geometrical simple, the number of elements for 12 mm mesh (solid plate) is exceeding 7690 elements, and the number of elements for 9mm mesh (perforated plate) is exceeding 26842 elements.

4.2.6 Time Settings

The initial time, $t = 0$, is set to the exact moment when the proctor hits the plate.

4.3 Solid Steel Plate - Simulation Results

In this chapter, the results from the simulations on the solid steel plate will be presented, categorized into 15 cm drop and 30 cm drop. This chapter is focused on each individual result with respect to values and behavioral patterns. The simulation results, on the other hand, will be discussed and compared to the conducted test experiment values in *chapter 7.4 Solidworks and Measurements Comparison*.

4.3.1 15 cm Drop Height – 1.71 m/s

In this subchapter, the results from the 15 cm drop height, i.e. 1.71 m/s, for the solid steel plate will be described.

4.3.1.1 Stress Distribution

Figure 41 shows the Von Mises stress distribution, obtained by the FEA of the solid steel plate. The analysis shows that the Von Mises stress is at its maximum in the middle of the plate, where the impact force hits the test object. The value is approximately 180 MPa at this point. Thus, it is less than the yield stress value of 355 MPa of the material, meaning that the solid plate will not go into plastic deformation for this specific load scenario.

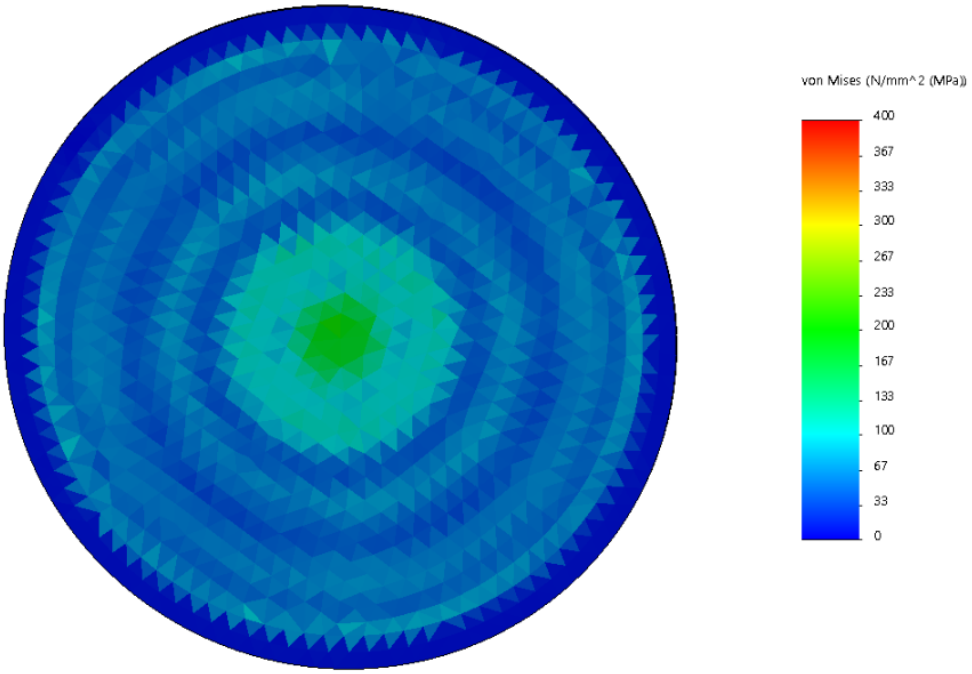

Figure 41: Von Mises Stress distribution (top view) for solid steel plate under 15 cm drop height scenario.

Figure 42 illustrates the Von Mises stress variation diagram which shows a maximum stress of 180 MPa, which is 50.7% of the static yield strength. The illustration also shows relatively large variation between max and min for each oscillation with the largest variation being 160 MPa.

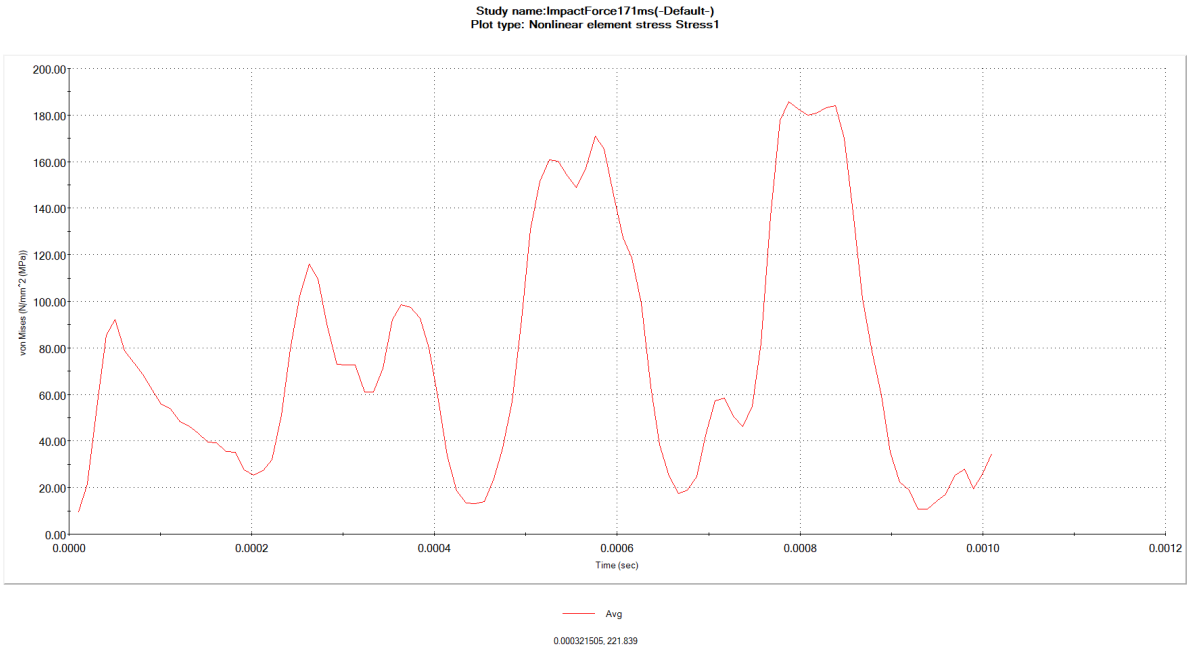

Figure 42: Von misses stress diagram vs time for solid steel plate under 15 cm drop height scenario.

4.3.1.2 Deflection

The deflection is shown to be approximately 2 mm at the maximum. This is quite a large value of deflection, having a steel plate thickness of 3 mm. Furthermore, the results show an axisymmetric pattern, with the deflection decreasing quite rapidly from the center of impact.

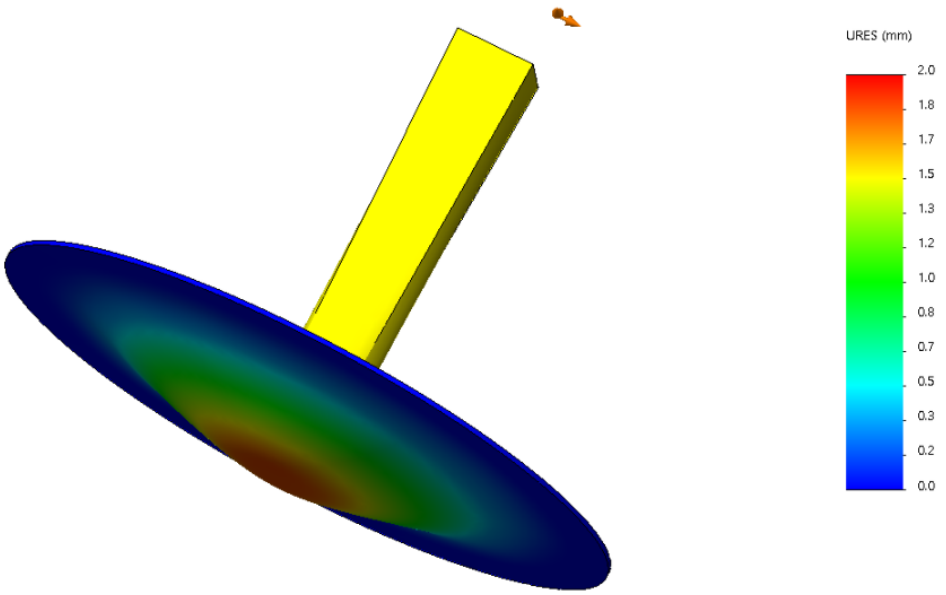

Figure 43: Illustration of Solidworks deflection values from a 4.8 kg mass released from a 15 cm drop height on a solid plate.

4.3.1.3 Strain Distribution

For the strain distribution some degree of strain can be seen to be concentrated around the supports of the plate.

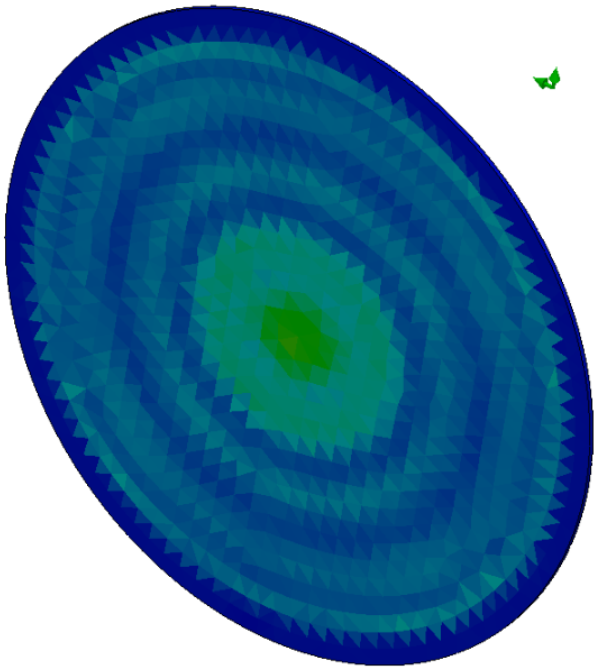

Figure 44: Strain distribution for solid steel plate under 15 cm drop height scenario.

The strain distribution shows a series of maxima and minima when moving away from the center. The same tendency was observed for the stress distribution described in section 1.2.1.1. This tendency is sometimes described as a ripple pattern.

4.3.2 30 cm Drop Height – 2.42 m/s

In this subchapter, the results from the 30 cm drop height, i.e. 2.42 m/s, for the solid steel, plate will be described.

4.3.2.1 Stress Distribution

Figure 45 shows the Von Mises stress distribution, obtained by the FEA of the solid steel plate, for the 30 cm drop height. The analysis shows the same results as for the 15 cm drop height, i.e. the Von Mises stress is at its maximum in the middle of the plate, where the impact force hits the test object. The value for the 30 cm drop height is approximately 270 MPa at this point. Thus, it is less than the yield stress value of 355 MPa of the material, meaning that the solid plate will not go into plastic deformation for this specific load scenario.

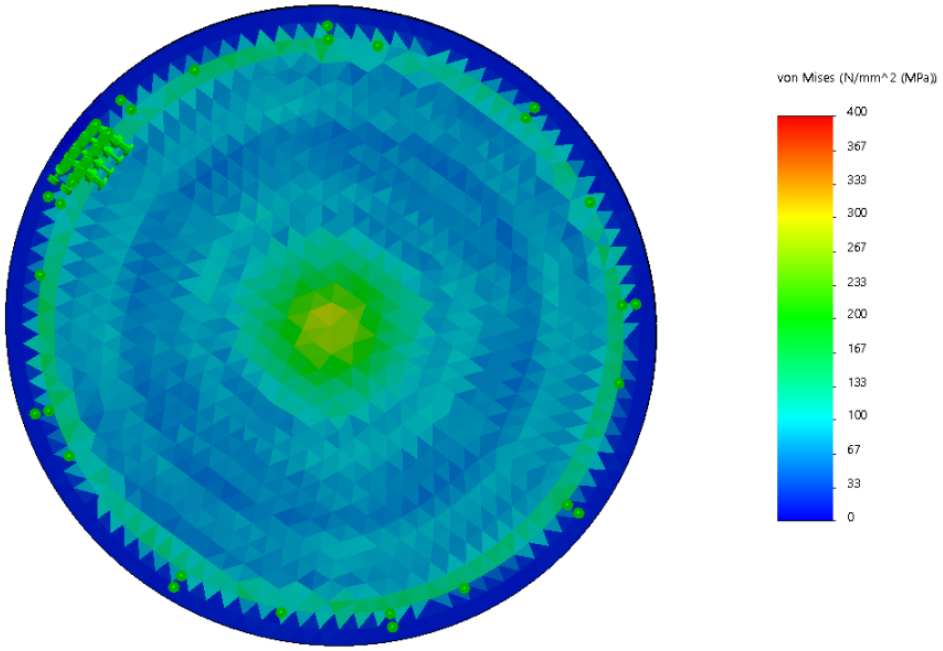

Figure 45: Von Mises stress distribution (top view) for solid steel plate under 30 cm drop height scenario.

The stress distribution shows a relatively large maxima and minima around the center. In addition, considerable stress can be seen around the support rim of the plate. It shows values of 233 MPa, which is approximately 86% of the maximum strain seen at the center of the plate (270 MPa). The stress concentrated around the rim of the plate is also larger than the maxima value of 133 MPa seen around the center.

Figure 46 shows the stress over time curve after impact. This shows that very large loading rate, with stress variation of 240 MPa at the most.

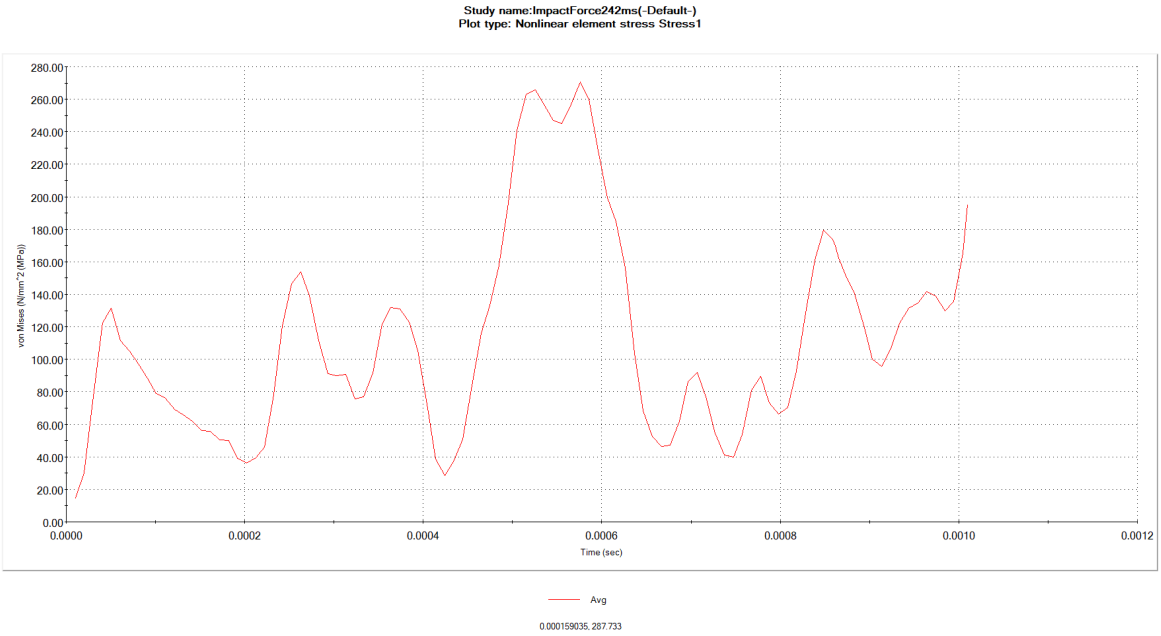

Figure 46 Von misses stress diagram vs time for solid steel plate under 30 cm drop height scenario.

4.3.2.2 Deflection

For increased impact energy, and drop height increased to 30 cm for the 4.8 kg mass, a larger area of high deflection is shown, with the maximum deflection estimated at 2 mm. Additionally, the simulation shows no deflection close to the support ring, noted by the circle green arrows in *Figure 47.*

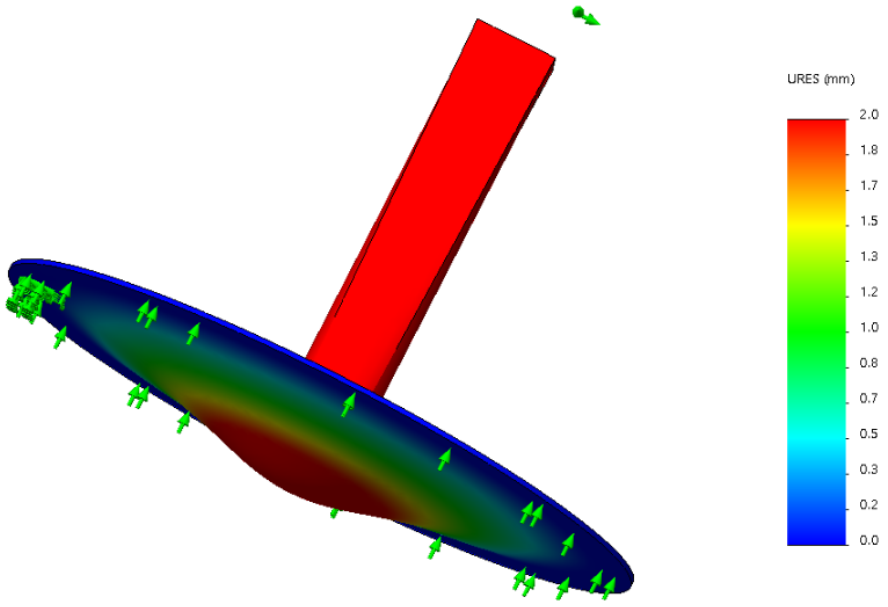

Figure 47: Illustration of SolidWorks deflection values from a 4.8 kg mass released from 30 cm drop height.

4.3.2.3 Strain Distribution

Similarly, as shown for stress distribution, the strain distribution is much less defined with respect to the visible maxima and minima around the center of impact.

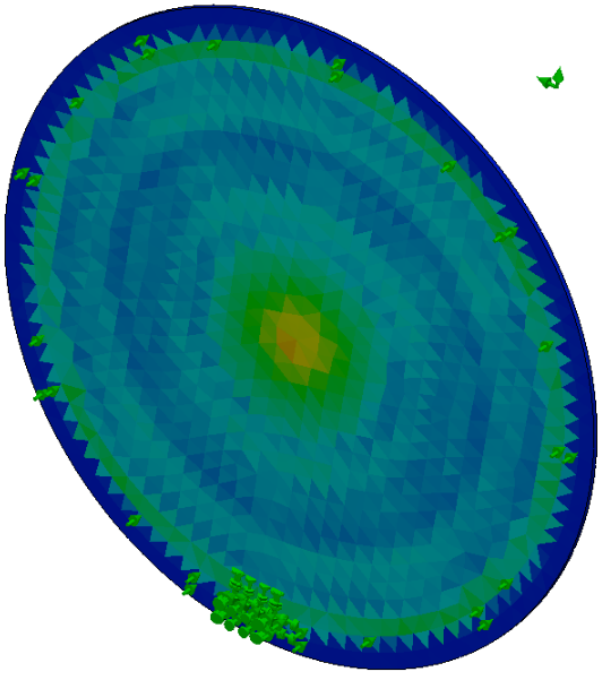

Figure 48: Strain distribution for solid steel plate under 30 cm drop height scenario.

4.4 Perforated Steel Plate - Simulation Results

In this chapter, the results from the simulations on the perforated steel plate will be presented, divided into a 15 cm drop and a 30 cm drop. The results will not be discussed in relation to each other in this chapter, the focus will be on each individual result, with respect to values and behavioral patterns. The simulation results will be discussed and compared to the conducted test experiment values later in *chapter 7.4 Solidworks and measurements comparison*.

4.4.1 15 cm Drop Height – 1.71 m/s

First, the results from the 15 cm drop height, 1.71 m/s, for the perforated steel plate will be presented in this subchapter.

4.4.1.1 Stress Distribution

The analysis of the 5 cm drop height, 1.71 m/s, for the perforated steel plate, shows that the Von Mises stress is at its maximum in the middle of the plate, where the impact force hits the test object. This is shown in *Figure 49*. The value is approximately 220 MPs at this point. Thus, it is less than the yield stress value of 355 MPa of the material, meaning that the solid plate will not go into plastic deformation, for the specific load scenario.

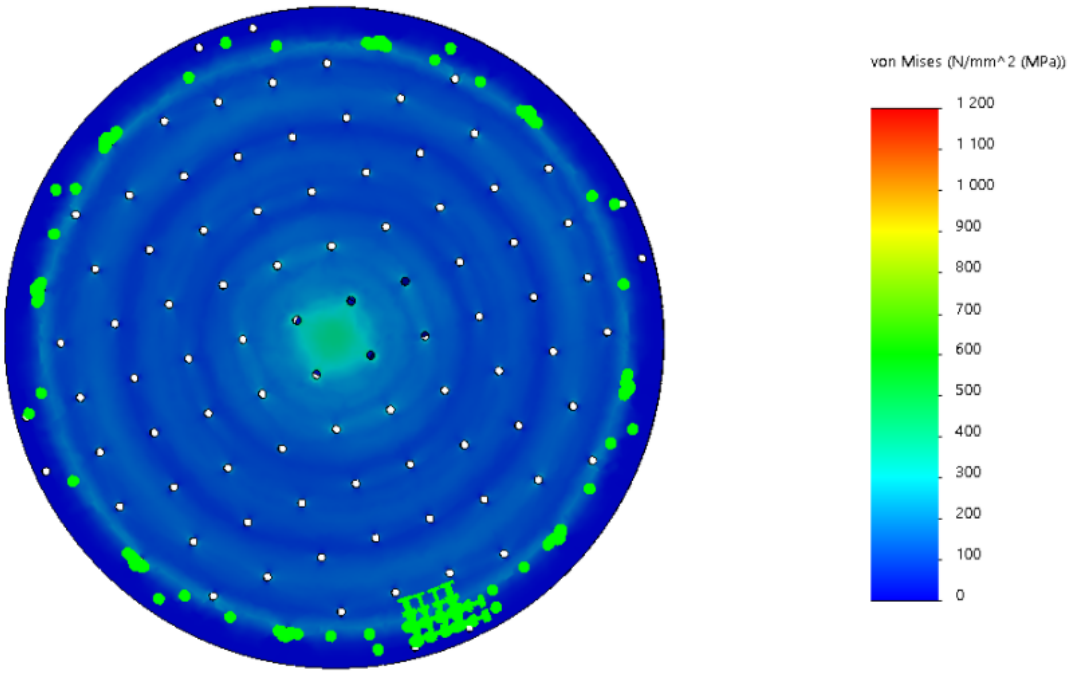

Figure 49: Von Mises stress distribution (top view) for perforated steel plate under 15 cm drop height scenario.

Ripple pattern as seen for the solid plate is also present for the perforated plate. The largest stress concentration for the perforated plate is being at center, at the outer part of the plate where the support ring is placed, as well as around the perforations.

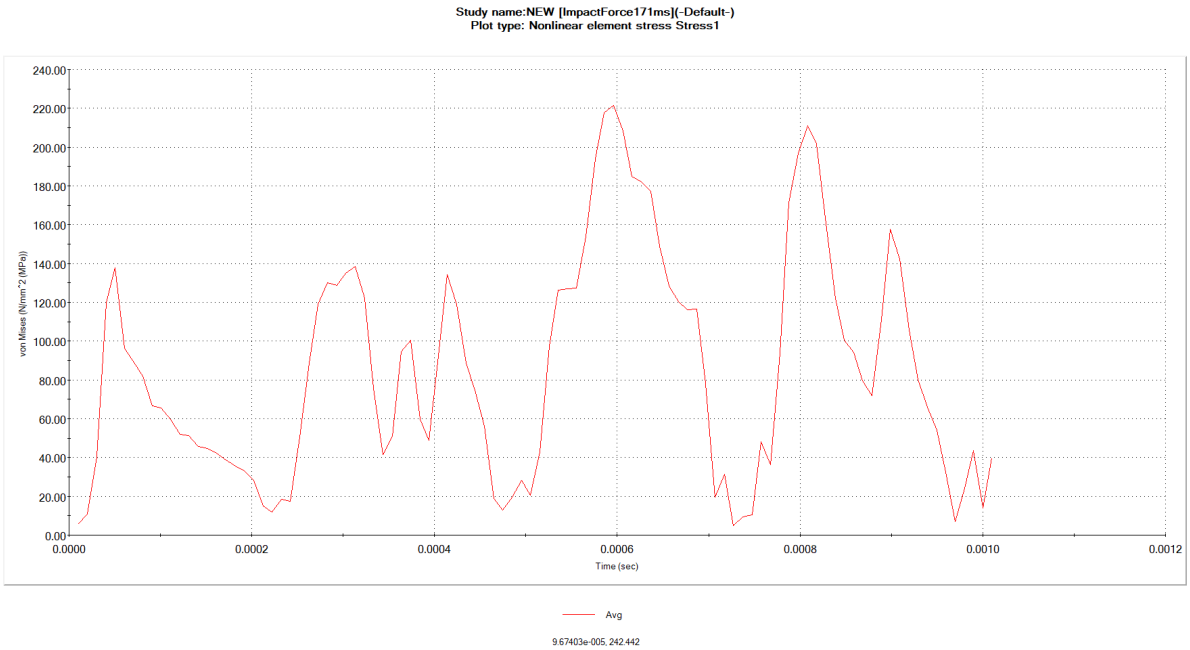

Figure 50: Von misses stress diagram vs time for perforated steel plate under 15 cm drop height scenario.

These results are to some degree similar to the results for the solid plate, as the loading rates are similar. However, the maximum peak values for the same 1 ms interval are larger for the perforated plate.

4.4.1.2 Deflection

Deflection of the perforated plate shows a maximum of 1.7 mm, which is reduced to roughly 0.7 mm at 12 cm radial distance from the center of the plate.

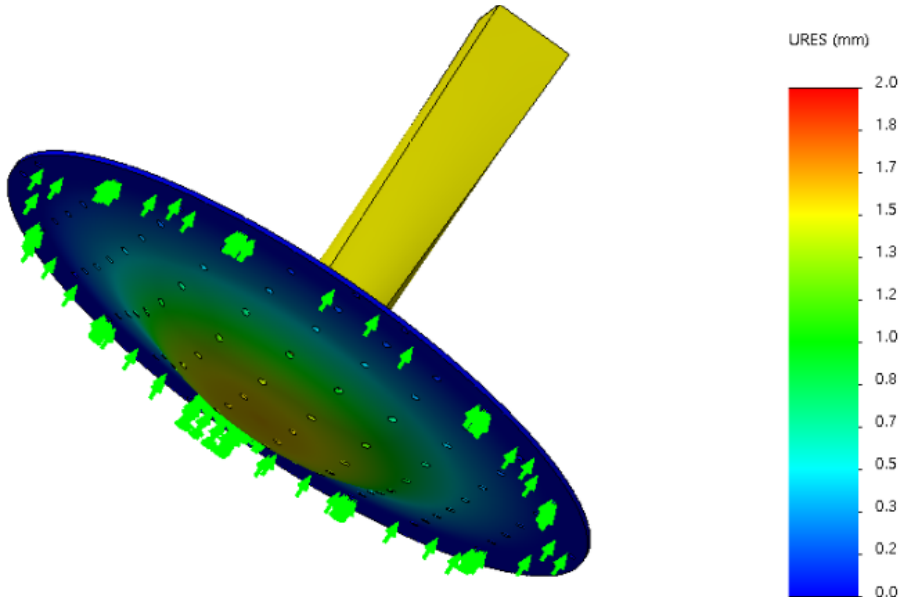

Figure 51: Illustration of SolidWorks deflection values from a 4.8 kg mass released from a 15 cm drop height on a perforated plate.

4.4.1.3 Strain Distribution

Building on the stress distribution diagram, it can be seen from *Figure 52* that strain is concentrated around the perforations. This concentration, however, is not symmetrical. Only two sides of the perforation have a maximum or a large value of strain, whilst the other two sides perpendicular to these sides have a minimum strain.

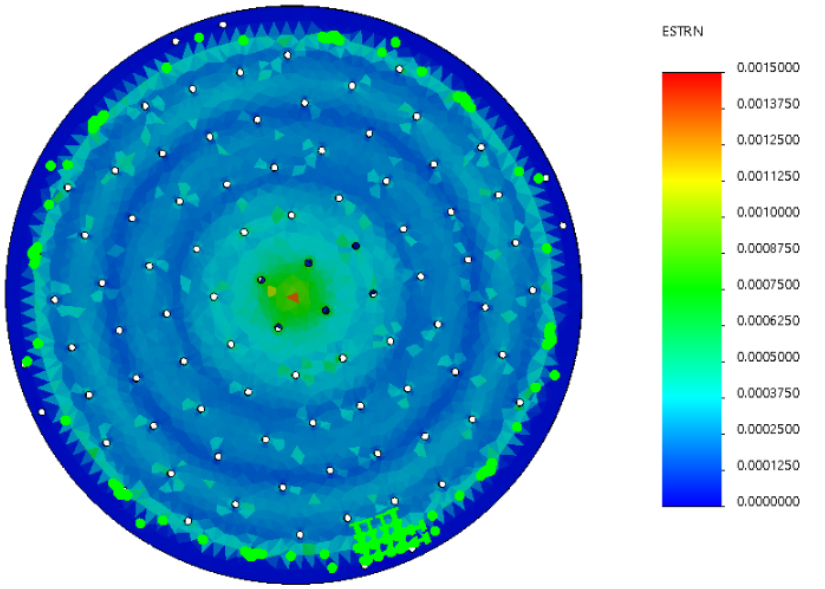

Figure 52: Strain distribution for solid steel plate under 15 cm drop height scenario.

This strain concentration is illustrated in *Figure 53*. The difference in strain surrounding the perforations is 500 µm/m, between the smallest value of strain (250 µm/m) and the largest value (750 µm/m).

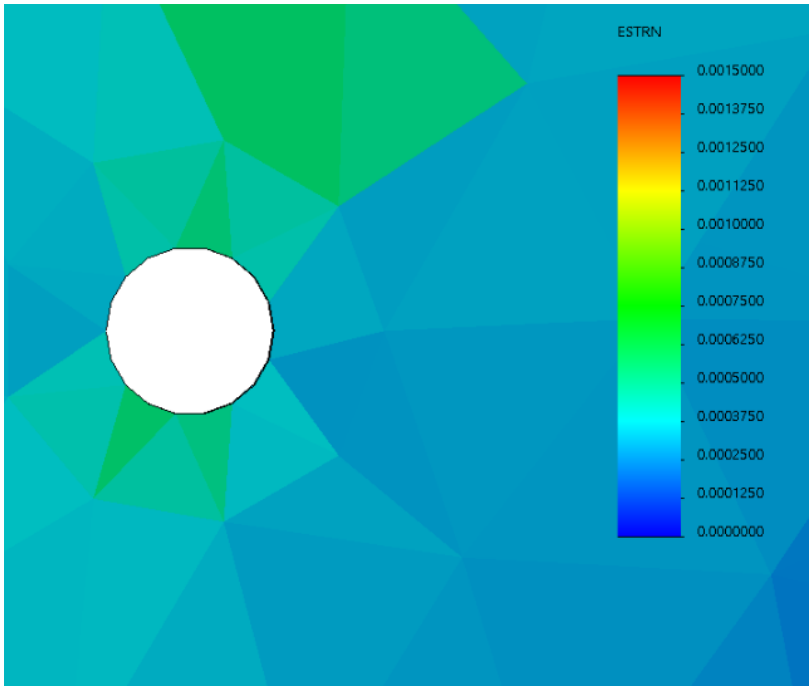

Figure 53: Close up view of the strain concentration around the perforation for 15 cm drop height scenario.

4.4.2 30 cm Drop Height – 2.42 m/s

In this subchapter, the results from the 30 cm drop height, i.e. 2.42 m/s, for the perforated steel plate be presented.

4.4.2.1 Stress Distribution

The analysis of the 30 cm drop height, i.e. 2.42 m/s shows that the Von Mises stress is at its maximum in the middle of the plate, at the point where the impact force hits the test object. The value is approximately 330 MPs and is slightly less than the yield stress value of 355 MPa of the material, meaning that the solid plate will neither go into plastic deformation for this specific load scenario.

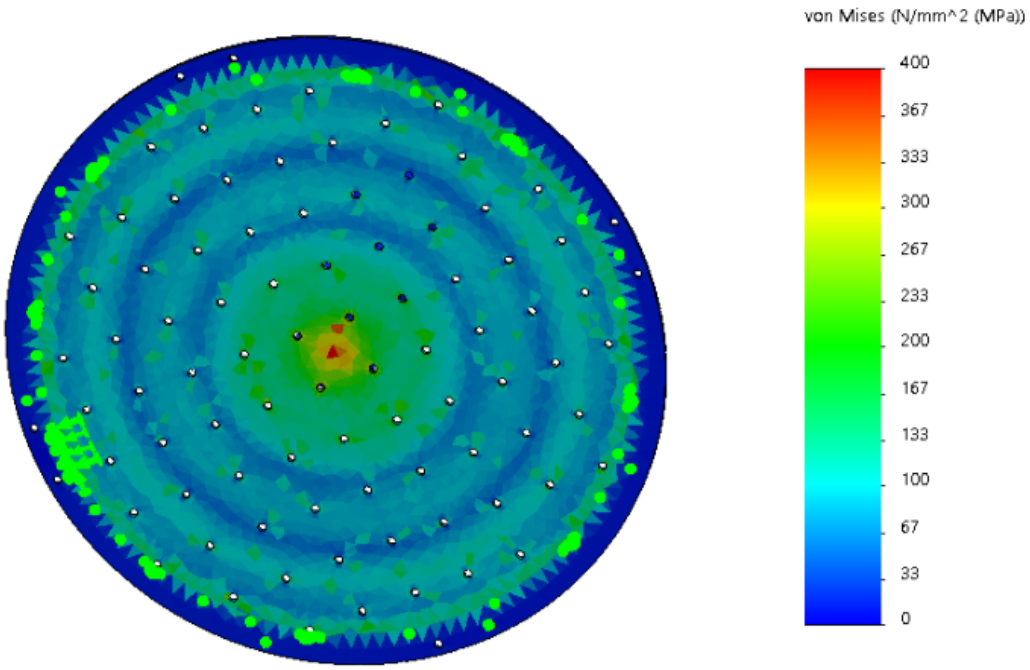

Figure 54: Von Mises stress distribution (top view) for perforated steel plate under 30 cm drop height scenario.

The values for strain as shown in *Figure 55*, exceed the value of 355 MPa, which is the yield point. In *chapter 7*, we will discuss how the yield point is not a static value for ductile materials, when subjected to dynamic loads.

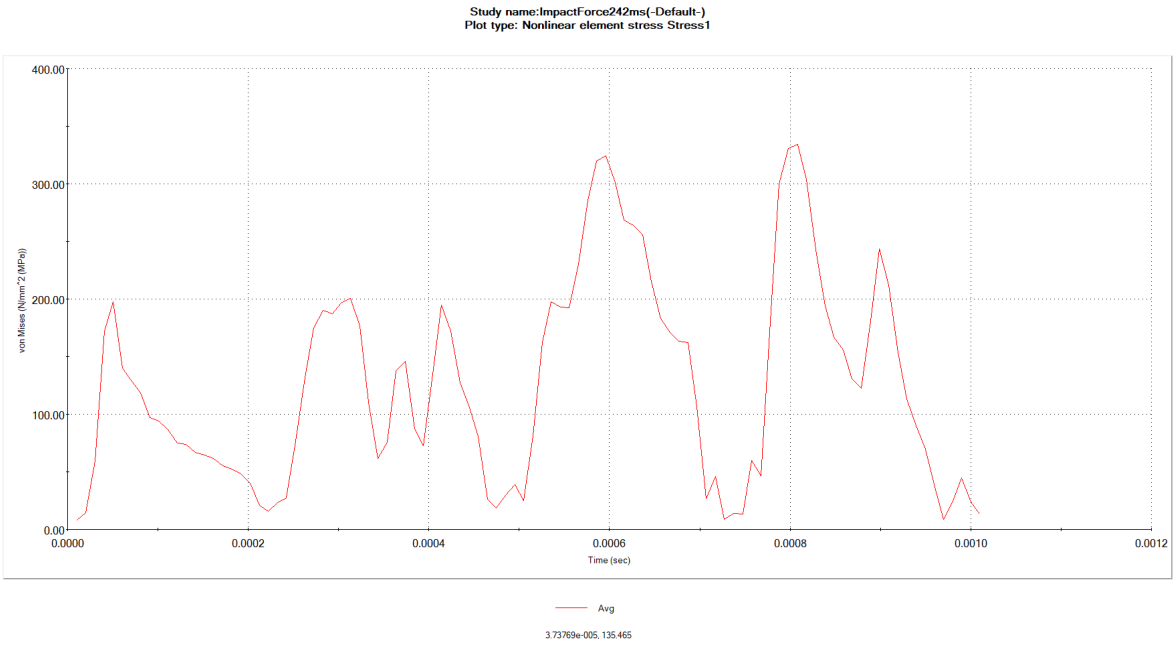

Figure 55: Von misses stress diagram vs time for perforated steel plate under 30 cm drop height scenario.

The overall stress over time curve for the center area on the plates, is shown to have a maximum value of 330 MPa, and dynamic loading of 310 MPa at larges, with a successive variation between minimum and maximum strain.

4.4.2.2 Deflection

The deflection distribution shows an area of approximately 12 cm where the deflection is 2 mm, which is, as mentioned, 66.6% of the thickness of the plate.

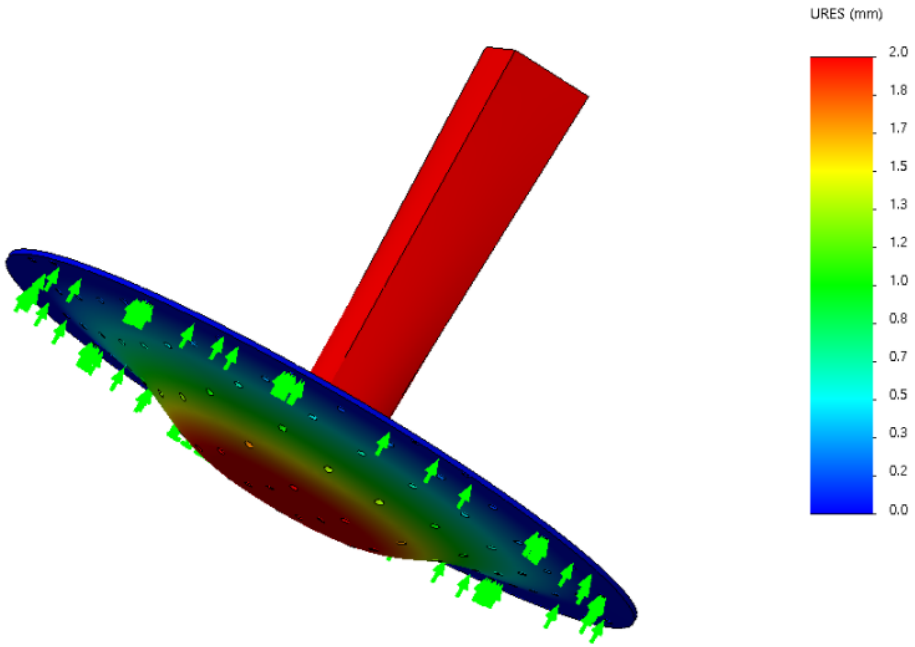

Figure 56: Illustration of SolidWorks deflection values from a 4.8 kg mass released from a 30 cm drop height on a perforated plate.

4.4.2.3 Strain Distribution

Largest concentration of strain is seen in the impact area of 5 cm around the center of the mass impact. Strain are again seen to be concentrated around the perforation in the plate.

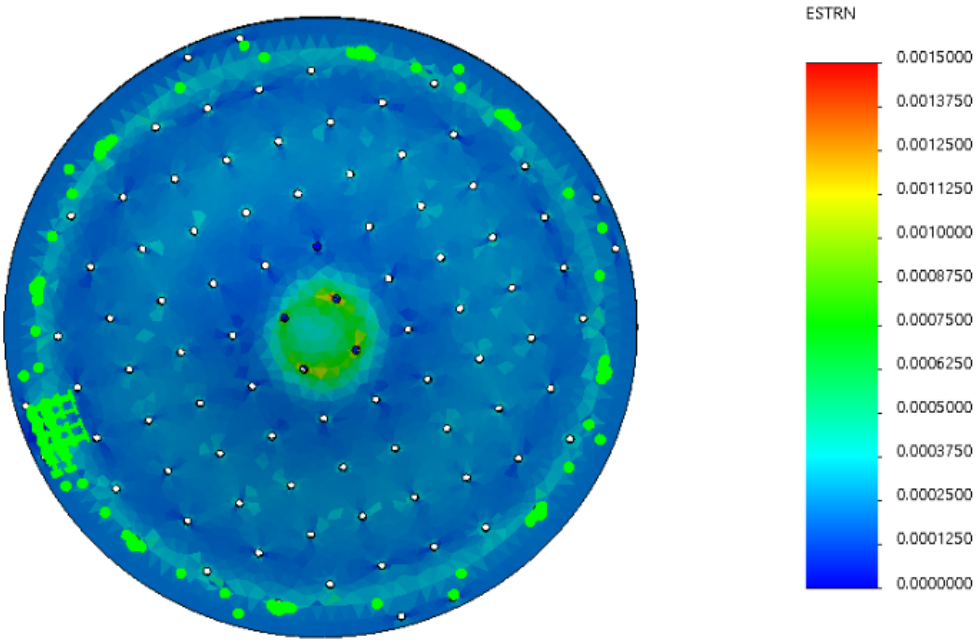

Figure 57: Strain distribution for perforated steel plate under 30 cm drop height scenario.

In *Figure 58*, the variation in strain around one of the center perforations varies between the largest value of 375 µm/m and smallest value of 625 µm/m.

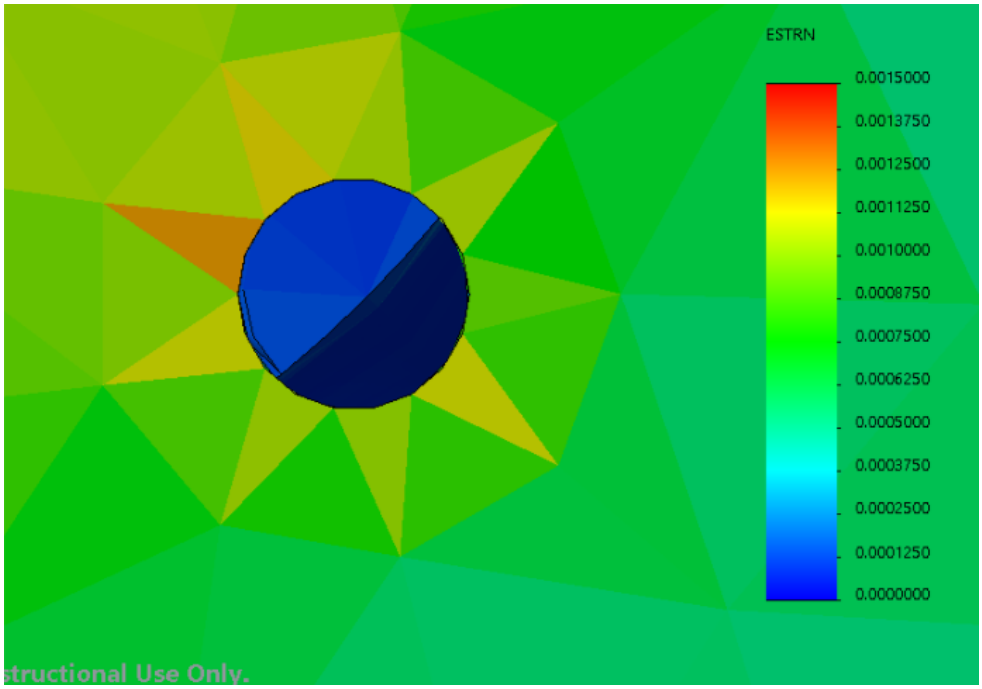

Figure 58: Close up view of the strain concentration around the perforation for 30 cm drop height scenario.

4.5 Simulation of Cap-X GRP Cover

The main objective of this thesis is to study the impact behavior of perforations in water versus air, which is intended to be applied to the protective Cap-X cover. GRP is the material used for the protection covers in Cap-X technology. However, we simplified the test objects for the experiment by solely examining the top horizontal surface of the protective cover and perform the tests with steel as the selected material. As pointed out in *chapter 3.3*, we decided to use a steel as it is a well defined material. In compare, GRP is a much more complex structure.

Due to cost and time limitations, the experimental tests were only performed on circular steel plates. However, by using Solidworks, simulations on a GRP Cover could also be performed, despite the tight budget.

Despite the fact that the geometry and material properties are not the focus of this thesis, it was decided to perform simulations on the GRP Cover. This was decided because of an interest of finding out how the structure behaves compared to steel plates, when subjected to a load. The simulation performed on the GRP Cover is elaborated upon in the following sub chapter. The simulation performed on the GRP Cover is elaborated upon in the following sub chapter.

4.5.1 Material

The material used for the simulation has its origin from GRP material used for the protection covers in Cap-X technology, given by Statoil. The material properties will not be outlined, as it is beyond the scope of this thesis.

4.5.2 The Test Object

The protective cover designed in Solidworks was based on the geometrical design from the 3D Cap-X model, provided by Statoil as shown *Appendix B*. The perforations used are based on "NORSOK standard" for maximum size allowed (Standards, 2005), as opposed to perforation size from model illustrations.

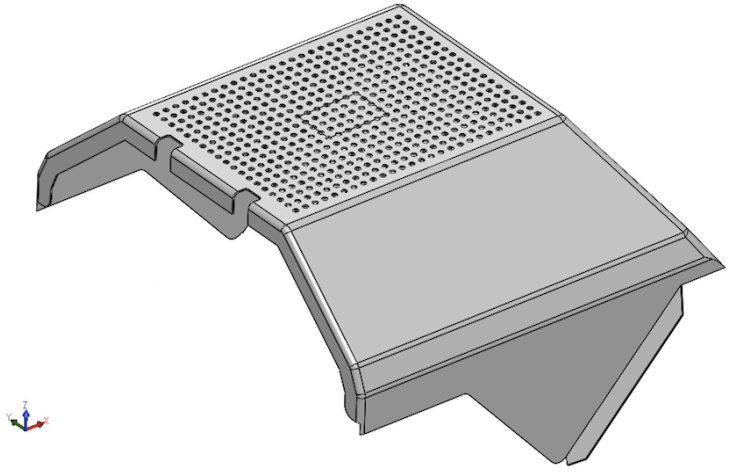

Figure 59: GRP Cover with perforations based on 3-D Cap-X model provided by Statoil.

4.5.3 Meshing

The meshing is set to a high quality 5mm mesh for the GRP Cover simulated, as illustrated in *Figure 60*.

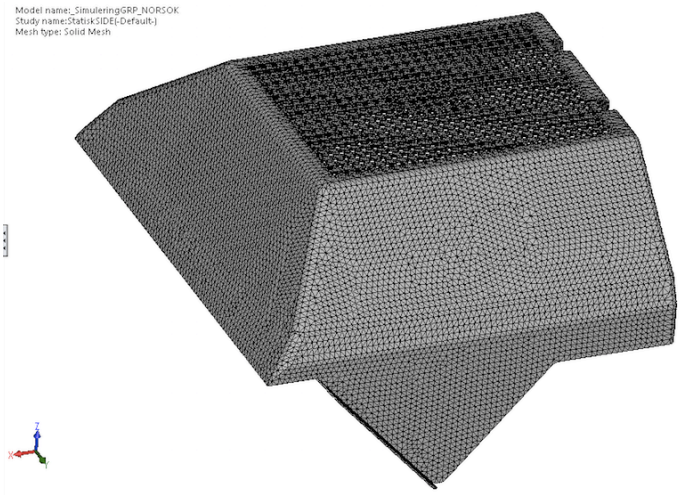

Figure 60: Meshing of CAP-X protection cover used in the simulations.

4.5.4 The Static Load

To simplify the simulation, a static load, instead of a dynamic load, was added. The force was added to two different locations in two separate simulations, one at the top and one on the side of the cap. The loads are illustrated in *Figure 61*. The size of the load was set to 1000 Newton.

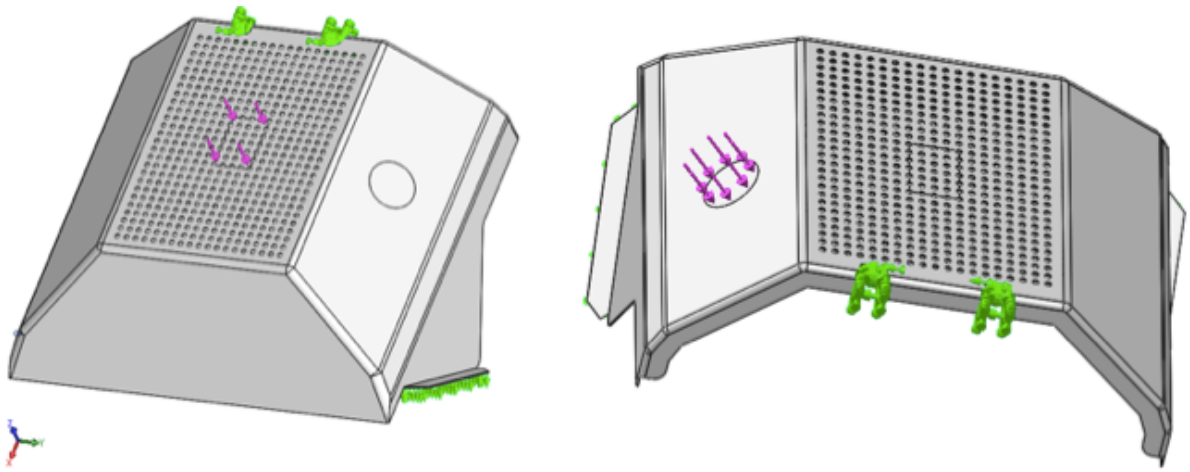

Figure 61: Static load on top of cover (left), deviated load on the side of cover (right).

4.5.5 Top Load – Results

The results from the simulation are divided into 3 parameters; (1) stress distribution, (2) displacement and (3) strain. The focus is on the tendencies rather than the single displayed values from the simulations. Overall, the distributions indicate that stress distribution is non-uniformly distributed, as shown in *Figure 62*. The largest stress concentration is inside the perforations, near the center of the top section. The second largest stress concentration is around the edges, connecting to the non-perforated GRP sections of the protection cover. This can be interpreted as some of the stress being transferred from the center to the sides of the protection cover. The simulation was done with the model being self-contained in this scenario, meaning that supports for the protection cover itself was not accounted for.

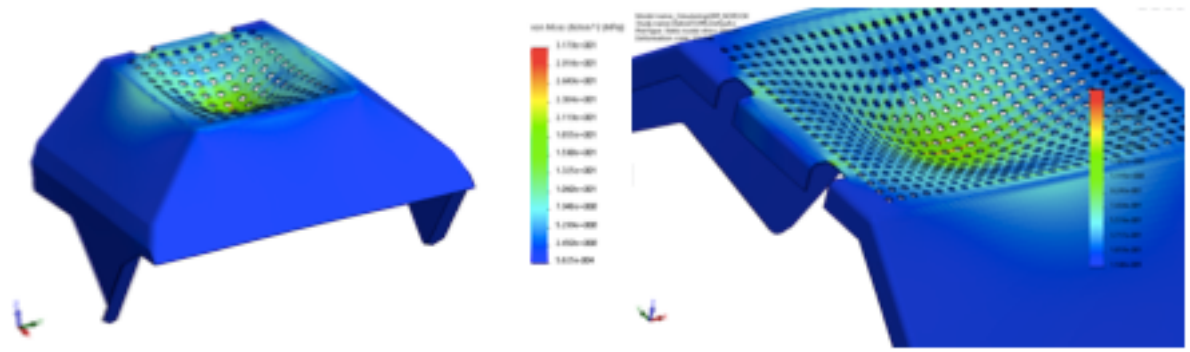

Figure 62: Von Mises Stress distribution on protection covers based on centric load.

The displacement results in *Figure 63* show significant variation based on the stress distribution. Displacement pattern is seen to be fully axisymmetric, with a ripple pattern like the perforated plate simulations.

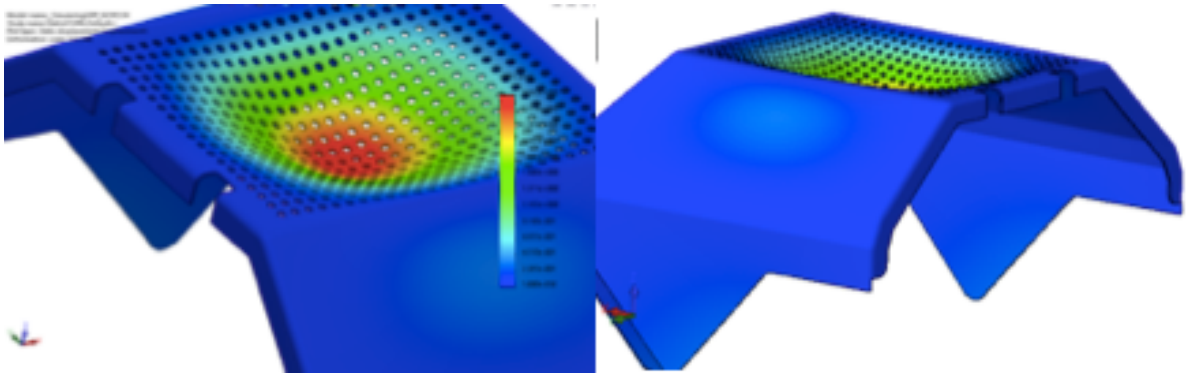

Figure 63: Displacement results on protection covers based on centric load.

Lastly, the strain distribution for the centrally placed load will be described. The top view in *Figure 64* show a clear indication of strain distribution, as "cold patches" of strain is located close to the top rim.

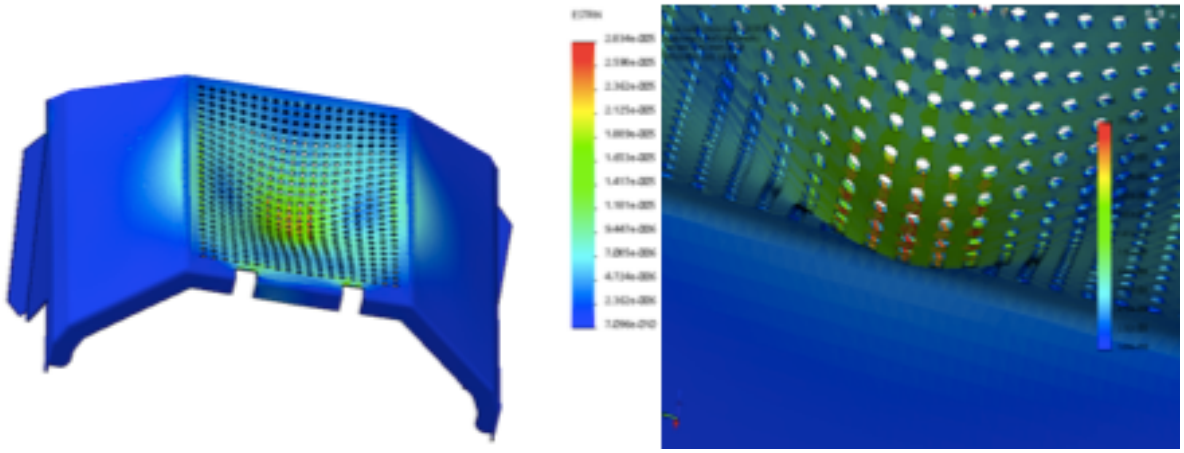

Figure 64: Strain distribution on protection covers based on centric load.

A closer inspection shows the perpendicular variation in maximum and minimum strain located around the perforations, which is where the largest value of strain on the plate is located.

4.5.6 Deviated Side Load – Results

The load based on the side of the protection covers, that act perpendicular to the surface, showed interesting results. Looking at the stress distribution, a large amount of stress is transferred to the corners of the structure and onto the lower and upper section of the protection cover. However, the stress is localized at a concentrated area, as the stress is rapidly reduced by 50% outside of the applied load region. This all being illustrated in *Figure 65*.

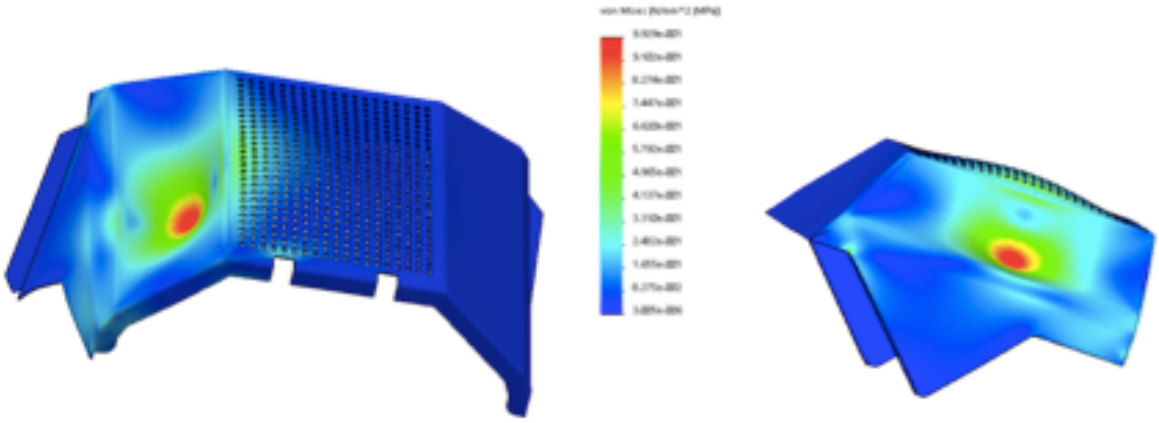

Figure 65: Von-Mises Stress distribution on protection covers based on deviated load.

The deflection again displays trends that differ greatly from the stress/strain distribution. In *Figure 66,* there are three regions of "localized" distribution patterns, separated by low values of deflection.

Outside of the load region, a large deflection is seen at the edges of the bottom of the protection covers. Also, deflection is seen at the top perforated section of the protection covers.

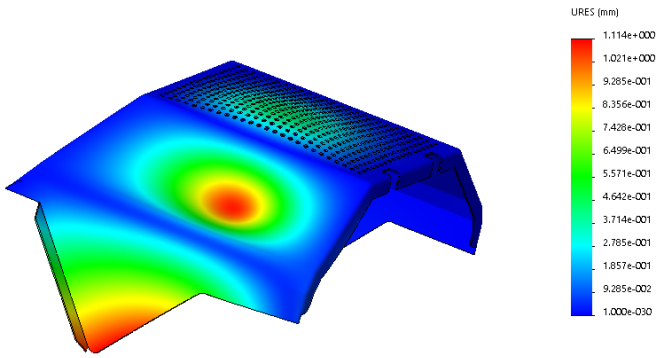

Figure 66: Displacement distribution on protection covers based on deviated load.

Figure 67 shows a side view of the strain distribution. It illustrates that the top section of the protection cover is subjected to negative strain. This is in opposition to the origin of the applied load, where the strain is positive.

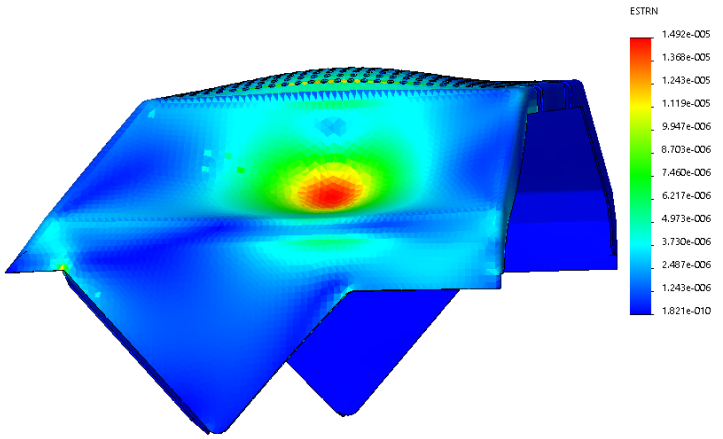

Figure 67: Strain distribution on protection covers based on deviated load.

5 Experiment

In this chapter the main tests conducted to measure strain from the experimental setups are explained in detail, with diagrams that includes all the parameters involved. Most importantly the procedure for each experiment type in both air & water is explained with regards to data sampling, proctor use, temperature, water depth etc.

5.1 Steel plates

The material used for the test objects in this thesis is Domex 355MC E. This is a hot-rolled, high-strength low-alloy (HSLA) steel, consisting of a fine grain structure with high mechanical properties (SSAB, n.d.). The test objects are produced by Svenskt Stål AB (SSAB) in Stavanger, based on the calculations and specifications given in *chapter 3.3 "Selection & Design of Plates Used for Impact Loading Experiment"*.

5.1.1 Material Properties

Table 4 lists the material properties of Domex 355MC E steel, while the material certificate is available in Appendix C: Material Certification.

Table 4: Material properties of Domex 355MC E steel.

	Abbreviation	***Value***	***Unit***
Young's modulus ***Modulus of elasticity***	E	208 000	GPa/MPa
Poisson's ratio	υ	0.285±0.005	1
Shear modulus	G, μ	83±2	GPa
Density	ρ	7850±20	Kg/m^3
Linear expansion coefficient	α	$12 \cdot 10^{-6}$	1/K
Thermal Conductivity	λ	45±2	W/Km
Specific heat	C_p	470±20	J/kgK
Thermal diffusivity		$= \lambda / (\rho * C_p)$ $=1.22\ 10^{-5}$	m^2/s
Resistivity		0.2 - 0.3	μΩm
Tensile Strength		500	$\frac{N}{mm^2}$
Yield Strength		355	$\frac{N}{mm^2}$

5.1.2 Solid Plate

Figure 68 illustrates the solid steel plate and its support ring used to conduct the experiments, where the plate is freely supported at the top of the ring.

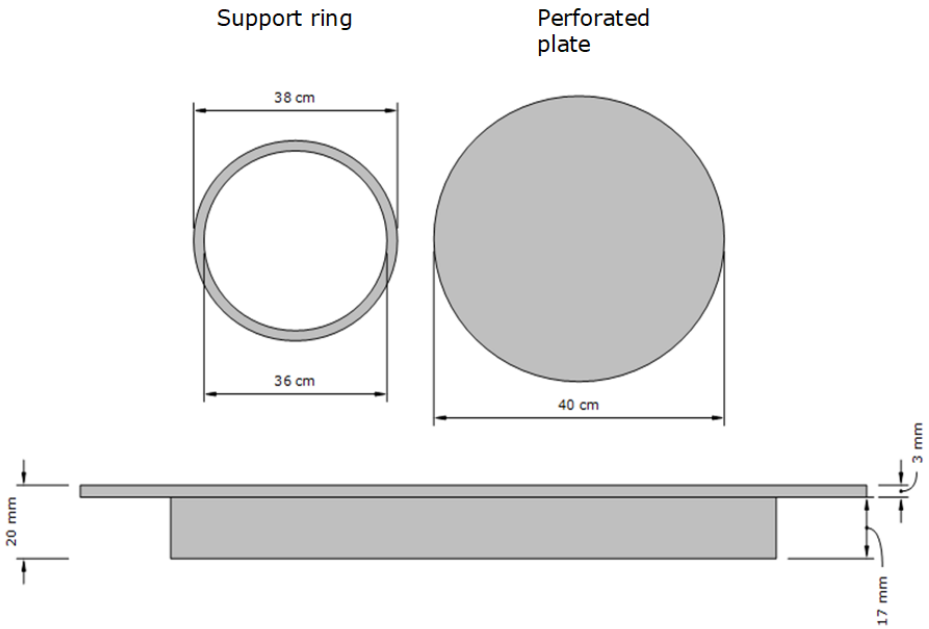

Figure 68: Solid steel plate and its support ring.

5.1.3 Perforated Plate

For the perforated plate, the overall dimensions are the same and the same support ring is used. The perforated plate together with the support ring is displayed in *Figure 69*.

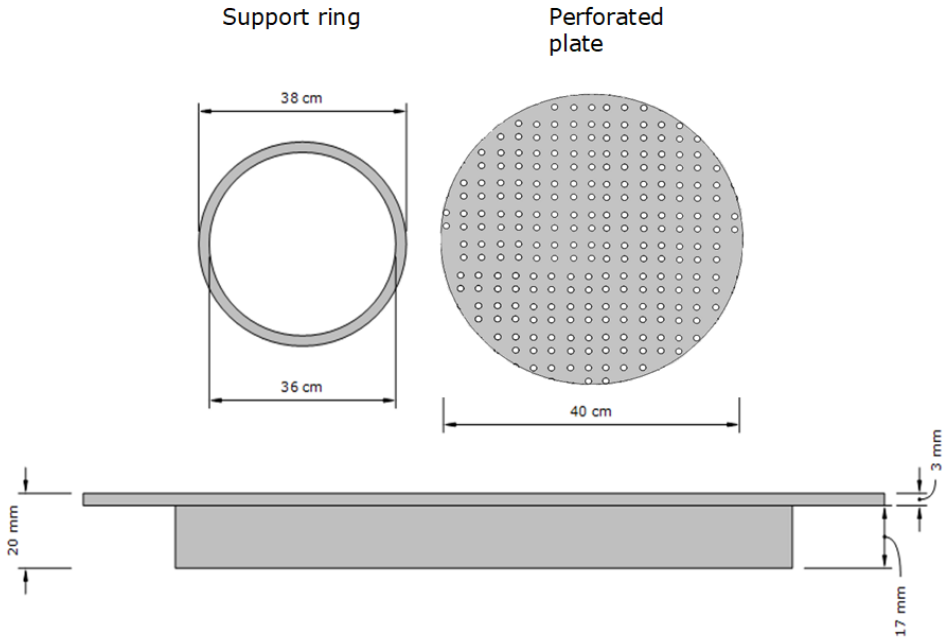

Figure 69: Perforated steel plate and its support ring.

5.2 Apparatus

In this sub chapter the design of the plates, frames, water tank, clamps, modified proctor etc. will be illustrated and explained. These are equipment that have been either made from scratch or heavily altered and modified to be used in the experiments. This section builds on some of the arguments mentioned in *chapter 2*.

5.2.1 Proctor

The modified proctor used in the first impact loading experiments is a tool normally used for to determine the dry density and the water content of the soil, based on the degree of compaction. With a maximum free fall height on the proctor is 30 cm with a moveable mass of 4.8kg (Vegvesen, 1996) is shown in *Figure 70.*

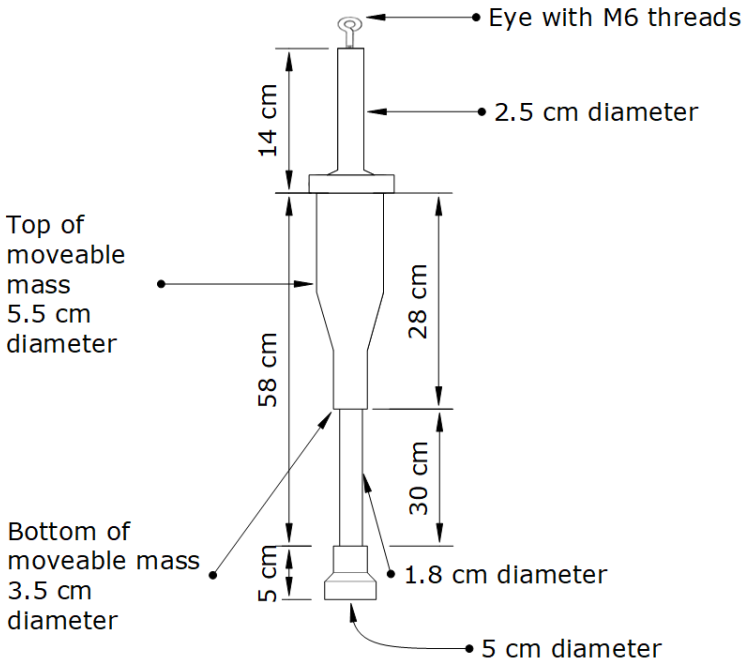

Figure 70: Proctor dimensions with lengths, diameter etc.

The only modification conducted on the proctor was to mill and make threads for the eye screw to suspend the entire proctor. Modified proctor was implement for this study as it was believed that it could best replicate pulse load, as data would then be more comparable to the simulated values as any mass resting on the surface influence, damping and corresponding response after the first impact.

5.2.2 Steel Frame

The steel frame used in the experiments was exclusively made for the proctor tests, an is illustrated in *Figure 71*.

This frame was a necessary component that was made when initial tests showed great instability as initial frame used was unable to contain the energy associated with the impact, resulting in large variations in measurements due to vibrations and movement of the entire apparatus (frame + proctor). Therefore, the main functions of the new frame were to have enough mass to prevent movement of apparatus. Secondly the clamps had to be centered and rigid to focus the impact energy of the proctor on the center of the plate and keep it as centered as possible.

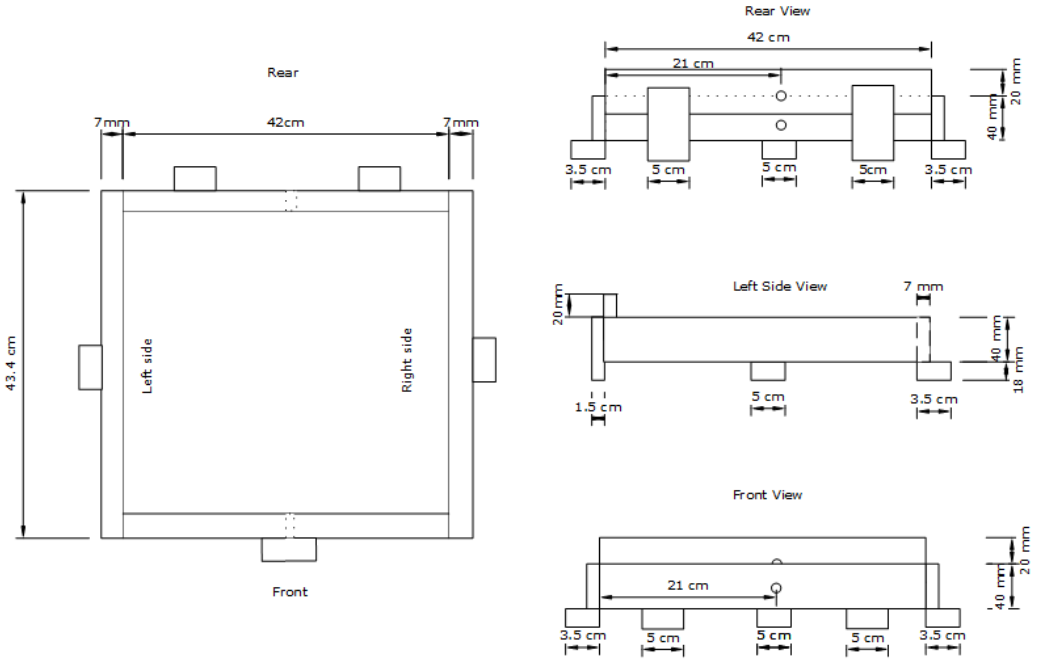

Figure 71: Steel frame used with proctor impact loading measurements.

Design selection is composed of steel plates with thickness 7mm that was welded together using stick welding. For the feet of the 3 sides are resting on the underside of the plate whilst the two feet on the side that is elevated by 2 cm are welded on the exterior. The elevated side was made to accommodate the two clamps. Mass of the frame by itself was not sufficient to remain stable during the tests, which weighed in at roughly 4kg with clamps. Sets of 2 kg weights were therefore used to nullify this issue, where 6 weights in total was used with two corners having an additional 2kg, making the total mass 16 kg.

Illustrations of clamps and masses used on the steel frame is shown in *Figure 72* The reason why the mass is important is because the clamps are integrated into structure, as entire function of the clamps would be nullified if the entire frame is moving. The clamps are not intended to be tightly fastened as their main function is to center to impact from the proctor. Having any degree of force applied means that it is more likely for the impact energy to dissipate into the frame instead of the plate.

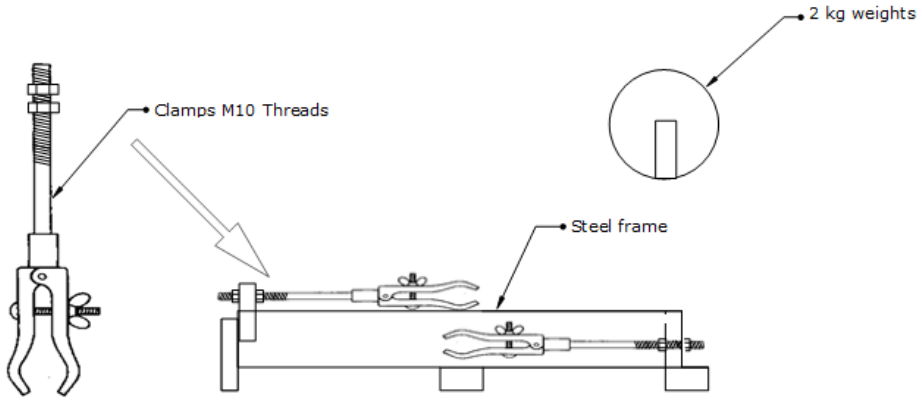

Figure 72: Steel frame and auxiliary components that are used with the frame.

5.2.3 Water Tank

Water tank constructed was important part of capturing the impact loading behavior of the steel plates underwater. Box frame is made from plywood with waterproof coating, with one side being made out transparent styrene-acrylonitrile resin(SAN) with marked name “plastglass”. The transparent material was important with regards to slow motion capture, which allows the height of bounce to be read from the measurement chart in the back of the box. The dimensions of the box were selected to accommodate the metal frame used in the proctor tests, and still have a minimum clearance of 5 cm. The total volume of this container being 133.86 liters when filled to the brim. An illustration of the water tank is seen in *Figure 73*.

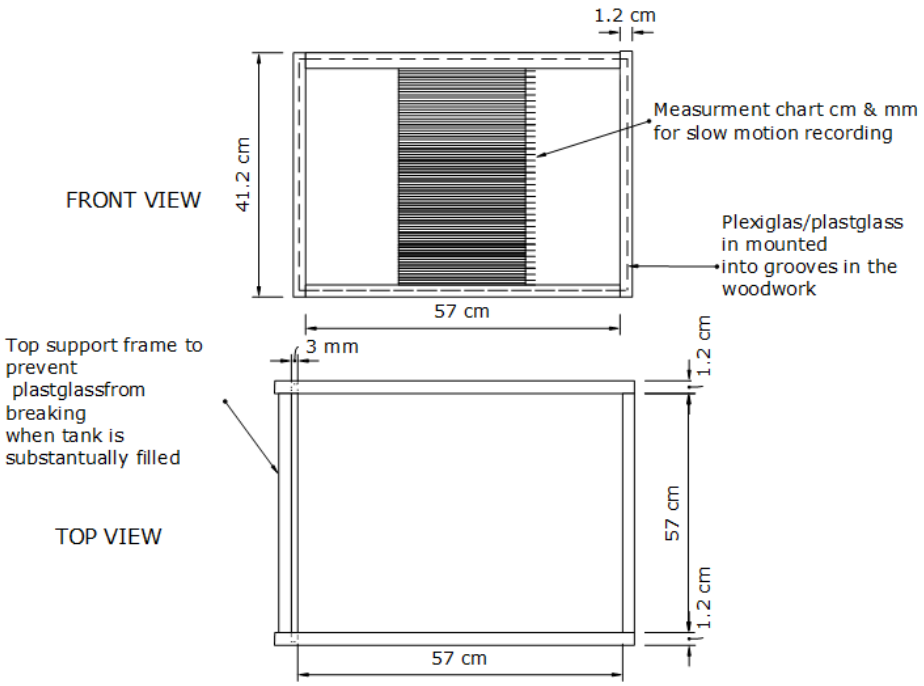

Figure 73: Work sketch of the water tank/tub used for the submerged experiments.

The measurement board was made for the experiments conducted in air in conjunction with slow motion capture footage. This simple construction had the same measurement board as the one used in the water tub with a scale of 40cm with millimeters marked as well.

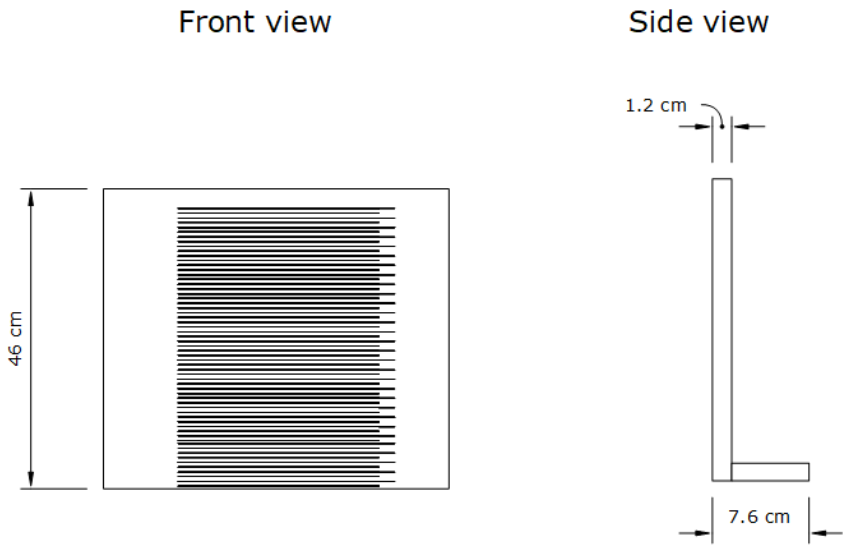

Figure 74: Measurement board used for tests in air/surface.

The back support of this board was weighted down to prevent it from being easily moved in addition to prevent it from toppling.

5.2.4 PVC pipe and Steel Ball

Last two components used for the experiments was PVC pipe and steel ball shown in *Figure 75*. The steel ball had a diameter of 4.8 cm and mass 440g, which was used for ball drop tests. The PVC pipe served as a guide for the ball. The selected length and dimensions used was 2.05 meters with an inner diameter of 7.5 cm.

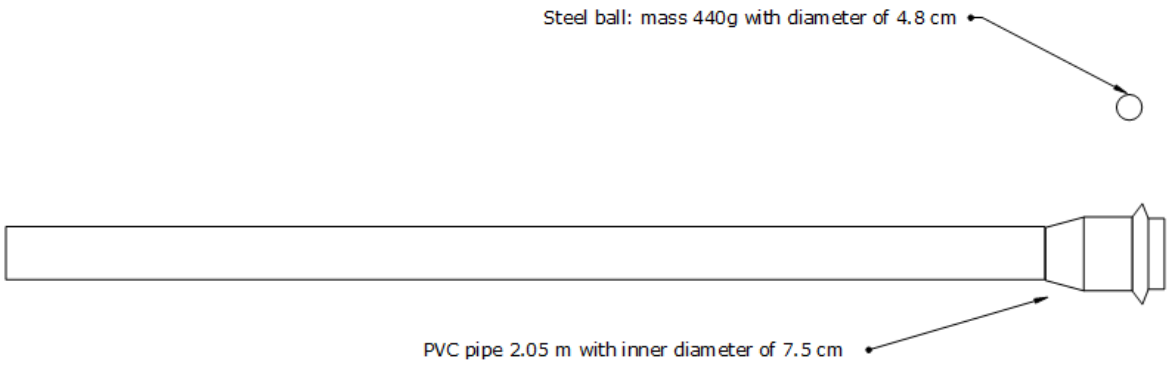

Figure 75: Illustration of PVC pipe and steel ball.

5.3 Measuring- and Data Processing Equipment

In this sub-chapter there will be a review of the equipment used to measure the strain in the material, in addition to the equipment used to forward, interpret and display the measured data.

5.3.1 Strain Gauge K-CLY41-3/120

In the experiment being described in this thesis, single directional strain gauge of type K-CLY41-3/120 are used. The strain gauge is illustrated in *Figure 76* (HBM, u.d.).

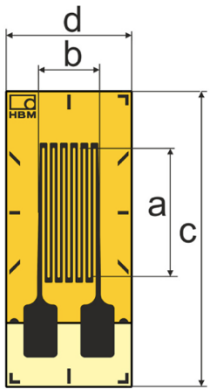

Figure 76: K-CLY41-3/120 Strain gauge.

For the solid plate, one strain gauge of the type shown in *Figure 76*, are used. For the perforated plate, six strain gauges of the same type, are mounted on the plate.

The midpoint of a solid plate will experience the greatest strain when lateral pulse load is applied. Consequently, when performing the measurement of the solid plate, the exact center of the plate was measured, and the strain gauge were carefully mounted on the center. Placement of the strain gauge for the perforated plate was selected with similar care, due to the fact that the stress behavior for perforated plate are not axisymmetric. The orientation was selected perpendicular to the vertical axis.

5.3.2 SCM-SG120 Adapter

The adapter used in the experiment, is the SCM-SG120 adapter. Coupling of a strain gauge and SCM-SG120 adapter, completes the quarter bridge of the strain gauge to a strain gauge full bridge (HBM, u.d.).

5.3.3 QuantumX – MX840B

QuantumX is a computer-based data acquisition hardware device (HBM, u.d.). This hardware will receive data from the strain gauges, through SCM-SG120 adapter, amplify the signals and forward them to the computer connected to QuantumX.

This tool provides a 24-bit analog-to-digital converter, has a sample rate up to 40 kS/s per channel, active low-pass filters and are renowned for their high accuracy up to 0.05% (HBM, u.d.).

5.3.4 Computer with Catman 5.2 Software

Catman 5.2 software is a data acquisitioning software (DAQ) which interprets the data received from QuantumX and allows for visualization, analysis and storage during the measurement and reporting after (HBM, u.d.). The software makes it possible to implement both k-factor and bridge type, in addition to calibrate the gauges, with output is given in [micrometer/meter] vs. time.

To summarize, the strain gauge is mounted on the steel plate. Strain gauge detects the change of resistance and transforms it into proportional surface strain. Signal continue through the wires and SCM-SG120, into the QuantumX hardware. The signal then amplified and forwarded to the Catman Software on the Computer. This sequence is illustrated in *Figure 77*.

Figure 77: Steel plate with strain gauge, QuantumX and Computer with Catman 5.2 Software.

5.3.5 iPhone for video recording

The first law of thermodynamics states that energy can neither be created nor destroyed, but it can be transformed from one form to another (Michael Moran, 2014). When a weight is hold over the test object, the weight has a potential energy. When the weight falls towards the object, the potential energy is being transformed to kinetic energy. The kinetic energy is dependent on the velocity and mass and increases exponentially with velocity (Michael Moran, 2014). When the weight hits the test object, some of the kinetic energy is transformed to the test object. This energy can be derived by comparing the height difference of the proctor before and after the weight hits the test object. The energy absorbed by the impact is measured. To accomplish this, an iPhone camera, with slow motion function, was used to record the height of rebound of the proctor.

5.4 Experimental Setup & Procedure

The two different setups used for the experiments to measure the impact loading will be explained, in addition to procedure for data sampling. With all the experiments conducted on the steel plates being subjected to impact load at the center of plates.

5.4.1 Proctor Tests in Air

The proctor tests conducted in this paper are conducted at two specific height levels, being 30 cm and 15 cm. Where these measurements are based on the impact from bottom of the moveable mass illustrated in *Figure 78*. With the modified proctor resting on the steel plate as shown in *Figure 79*.

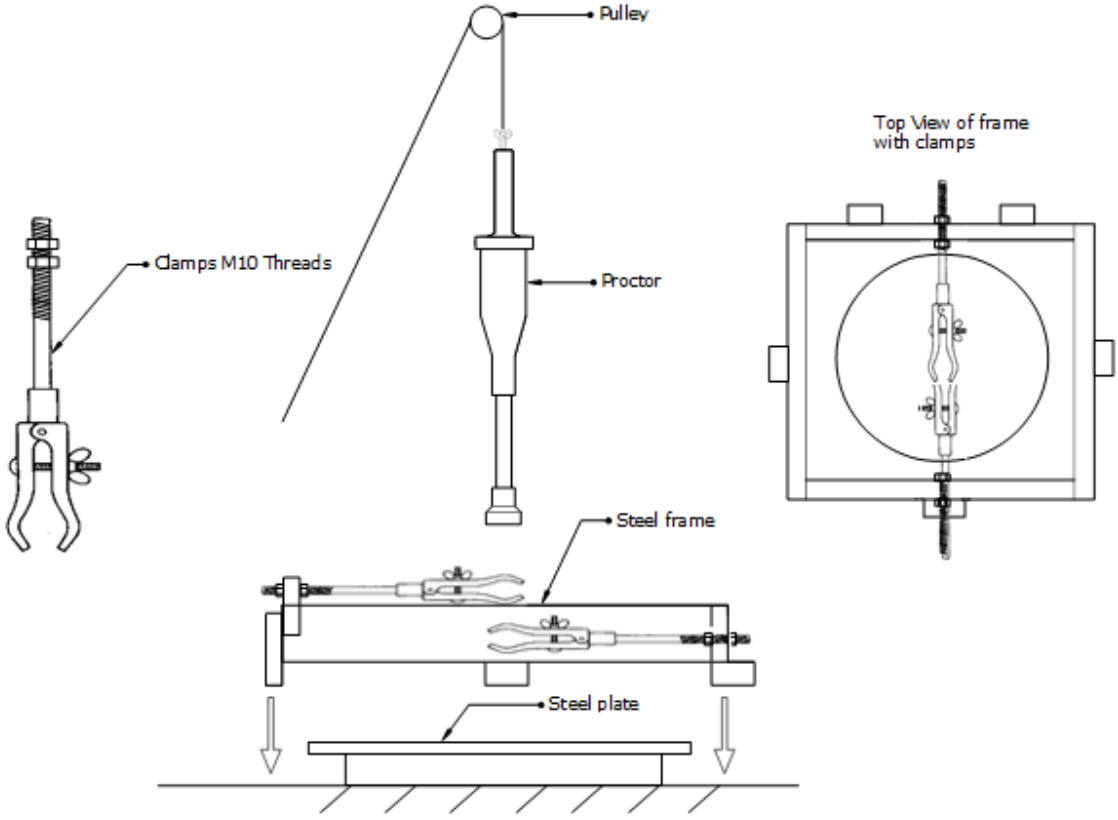

Figure 78: Components involved in modified proctor tests.

For the proctor tests it was centering that was the most delicate part of the procedure, to ensure that center of mass for the proctor was as close as possible to the center of the plate. Due to the nature of impact loading tests, in addition to freely supported plates, meant that plate had to be routinely checked, whether a measurable shift had occurred, which required the centering to be re-measured. In air these centering measurements had to be done for between every run, especially for the 30 cm proctor tests as plate bounce into the air. As the connected strain gauges had a large amount of wiring for the perforated plate with 6 strain gauges, making sure that the wires were not in being squeezed by the plate. This was a much simpler issue for the solid plate which only had a single strain gauge.

When conducting these experiment, the initial conditions was of great importance. As the impact load would be delivered with a modified proctor, normally used for soil compaction tests. This tool is originally considered to be resting on the ground, when being used. The issue with this is that the initial displacement at the center of the plate will then be a function of the mass of the proctor tool in addition to its own weight.

This means that any analytical function describing impact loading behavior would be very difficult to implement, as most these are based on Heaviside step function when describing impact. Therefore, equation for electrodynamic behavior such as the ones described *chapter 3* would not be applicable as this load would not be considered a pulse load. However, the results from experiment conducted using this approach would still make it possible to determine the impact of perforations, as any damping effected afforded to the steel plates occur if displacement of steel plate occurs in fluid. This will remain true for all cases of initial deflection if elastic behavior of material is within linear range.

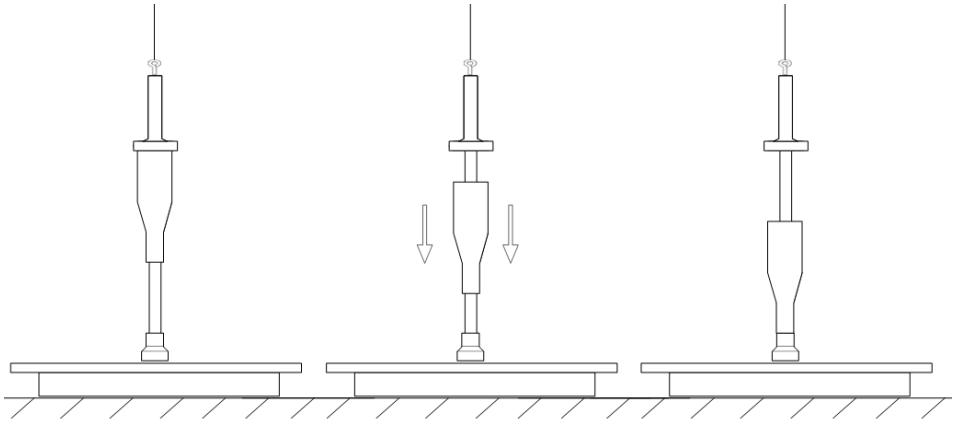

Figure 79: Process of impact loading by using the modified proctor starting from rest at specific height (to the left) until impact on steel plate.

The approach that was taken to achieve the impact most similar to a pulse load, proctor would then have to be suspended just above the surface of the plate, as shown in *Figure 79*. This can be achieved by using attached strain gauges to measure the point where to proctor is touching the surface of the steel plate without applying any load. This was easier said than done but the resting strain was reduced to roughly 5-10 μm/m. As the proctor was suspended using a nylon rope, the elasticity prevented this from perfectly stable as rope elasticity modulus is 3.9 GPa (19/1000th that of steel).

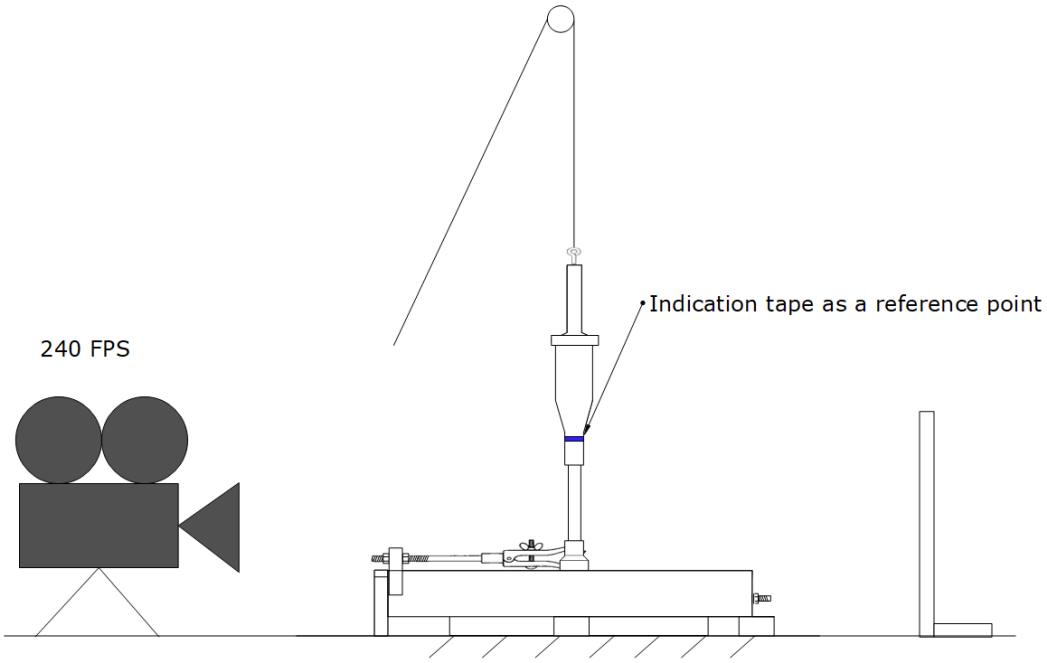

Figure 80: Sketch of slow motion camera set up for the impact loading tests.

The final step of the procedure for each test was the data sampling and recording of the event itself. This was achieved using a selfie stick wirelessly connected to the iPhone, which was activated "simultaneously" by hand. The signal was then given to release the mass. To get accurate results from the recorded footage the alignment between camera the frame and the measuring board was very important. Camera had to be perpendicular to these surfaces in addition to the camera having to be horizontally facing(90^o angle with the vertical component). Also making sure to check the distance from the steel frame and the camera and the measurement board to keep it as consistent as possible. Since all the tests conducted with the water tub had a measurement chart installed inside the tank, the board as shown for air tests in *Figure 80* was not used for the tests performed in water.

5.4.2 Proctor Tests in Water

Having gone through the process for the proctor tests in air, there are little difference between the actual procedure and setup in water shown in *Figure 81*.

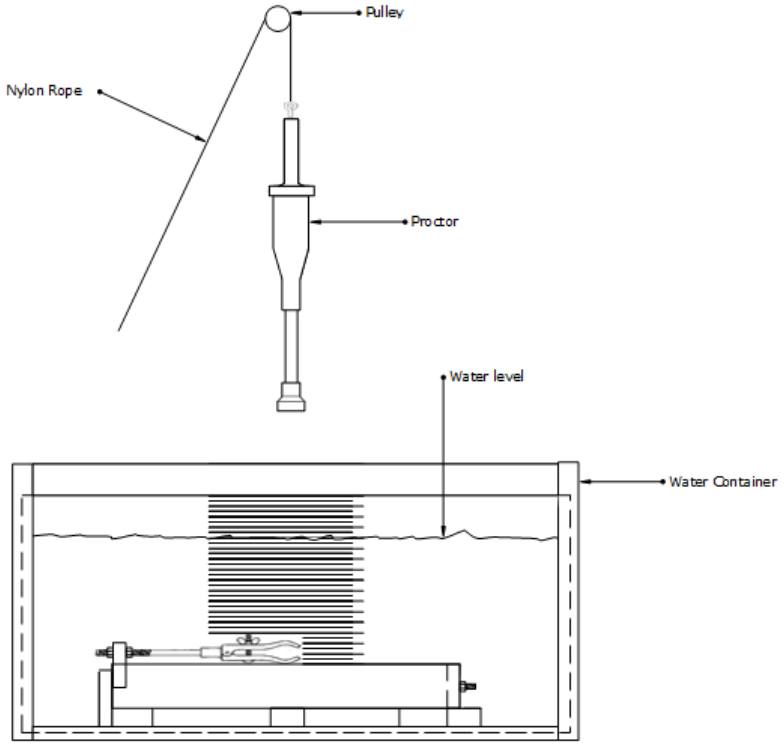

Figure 81: Front view of modified proctor setup in water.

Major difference is the addition of water which requires an accurate measurement of the water level as well as accurate temperature measurements. Temperature measurements are mostly for reference sake but are also important for material property calculations which will be explored further in the discussion *chapter 7*. Water level for proctor tests were done with water levels at 36 cm with the surface of the plate being 34cm below the surface, which is portrayed in *Figure 82*. The illustration is not to scale but serves to illustrate how much of the proctor is below water. Measurement of the water level includes the proctor, frame, plate being submerged into the water. The moveable mass (4.8kg) section of the proctor alternates between being submerged and not submerged.

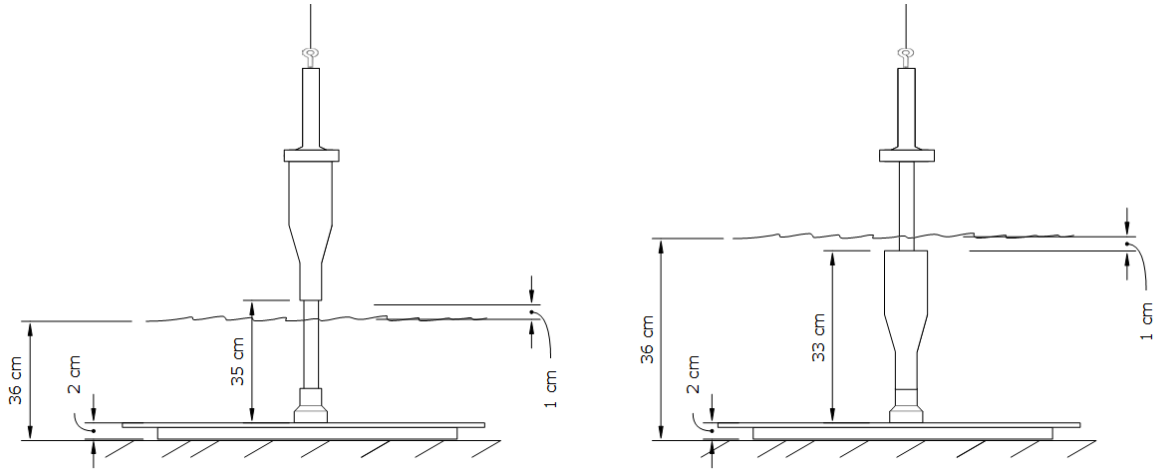

Figure 82: Showing difference between proctor before and after release with regards to submersion (drawings not properly scaled).

Due to the large capacity of the water tub, the change in water level is only 1.8 mm and was neglected, as this amounts to only 0.5% change in total water height.

5.4.3 Ball Drop Test in Air

Ball drop tests conducted. have a much simpler setup than the modified proctor tests. This experiment incorporates the use of 440 g steel ball with diameter of 4.8 cm, which is made of hardened steel. Setup is as shown in *Figure 83.*

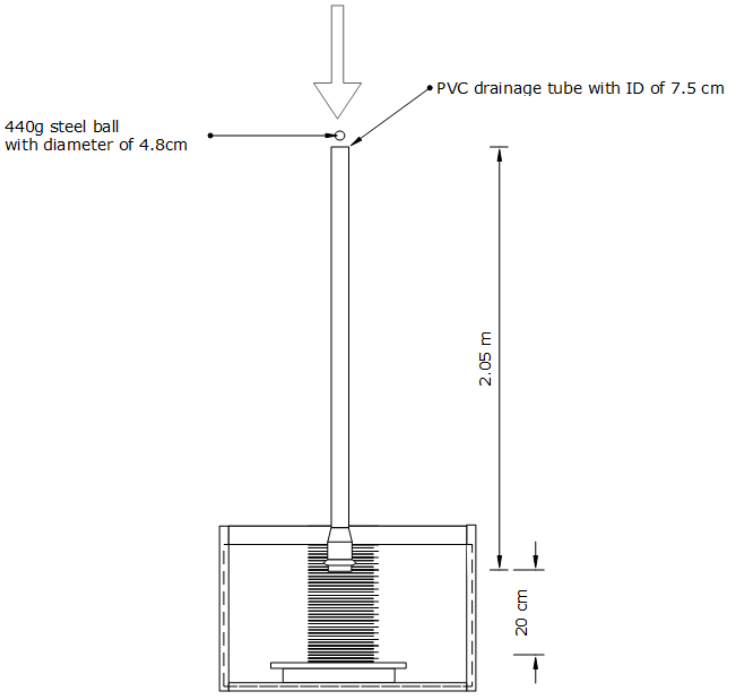

Figure 83: Setup for ball drop experiment in air.

Setup for this type of experiment was more centered around PVC pipe, as it had to be fastened and levelled properly to ensure that it was completely vertical. Pipe was fastened to a guard rail above setup area using gaffer tape. The height of the PVC pipe above the steel plate was selected based of the approximate bounce height of the steel ball. Any lower height above the plate than 20 cm would mean that the bounce height would not possible to be recorded, as the PVC pipe is not transparent.

5.4.4 Ball Drop Test in Water

Lastly are the ball drop tests conducted for a submerged plate in *Figure 84*, which has the same core procedure as the aforementioned tests conducted in air.

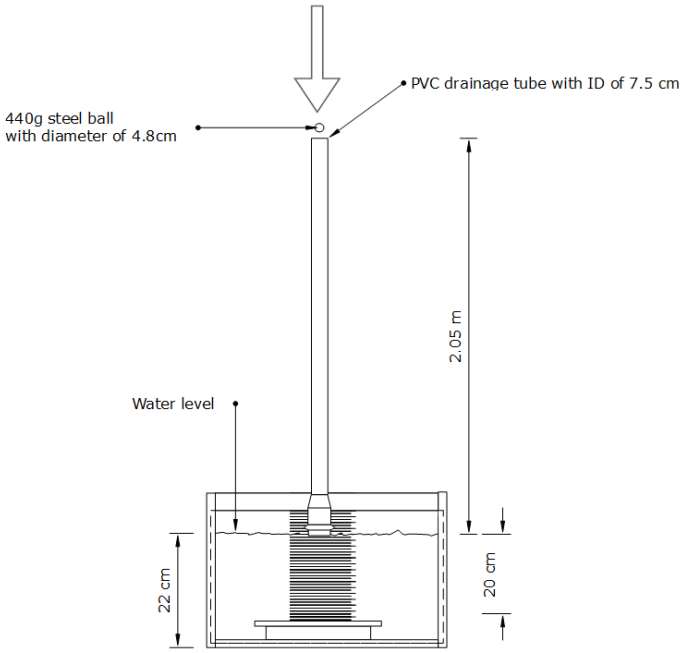

Figure 84: Ball drop test in water.

The water level for all the ball drop methods conducted had a measured water height of 22cm of water. Similar to the proctor tests done in water, the change in water level due to the mass is being submerged into the tub is ignored, as the increase in water level is so small (roughly 0.17 mm water level change due to ball being submerged into the water).

6 Results

In this chapter, the results from the conducted experiments will be presented, categorized into air, water, height, for both solid and perforated plates. The results will not be discussed in relation to each other in this chapter, but will instead focus each individual result with regards to values and behavior etc. These values presented are based on the center strain gauges for solid and perforated plates.

Due to nature of tests conducted, there exists a certain degree of variation between each measurement. Therefore, the average first peak maximum from all the tests conducted was used to form an average, and then the results that show the closest behavior to this is presented in this section marked as red in the tables. This variation however, is not significant initial peak in the impact loading response, which is the focus in this segment (detailed analysis of full impact response in *chapter 7*. The rest is presented in tables as reference statistics which include averages for peaks, standard deviation, bounce height etc. Additionally, for each of the type of plate and corresponding height (e.g. 15cm 30 cm or 2.25 m), the same scales are used to quickly discern the difference in the results. In all the cases, the scale is based around the first maximum.

Equations used are the arithmetic mean and sample standard deviation (Anon., 2018).

$$\bar{x} = \frac{1}{n}\sum_{i=1}^{n} x_i$$ *Equation 18*

Arithmetic mean used to determine the sample average from the measurements with "x_i" being the measured strain from measurement "i" from a total number of measurements "n"

$$S_{n-1} = \sqrt{\frac{1}{n-1}\sum_{i=1}^{n}(x_i - \bar{x})^2}$$ *Equation 19*

Even with the presence of slow motion footage, the velocity of the mass could not be accurately approximated to reasonable accuracy. This was tested using proctor tests in air for 30cm where the bottom of the mass showed approximately 3 ±1 m/s. For some of the tests they showed the same value of 2.42 m/s one gets when calculating velocity before impact using energy balance equation. This degree of inaccuracy was not acceptable, and calculations was used instead to approximate velocity before impact.

6.1 Proctor 30 cm - Solid Plate

Scale selected to represent these results were -200 < y < 1100 µm/m for the y-axis, and -0.05 < x <0.4 sec centered around the maximum from initial peak.

6.1.1 Proctor 30 cm - Solid Plate in Air

Results for the test on solid plate in air is shown in *Figure 85*. The solid plate measurements for 30 cm proctor test showed a first peak response from initial impact at 989.4 µm/m, with the second 335.7 and third being 145.4 µm/m. Where the second peak is 33.9% of the initial peak strain, and the third being 43.3% of the second peak. The bounce height was also very consistent showing approximately 6 cm ± 0.5cm

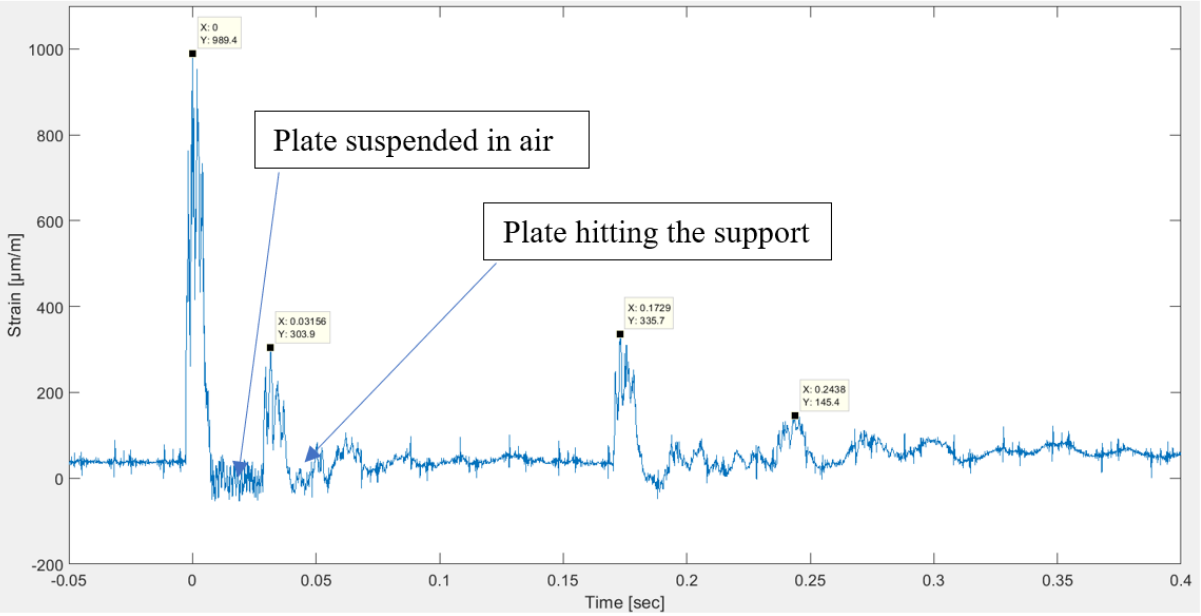

Figure 85: Impact loading response from 30 cm proctor test on solid plate in air, measurement #3.

The plate hitting the rim also produces a sizeable peak at 303.9 µm/m being roughly equivalent in size to the second impact, being 30.7% of the initial peak.

Table 5: Measurement, averages and standard deviations for strain gauge 1, center strain gauge.

Measurement nr #	first peak maximum [µm/m]	Average first peak maximum [µm/m]	Standard deviation first peak maximum [µm/m]
1	960.9	998.92	101.93
2	1097		
3	989.4		
4	1062		
5	1111		
6	1066		
7	918.3		
8	1038		
9	741		
10	1072		
11	966.5		
12	964.9		

The tabulated measurements showed an average first peak maximum of 998.92 µm/m, with standard deviation of 101.93 µm/m, equivalent to 10.2% of average maximum. Other than measurement #9, which had the largest variation from the average maximum, the overall results can be said to be fairly precise.

6.1.2 Proctor 30 cm - Solid Plate in Water

Tests conducted with total water level of 36 cm, where the plate is self being 34 cm below the surface, with water temperature of 15 °C. Bounce height was not large enough to be accurately measured as it was less than 0.5 cm. The initial impact yields a peak of 1015 µm/m, whilst the second peak at 230.3 µm/m as shown in *Figure 86*.

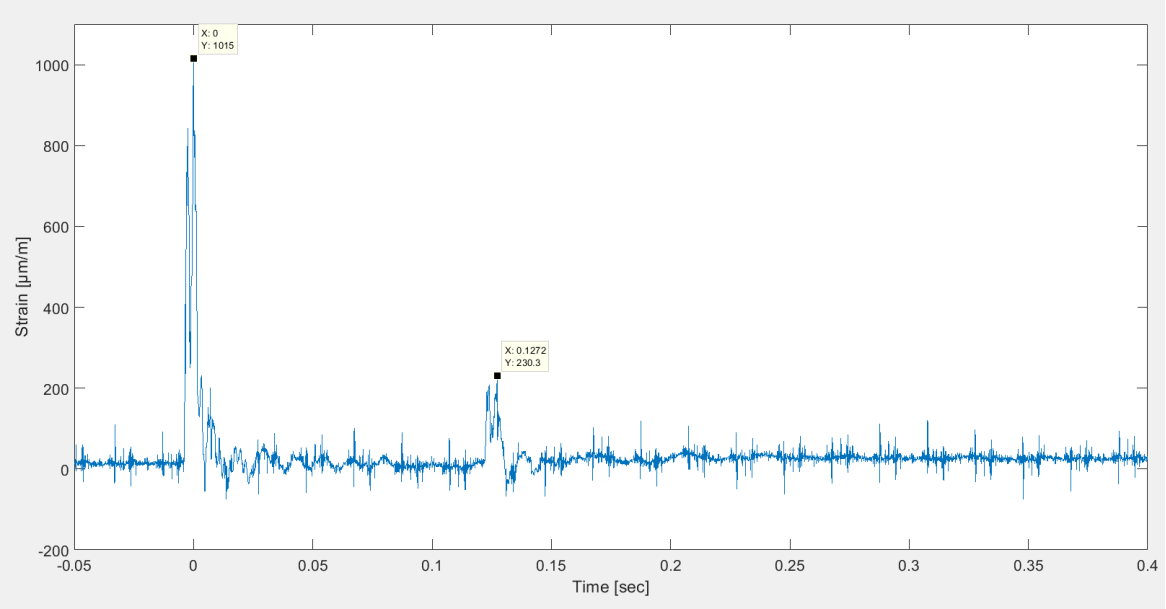

Figure 86: Impact loading response from 30 cm proctor test on solid plate in water, measurement #1.

Plate shown to be stable on support ring, such that no observable peak is seen in between the first and second impact. The averages and standard deviations for all the measurements are shown in *Table 6*. Results from the measurements showed an average maximum of 1029.64 µm/m, with a standard deviation of 66.83 µm/m, being equivalent to 6.5 %

Table 6: Measurement, averages and standard deviations for strain gauge 1, center strain gauge.

Measurement nr #	first peak maximum [µm/m]	Average first peak maximum [µm/m]	Standard deviation first peak maximum [µm/m]
1	1015	1029.64	66.83
2	966		
3	962.9		
4	965.1		
5	1125		
6	1093		
7	1155		
8	959		
9	1043		
10	1012		
11	1061		
12	998.7		

6.2 Proctor 15 cm - Solid Plate

Scale selected to represent 15 cm drop proctor tests results were -200 < y < 800 µm/m for the y-axis, and -0.05 < x <0.4 sec centered around the maximum from initial peak.

6.2.1 Proctor 15 cm - Solid Plate in Air

The results show a first impact of 664.1 µm/m with the second and third impacts at 300.4 and 135.7 µm/m respectively illustrated in *Figure 87*. This shows the second peak being equivalent to 45.2% of the first impact, and the third impact being 45.2% of the second impact. The first bounce being an average of 4 ± 0.5 cm second bounce height for these tests where less than 0.5 cm and could therefore not be accurately determined.

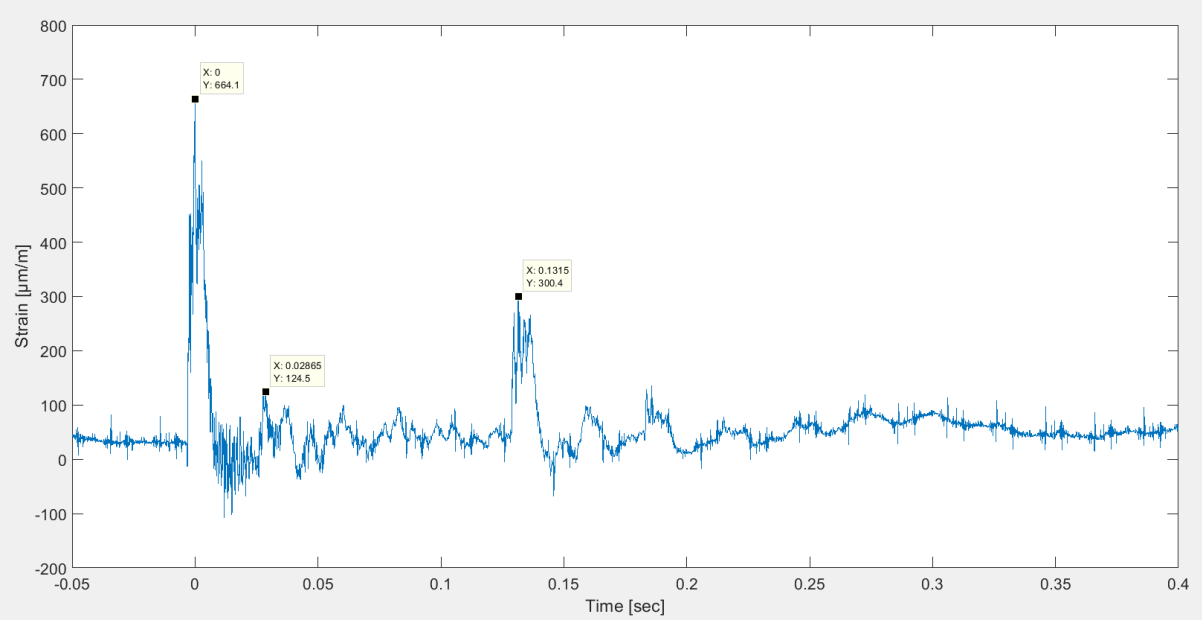

Figure 87: Impact loading response from 15 cm proctor test on a solid plate in air, measurement #10.

Impact from the plate colliding with support ring shows a response of 124.5 µm/m being 18.75% of initial impact.

Table 7: Measurement, averages and standard deviations for strain gauge 1, center strain gauge.

Measurement nr #	first peak maximum [µm/m]	Average first peak maximum [µm/m]	Standard deviation first peak maximum [µm/m]
1	863.5	660.60	69.98
2	642.3		
3	623.8		
4	646.4		
5	619.5		
6	651.9		
7	634.2		
8	631.8		
9	588.9		
10	664.1		
11	652.3		
12	708.5		

The overall average from the measurement showed an average first impact response of 660.6 µm/m with a standard deviation of 69.98 µm/m, equivalent to 10.6% variation from the mean average.

6.2.2 Proctor 15 cm - Solid Plate in Water

Tests conducted with total water level of 36 cm with temperature of 16 °C. Mass bounce height being zero for all the measurements. The initial impact was 700.9 µm/m with the second impact at 152.5 µm/m, with the second impact being equivalent to 21.8% of the initial one. Illustrated in *Figure 88.*

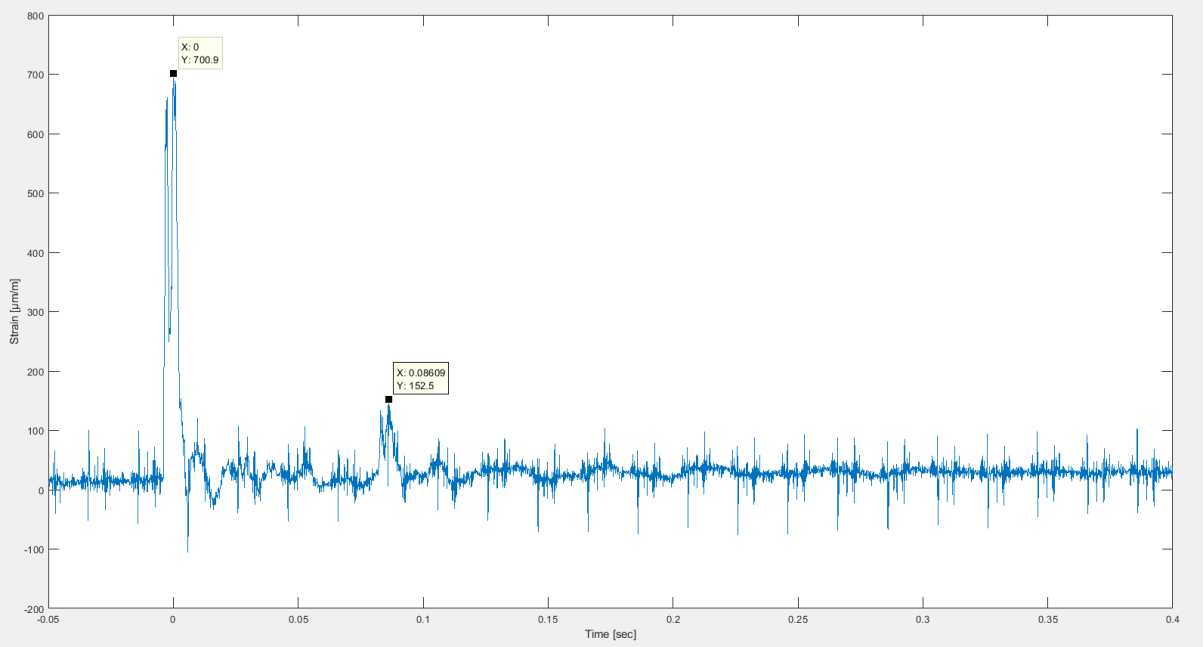

Figure 88: Impact loading response from 15cm proctor test on solid plate in water, measurement #8.

Due to relatively stable plate, there is no noticeable impact between the plate and support ring. The tabulated values are shown in *Table 8*. The average peak maximum from these measurements was shown to be 701.4 µm/m with a standard deviation of 31.17 µm/m, equivalent to 4.44% variation between the results.

Table 8: Measurement, averages and standard deviations for strain gauge 1, center strain gauge.

Measurement nr #	first peak maximum [µm/m]	Average first peak maximum [µm/m]	Standard deviation first peak maximum [µm/m]
1	747.1	701.3667	31.16981
2	730.5		
3	748.8		
4	696.5		
5	703.2		
6	696.6		
7	722.3		
8	700.9		
9	657.6		
10	674.2		
11	657		
12	681.7		

6.3 Proctor 30 cm - Perforated Plate

Scale selected to represent these results were -200 < y < 1100 for the y-axis, and -0.05 < x <0.4 sec centered around the maximum from initial peak.

6.3.1 Proctor 30 cm - Perforated Plate in Air

Results presented in *Figure 89*. For the proctor test in air the peaks show value of 992.4, 419.7 and 124.1 µm/m, for which the second peak is 42% of the first peak, and the third peak is 29.6%of the second peak. With the bounce height being consistently 6 ± 0.5 cm and the second bounce being 1 cm for all the measurements with little to no discernible difference.

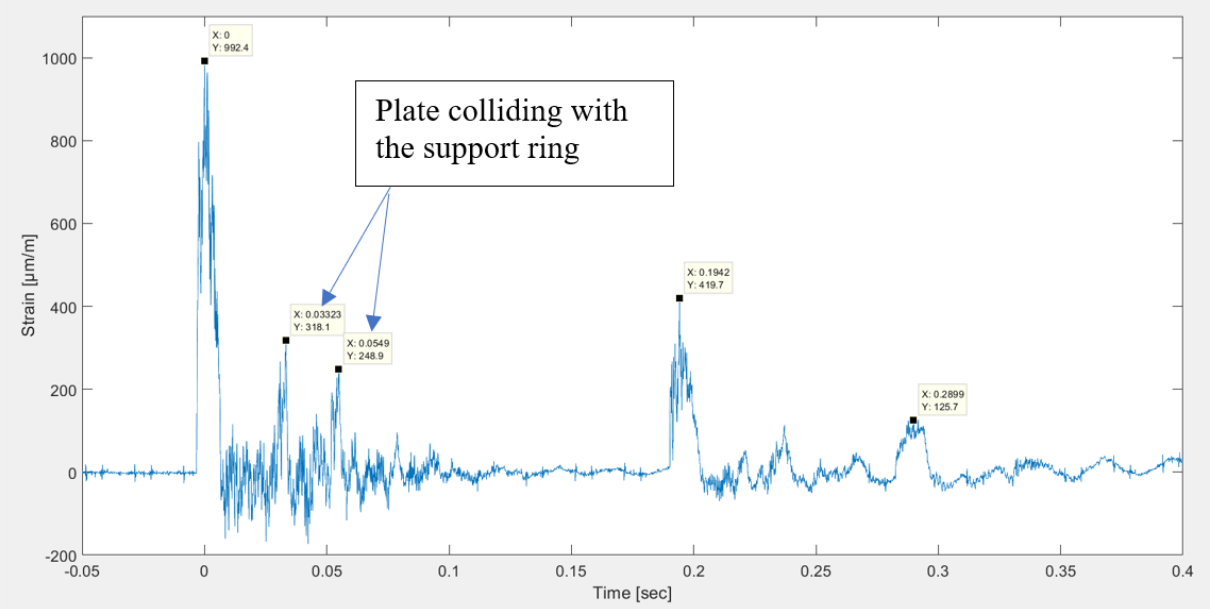

Figure 89: Impact loading response from 30 cm proctor test on a perforated plate in air, measurement #10.

The collisions of the rim can be clearly seen as and values of these are 315.8 and 248 µm/m, which are significant peaks in the overall impact loading response.

Table 9: Measurement, averages and standard deviations for strain gauge 1, center strain gauge.

Measurement nr #	first peak maximum [µm/m]	Average first peak maximum [µm/m]	Standard deviation first peak maximum [µm/m]
1	928.6	1006.89	59.51807
2	1107.0		
3	944.4		
4	959.0		
5	1012.0		
6	1073		
7	1040		
8	1050		
9	962.5		
10	992.4		

The measurements are fairly concentrated around 1006.9 µm/m with a standard deviation of 59.5 µm/m, which is roughly 5.9% variation between the results.

6.3.2 Proctor 30cm - Perforated Plate in Water

Water level 32cm and the temperature measured to 18 °C and an average first bounce of 1cm for all the results, with no discernible bounce on the footage for consecutive bounces. The results being illustrated in *Figure 90.* The peak response are 778.4 for the first and 125,6 µm/m for the second, which the second peak is 16% of the initial impact.

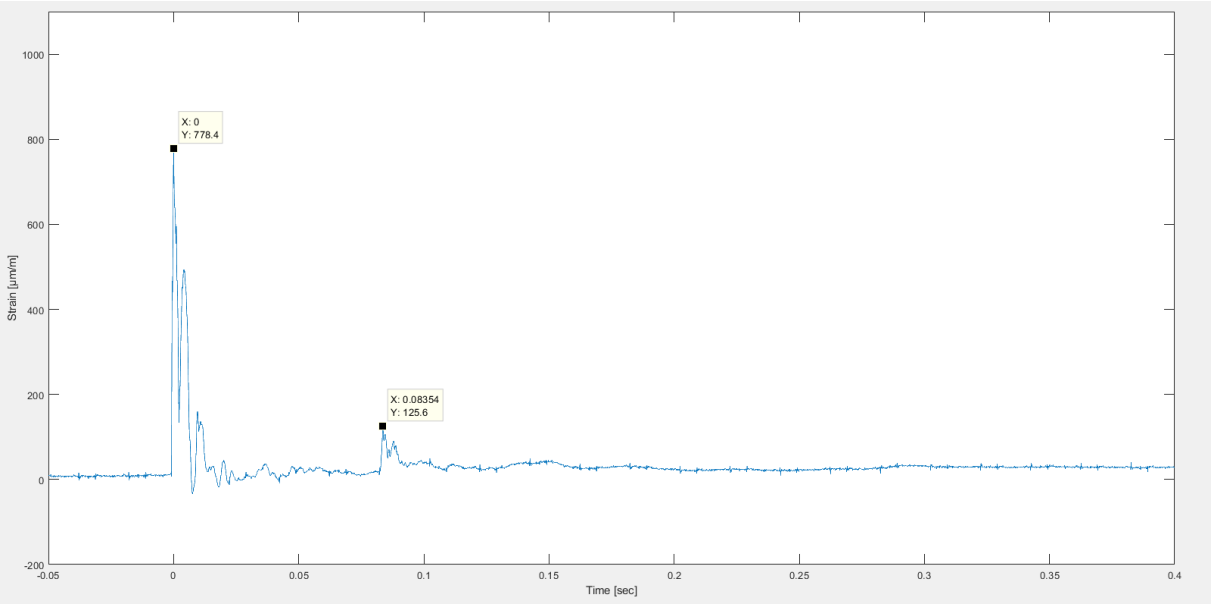

Figure 90: Impact loading response from 30 cm proctor test on a perforated plate in water, measurement #2.

Based on *Table 10*, the peak distribution and averages show values of 780.5 µm/m and a standard deviation of 47.6 µm/m, which shows a variation between the results of approximately 6.1%.

Table 10: Measurement, averages and standard deviations for strain gauge 1, center strain gauge.

Measurement nr #	first peak maximum [µm/m]	Average first peak maximum [µm/m]	Standard deviation first peak maximum [µm/m]
1	811.8	780.5	47.6
2	778.4		
3	858.7		
4	764.8		
5	818.1		
6	738.5		
7	765.5		
8	687.3		
9	810.2		
10	771.7		

6.4 Proctor 15cm - Perforated Plate

Scale selected to represent these results were -200 < y < 800 for the y-axis, and -0.05 < x <0.4 sec centered around the maximum from initial peak.

6.4.1 Proctor 15cm – Perforated Plate in Air

Measured bounce height was recorded to be 4 ± 0.5cm with second being less than 1cm. The first to third peak responses was seen at values of 690.5,271.2 and 191.7 µm/m displayed in *Figure 91* The second peak being 39.2% of the first and the third being 70.6% of the second.

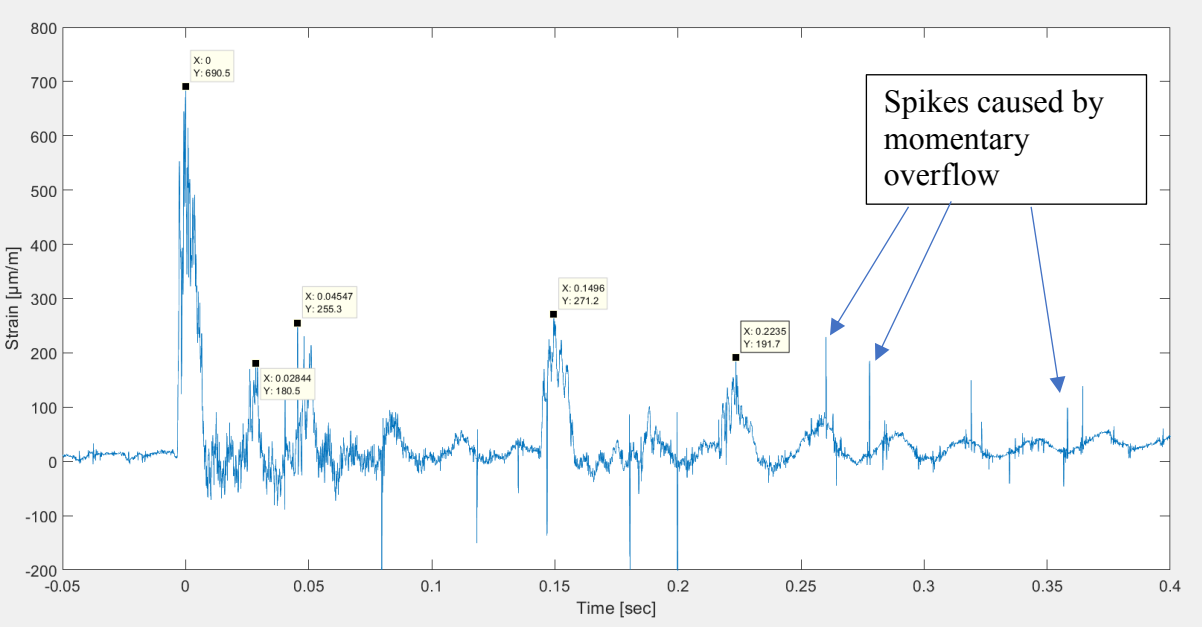

Figure 91: Impact loading response from 15 cm proctor test on a perforated plate in air, measurement #6.

These results showed some degree of overflow, but values of caused by this can be easily determined, based on their sporadic nature. Therefore, these spikes do not impact the accuracy of the measurements. Corresponding averages and standard deviation from the measurements are shown in *Table 11*.

Table 11: Measurement, averages and standard deviations for strain gauge 1, center strain gauge.

Measurement nr #	first peak maximum [µm/m]	Average first peak maximum [µm/m]	Standard deviation first peak maximum [µm/m]
1	757.9	683.24	54.6
2	670.4		
3	723.7		
4	569.1		
5	714.3		
6	690.5		
7	705.9		
8	620.7		
9	711.1		
10	668.8		

Measurements conducted displayed an average maximum peak of 683.24 µm/m, with a standard deviation of 54.6 µm/m. The standard deviation equivalent to 7.99%, indicating a good degree of precision.

6.4.2 Proctor 15 cm - Perforated Plate in Water

The measurements in water show that the initial impact response is 473.5 µm/m, whilst the second is only 64.62 µm/m being 13.6% of the initial peak, shown in *Figure 92*. Tests were conducted with water level at 36 cm at temperature of 18 °C. Recorded bounce height for these measurements were equivalent to zero

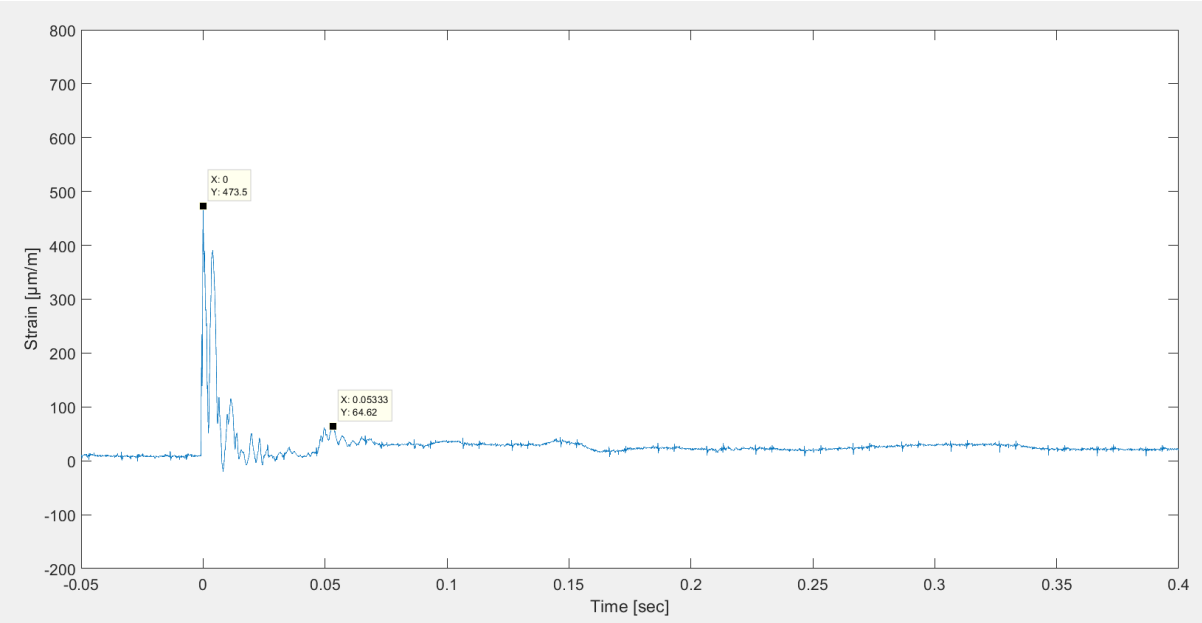

Figure 92: Impact loading response from 15 cm proctor test on a perforated plate in water, measurement #4.

Impact loading response from 30 cm proctor test on a perforated plate in water, measurement #2.

Table 12: Measurement, averages and standard deviations for strain gauge 1, center strain gauge.

Measurement nr #	first peak maximum [µm/m]	Average first peak maximum [µm/m]	Standard deviation first peak maximum [µm/m]
1	497.2	474.44	56.75
2	502.1		
3	377.1		
4	473.5		
5	396.3		
6	508.1		
7	442.3		
8	523.4		
9	560.7		
10	463.7		

The overall measurements showed an average peak maximum of 474.44 µm/m with a standard deviation of 56.75 µm/m, equivalent to a variation in the results of 11.96%

6.5 Ball Drop Method 2.25m

In this section, the results from impact loading achieved by dropping a hardened steel ball from 2.25m will be presented. Height measurement was determined using laser measurement device. Due to the large amount of kinetic energy, the object was seen to have significant bounce heights as a result. The corresponding bounce height is presented in the table for each measurement. The tables however, only include the first bounce height as the consecutive bounces are less than 0.5 cm and can therefore not be accurately measured using the footage at hand.

6.5.1 Solid Plate

For the solid plate, the scale for the x-axis was selected to display -0.05 sec before peak and showing 0.5 sec after impact. The y-scale limits were set to -600<y<1800 µm/m. Time scale was extended to capture the third impact from the steel ball.

6.5.1.1 Ball Drop Method 2.25m - Solid Plate in Air

Measurement for solid plate ball drop showed three characteristic peaks illustrated in *Figure 93*, with first at 1720 µm/m, and the second and third at 235.4 and 49.3 µm/m respectively. The second bounce being 13.7% of the first, and the third is 20.9% of the second impact.

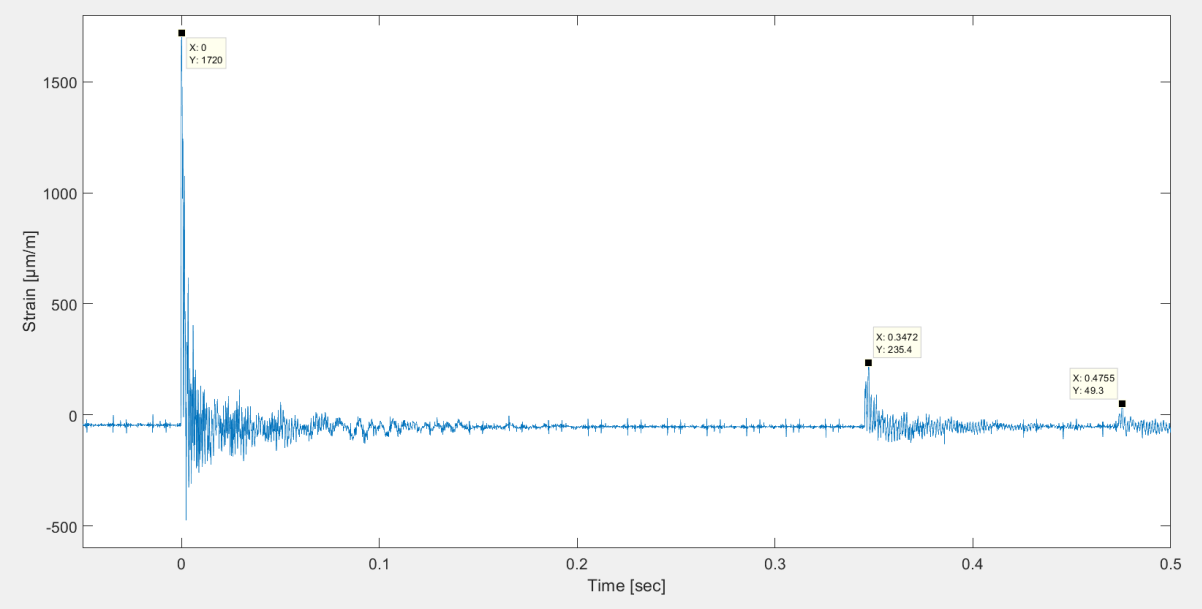

Figure 93: Impact response from ball drop test on a solid plate in air, measurement #8.

Little indications of significant plate to support rim collisions.

Table 13: Measurement, averages and standard deviations for strain gauge 1, center strain gauge for strain and bounce heights.

Measurement nr #	first peak maximum [µm/m]	Bounce height [cm]	Average first peak maximum [µm/m]	Standard deviation first peak maximum [µm/m]	Average Bounce height [cm]	Standard deviation bounce height [cm]
1	1400	16	1730.77	464.12	16.23	3.03
2	1617	17				
3	1150	18				
4	1328	15				
5	3067	13				
6	1922	15				
7	1923	17				
8	1720	18				
9	1577	17				
10	1667	18				
11	1595	9				
12	1933	22				
13	1601	16				

Based on all the results the average peak maximum was at 1730.77 µm/m with a standard deviation of 465.12 µm/m equivalent to 26.87% variation from the mean average. The bounce height from the first impact also showed an average of 16.23 cm with a standard deviation of 3.03 cm, equivalent to a variation of 18.67% from the mean average. The bounce height beyond the first was not accurately measurable as it was below 0.5 cm.

6.5.1.2 Ball Drop Method 2.25m – Solid Plate in Water

For the test done for solid plate in water, with total water level of 22 cm and temperature of 11.1 °C. The characteristic first and second impact of 1784 µm/m, with the second being 356.4 µm/m displayed in *Figure 94*. Second impact being equivalent to 19.97% of the initial impact.

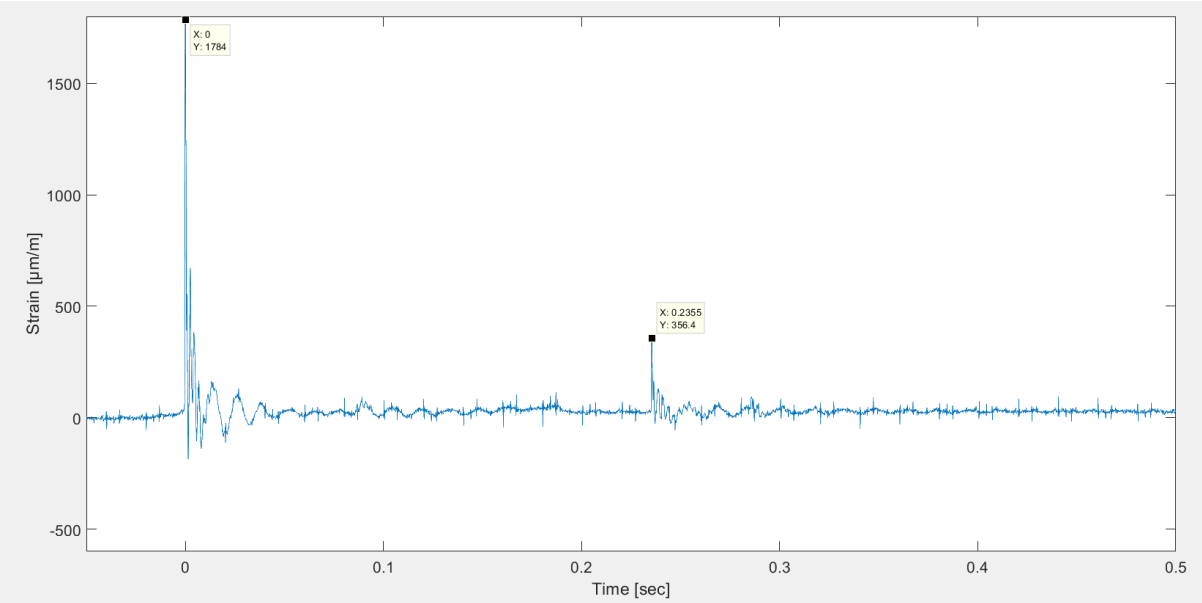

Figure 94: Impact response from ball drop test on a solid plate in water, measurement #9.

Plate remains fully stable on the support ring for the first and second impact.

Table 14: Measurement, averages and standard deviations for strain gauge 1, center strain gauge for strain and bounce heights.

Measurement nr #	first peak maximum [µm/m]	Bounce height [cm]	Average first peak maximum [µm/m]	Standard deviation first peak maximum [µm/m]	Average Bounce height [cm]	Standard deviation bounce height [cm]
1	1933	3	1778.46	235.99	6.62	1.67
2	1524	4				
3	1417	5				
4	1685	6				
5	2163	7				
6	1652	7				
7	2000	7.5				
8	2135	8.5				
9	1784	7				
10	1701	8				
11	1908	8				
12	1509	7				
13	1709	8				

Average first peak response based on the tests was 1778.46 µm/m with a standard deviation of 236 µm/m, being a variation of 13.26%. The bounce height resulting from the initial impact was equivalent to an average value of 6.61 cm, with a standard deviation of 1.67 cm, equivalent to a variation of 25.26% from the mean average.

6.5.2 Perforated Plate

For the perforated plate, the scale for the x-axis was selected to display -0.05 seconds before peak and showing 0.4 sec after impact. The y-scale limits were set to -600<y<1500 µm/m

6.5.2.1 Ball Drop Method 2.25m – Perforated Plate in Water

The results from the impact loading tests a large amount of high frequency vibrations as the perforated plate is impacted by the steel ball. From the slow-motion footage of the impact the plate can be seen to be elevated roughly 2 cm on average due to the initial impact. The value of the if these abrupt peaks are in the order of magnitude 982.1,389.5 and 263.9 µm/m for the first to third occurrence. This being illustrated in *Figure 95*.

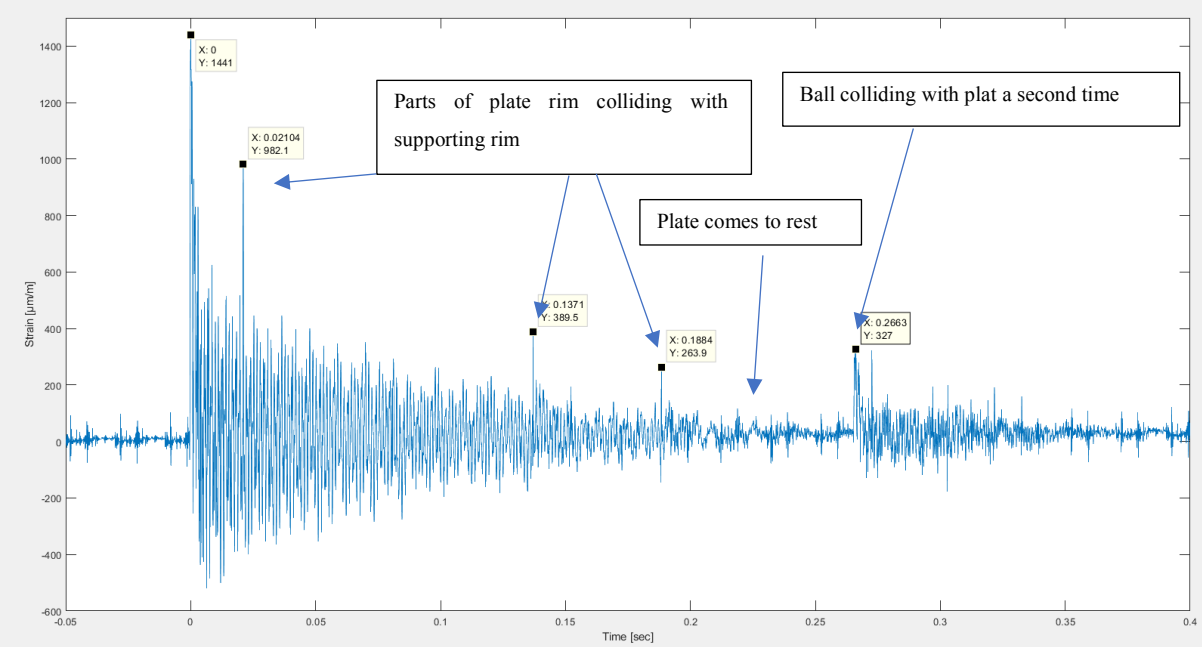

Figure 95: Result from ball drop tests in air from 2.25 m on the perforated steel plate, Measurement #4.

The number of conducted tests showed that the average first peak maximum is 1386.71 µm/m and standard deviation of 516.31 µm/m. Only a total of two bounces were visible in the results, which is clearly indicated in the graph.

Table 15: Measurement, averages and standard deviations for strain gauge 1, center strain gauge for strain and bounce heights.

Measurement nr #	first peak maximum [µm/m]	Bounce height [cm]	Average first peak maximum [µm/m]	Standard deviation first peak maximum [µm/m]	Average Bounce height [cm]	Standard deviation bounce height [cm]
1	1047	6	1386.71	516.31	10.54	3.91
2	1082	20				
3	1180	14				
4	1441	7				
5	2457	8				
6	2248	11				
7	1569	9				
8	873.8	11				
9	1186	8				
10	1031	10				
11	1139	12				

Large standard deviation observed in the result for the maximum of the first peak. As the standard deviation is roughly 37% of the average peak value. Average bounce height observed being 10.54 cm with a standard deviation of 3.91, being 37% of the average bounce height.

6.5.2.2 Ball Drop Method 2.25m – Perforated Plate in Water

Results from the perforated plates, where measurement nr. 9 was selected as a representative response for the average impact. Water level at 22 cm, with the water temperature at 25 °C

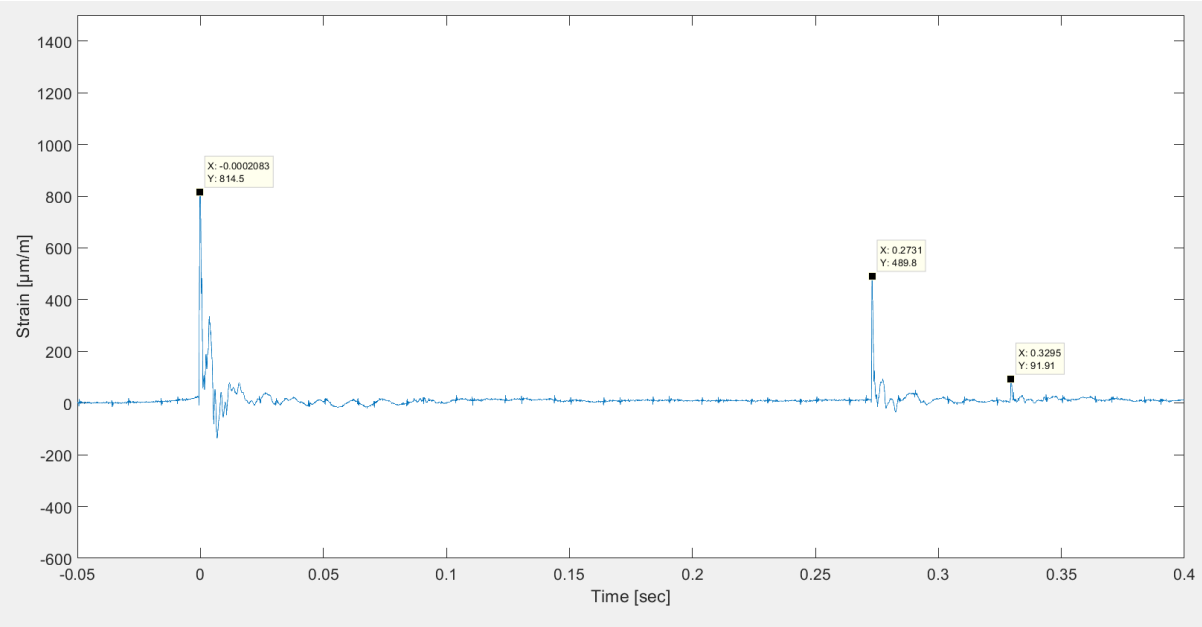

Figure 96: Result from ball drop tests in water from 2.25 m on the perforated steel plate (measurement #9).

In *Figure 96* three visible peaks are shown in the results but the height of the second bounce being less than 1 cm meant that the third is even less feasibly detected. However, the measurement indicates that plate itself is not lifted of its supports, even for impact energy of 9.7 J. The peak impact response of 814.5, 489.5 and 96.1 µm/m from the first to the third peak. Where the second peak is 60% of the first, and the third is 19.6% of the second peak. The deviation is 19.6% of the average value of the first peak maximum. It is important to note however that the third peak was not consistently present for all the measurements, as some only had two peaks.

Table 16: Measurement, averages and standard deviations for strain gauge 1, center strain gauge for strain and bounce heights.

Measurement nr #	first peak maximum [µm/m]	Bounce height [cm]	Average first peak maximum [µm/m]	Standard deviation first peak maximum [µm/m]	Average Bounce height [cm]	Standard deviation bounce height [cm]
1	815.9	7	823.3	161.7	6.1	1.2
2	989.6	9				
3	967.6	6				
4	941.9	6				
5	605.5	5				
6	529	5				
7	930.9	5				
8	858.5	5.5				
9	824.9	6				

The results in water indicate non-significant variation in the average bounce height as the standard deviation is 19.6% of the average bounce height. Interestingly the results show that percentage wise the standard deviation is identical to the first maximum and bounce height but is most likely coincidental in this case.

7 Discussion

In this chapter the results will be compared and discussed with regards to a multitude of factors, ranging from dampening effect in water, bounce & impact correlation, material properties & behavior and more. Overall this chapter aims to give answers to what was discovered in *chapter* 6, in addition to raising questions pertaining to the nature of impact loading measurements.

7.1 Comparison Between Results of Plate in Water and in Air

This section will tackle the important thesis question from the observed behavioral differences of the solid and perforated plate, in air and water.

7.1.1 "Cushioning effect" of Submerging Plates in Water

Submerging any material into a new medium play an important role with regards to material behavior and its response as shown from the results. Cushioning effect as it is referred to in this paper is the dampening or reduction in strain when submerging a material in a fluid denser than air such as water. The investigation conducted however lacked the accurate tools to directly measure the impact velocity, as this would require a slow-motion camera capable of filming at least 1400 frames per second. Capture rate should always at least twice as large as what you intend to capture (Nyquist frequency). Whilst camera used only had the capability of 240 frames per second. This was especially an issue when considering the maximum velocity seen from ball drop tests in air with velocity of 6.64 ms^{-1}. For the camera used (240 FPS), the time between each frame was 1/240 sec. However, in that given time frame the ball would has already moved 2.76 cm. Based on general sampling theory the largest velocity recordable is therefore 1.2 ms^{-1}. Unfortunately, even for the smallest velocity seen from the proctor drop from 15 cm was not possible as these velocities also exceed 1.2 ms^{-1}.Therefore, it was not possible to determine the velocity based on the footage, and the reason why impact velocities was calculated instead. Considering these limitations with regards to capture rate, it was therefore not possible to accurately discern the difference between velocity for the tests done in water & air.

The impact loading response and the kinetic energy of the mass before impact is very important and this is amount of energy is referred to in this paper as impact energy. This was calculated using equations from chapter "force impact energy balance". As mentioned in theory chapter is that when one is not able to determine mass velocity from video footage, then calculated values must suffice. Since one of the major goals is to determine the degree of damping effect.

Therefore, a conservative calculation of the velocity was preferred to confirm the difference between air and water tests.

For the proctor, the velocity was calculated based on an approximated 4 cm diameter surface area, as smallest area with a drag coefficient "$C_d = 1$ (based on long cylinder high Reynolds number), as the approximated value used in the calculations. *Figure 97* illustrates the approximated geometry used for the drag calculations.

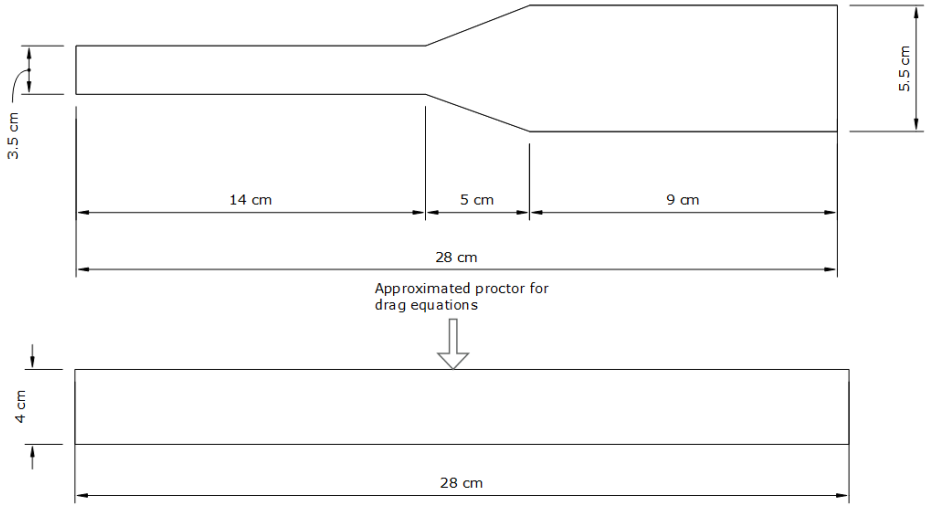

Figure 97: Drag equation approximated geometry for moveable mass in the proctor tests.

Additionally, the proctor is assumed to be fully submerged for drag and final velocity calculations, whilst the moveable mass has traveled 15 cm in water, only 50% of the mass is has travelled and been submerged in water. This ensures that drag is not under estimated in the calculations.

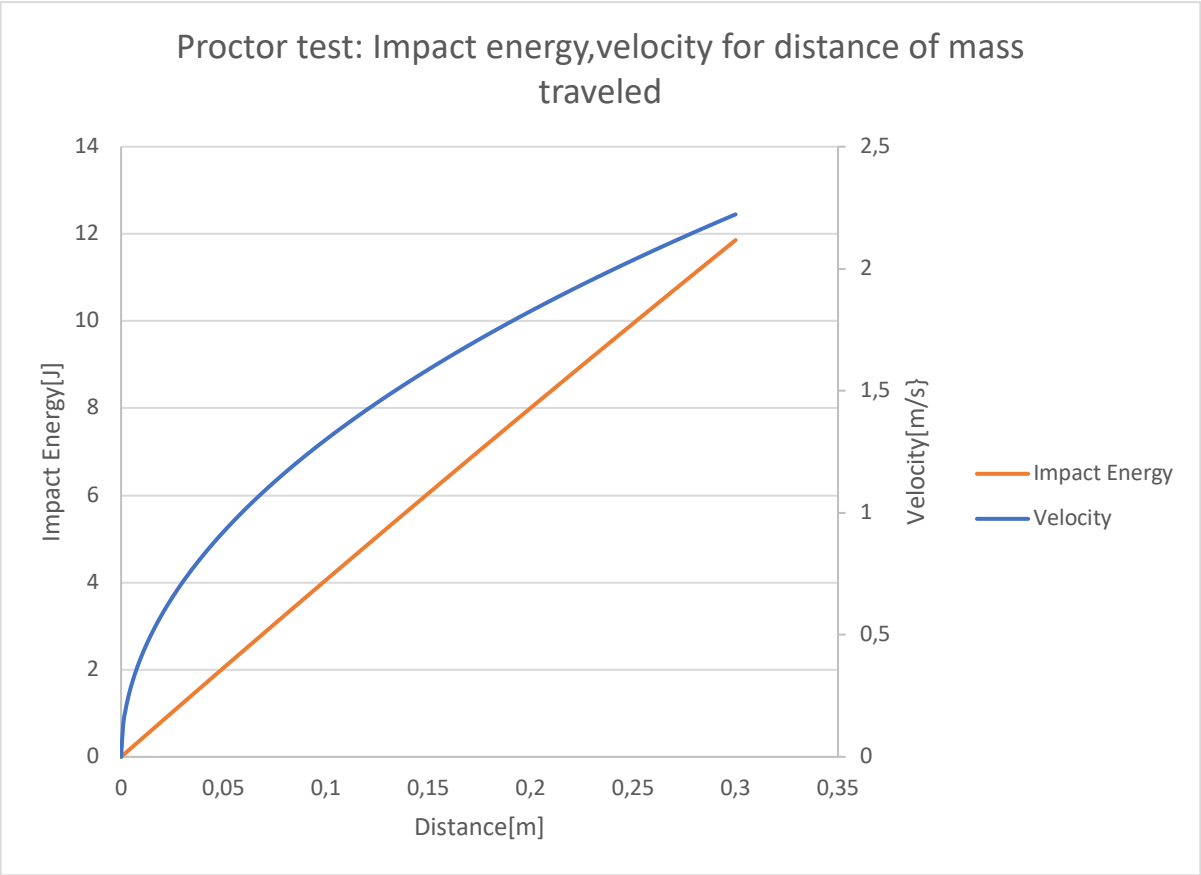

Figure 98: Proctor test: Impact energy, velocity for distance of mass traveled.

Having done these calculations, impact velocity & impact energy for 15 cm and 30 cm proctor test can be estimated. *Figure 98* illustrates calculated impact energy and velocities as mentioned.

The same was done with the ball drop test, where drag was based on the high turbulent value "C_d" of 0.5 with entrance velocity based on 2.05 m of frictionless free fall in air, as shown in *Figure 99*. Effect of surface interface upon impact is ignored and turbulent drag coefficient is used.

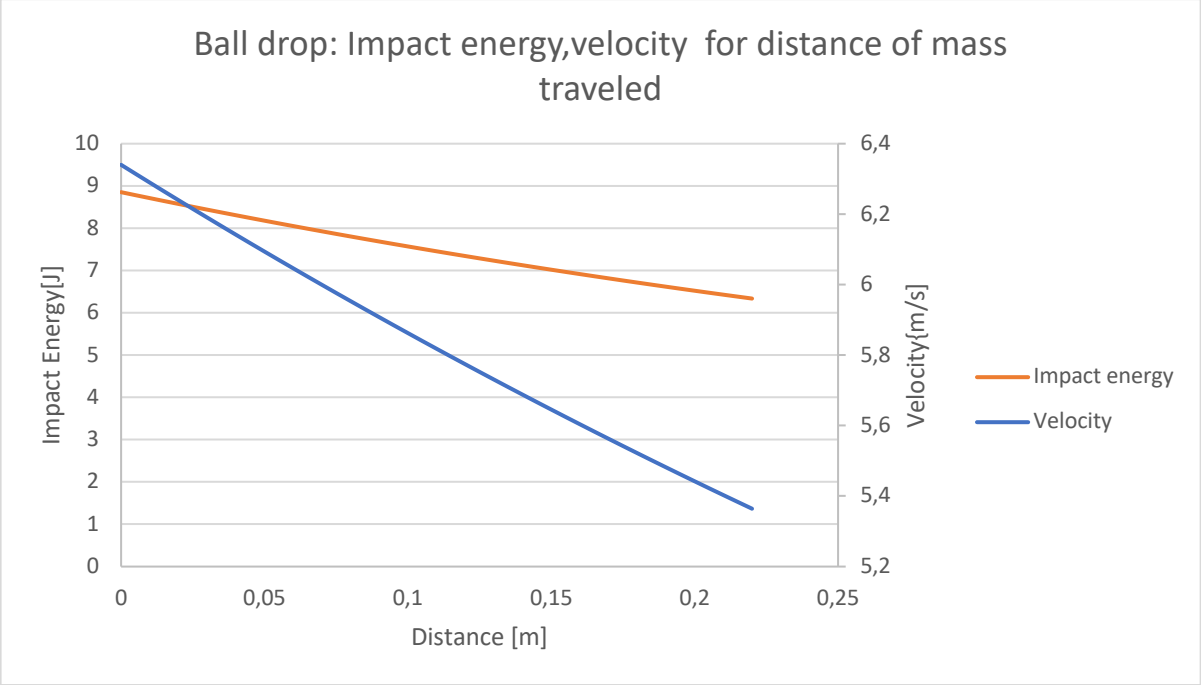

Figure 99: Ball drop test: impact energy, velocity for distance of mass traveled.

Values of impact energy and velocity can then be simply read of graph as the steel sphere has traveled 20 cm in water before impact.

Table 17: values for experiment type with their corresponding impact velocities and impact energy.

Fluid medium	Experiment type	Impact velocity[m/s]	Impact energy[J]
Air	30 cm proctor	2.42	14.12
	15 cm proctor	1.71	7.06
Water	30 cm proctor	2.22	11.856
	15 cm proctor	1.587	6.04
Air	2.25 m ball drop	6.34	8.84
Water	2.25 m ball drop	5.44	6.52

Comparing the average maximum peak based on all the different approaches combined with the calculated values of impact energy, it should be feasible to determine the degree of cushioning that occurs due to the plates being submerged.

7.1.1.1 Proctor Tests

Presentation of the results includes the standard deviation for all the measurements to give a clear indication of variation between the results in air and in water for both plate types. In addition to see of values are close to overlapping.

Table 18: Values for impact energy and corresponding peak averages and standard deviation for proctor tests in air & water.

Plate type	Experiment type	Impact energy [J]	First peak strain [µm/m]	Standard Deviation [µm/m]
Solid	30 cm proctor (air)	14.12	998.92	101.93
	15 cm proctor (air)	7.06	660.6	69.97
	30 cm proctor (water)	11.856	1029.64	66.83
	15 cm proctor (water)	6.04	701.37	31.17
Perforated	30 cm proctor (air)	14.12	1006.89	59.52
	15 cm proctor (air)	7.06	683.24	54.6
	30 cm proctor (water)	11.87	780.5	47.6
	15 cm proctor (water)	6.04	474.44	56.75

7.1.1.1.1 Solid Plate

First by evaluating the proctor tests for the measurements done with the solid plate, it was shown that that the results in air and water with regards to initial impact are virtually the same, with the measurements in water showing marginally larger values than the ones conducted in air, these values being displayed in *Figure 100*. These are very interesting results as one would expect the values from the impact to be greater in air as opposed to in water, as impact energy is reduced by traveling through fluid. The values based on the best fit line indicates strain for impact energy 6.04 J. Strain in air is estimated at 611.7 µm/m as compared to the measured the 701.36 µm/m, being 14.6% larger strain in water than in air. For impact energy of 14.12 J the expected impact in water is 1157.42 µm/m compared to measured 998.91 µm/m in air being a difference of 15.87% .

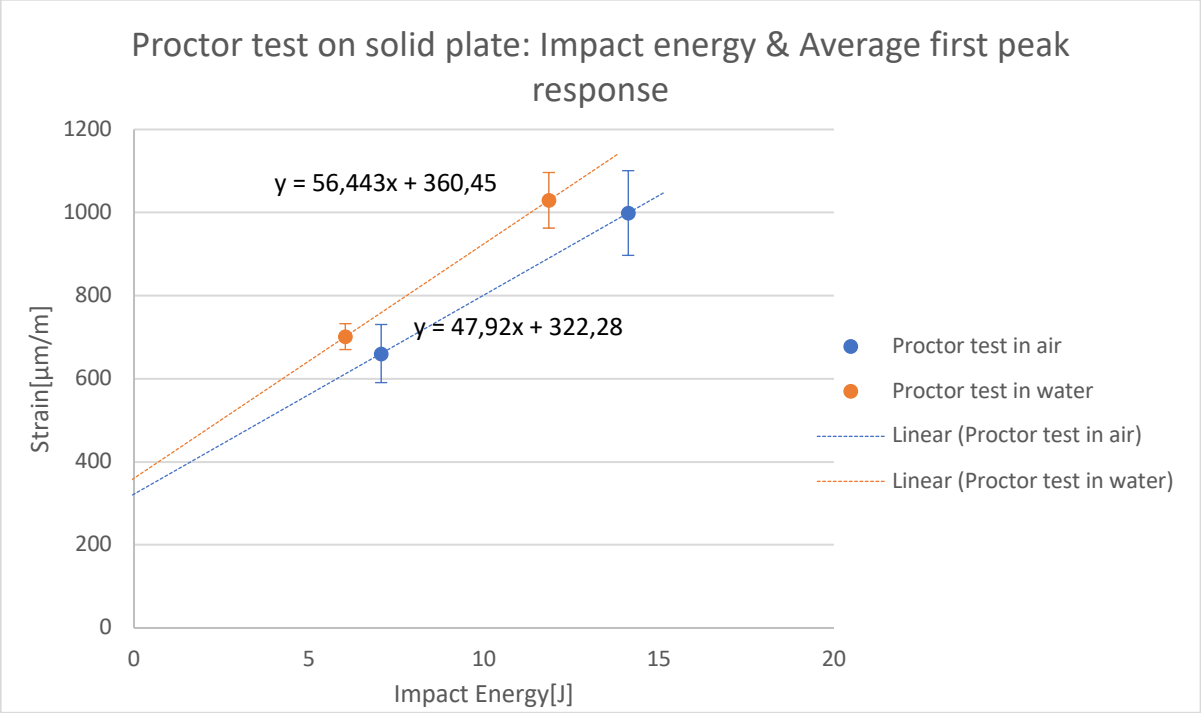

Figure 100: Illustration of the impact strain & impact energy correlation for solid plate from proctor tests.

When considering the error bars, a notable degree of overlap can be seen between the air and water correlation. This makes the seemingly large variation smaller as the proctor test in air overlap percentage is roughly 22.4% for at 11.856 J and 19% at 6.04 J. Additionally the impact energy calculation being conservative also contributes to a larger impact strain / impact energy ratio than reality. The most probable explanation is therefore that the difference between the results in air and water is marginal, but due to approximation such as overlap from experimental variation. This can be explained assuming energy is the same (no energy is lost) then the results in air and water would become identical.

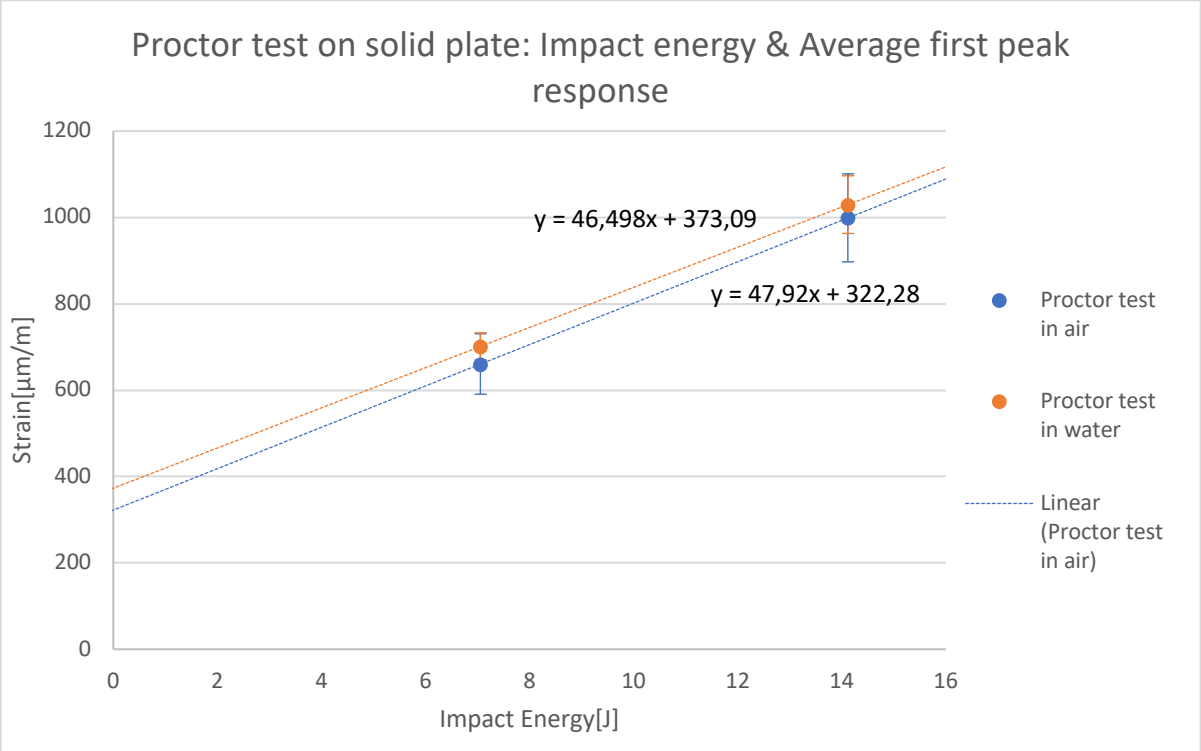

Figure 101: Illustration of impact strain vs impact energy correlation when energy loss is assumed to be zero in water.

With difference in impact energy assumed zero shown in *Figure 101* there is only a slight larger value for air than in water, but the difference is only 3% and with the standard deviation from the results the data points have a 100% overlap as compared to the previous 19-22%. However, it is important to note that variation due to background noise was not incorporated into the results due to complexity with regards to weighting the noise response at each point in time with the statistical variation due to the measurements themselves. This difference is not major but would more than make up for 5% difference between the two.

7.1.1.1.2 Perforated Plate

Looking at the perforated plate the behavior, the results being represented in *Figure 102.*

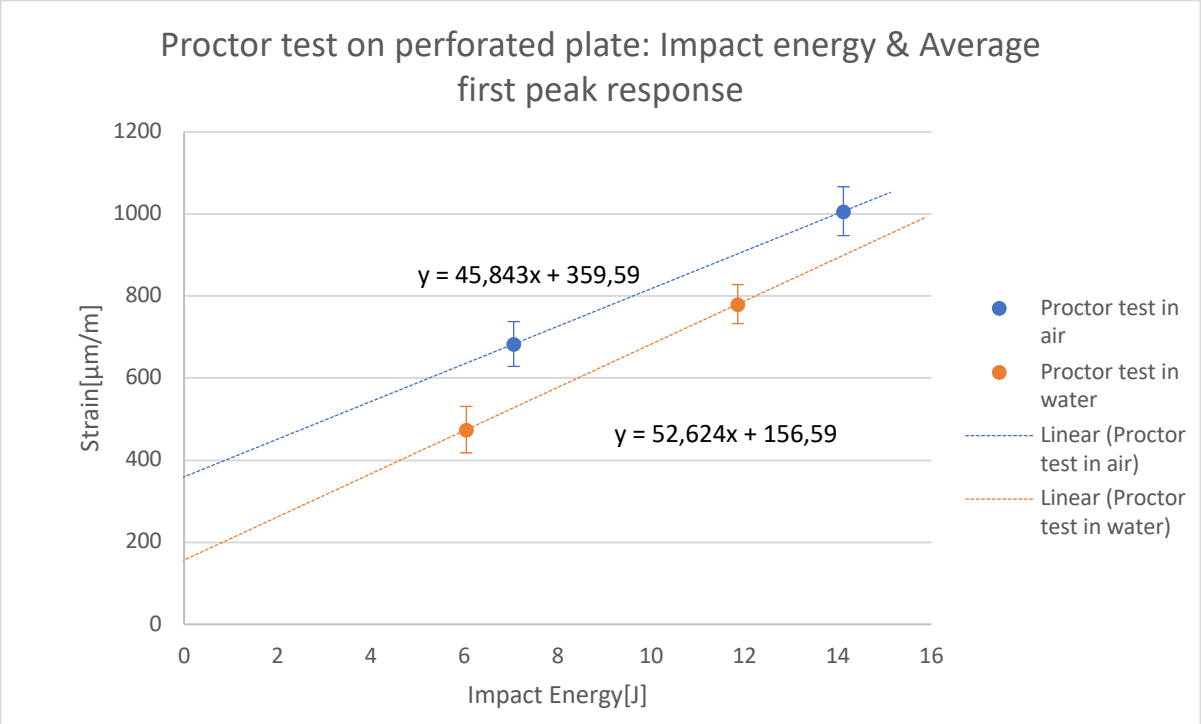

Figure 102: Illustration of the impact strain & impact energy correlation for perforated plate from proctor tests.

Based on these values, it seems to indicate a clear difference between the measurements conducted in water as opposed to the ones in water. The difference however is reduced as impact energy increases, such that the largest difference is at 6.11 J with 34.8% larger strain in air is expected. The least amount of variation between air and water is when impact energy is 14.12 J, where strain is 12.2% larger in air (based on point values only). Taking into consideration the error bars there is no % overlap at 11.856 J and 6.04 J. The % difference is however quite small being 1.5% and 8.8% at 11.856 J and 6.04 J respectively. In terms of strain this is 840.5 and 828.1 µm/m in air and water at 11.856 J, and 578.3 and 531.2 µm/m in air and water at 6.04 J.

Lastly if we do the same assumption & comparison as conducted for the solid plate, by assuming the no loss in energy from the mass moving through water, the maximum achievable difference between impacts in water and in air can be shown. This being illustrated in *Figure 103.*

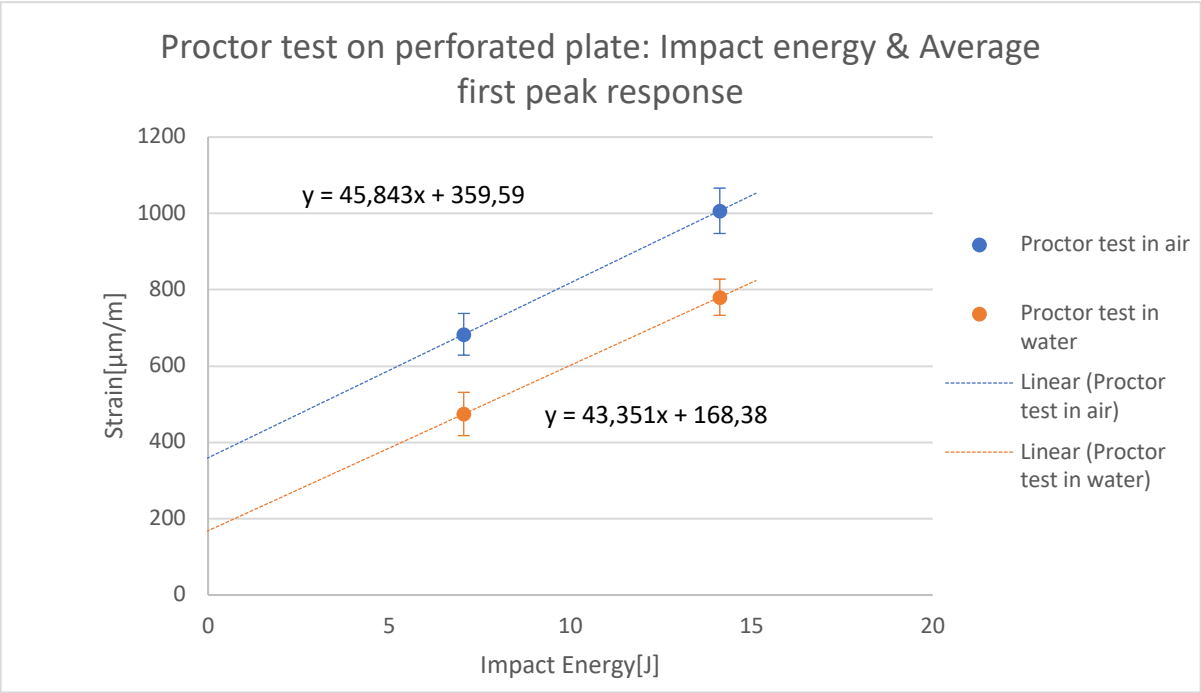

Figure 103: Impact strain & impact energy correlation for perforated plate when zero energy loss is assumed in water.

Lastly the energy loss is assumed to be zero, as was done for solid plate proctor tests. When energy loss is assumed to be zero a large gap between the two emerges. The ratio between the strain and impact energy can also be used to indicate the difference between air & water. This being a particularly good option for ball drop tests done on the perforated plates as proper measurements was only done for 2.25 m.

Table 19: values for impact energy and corresponding peak averages and standard deviation for proctor tests in air & water.

Plate type	Experiment type	Fluid medium	Impact energy [J]	Strain [µm/m]	Strain/impact energy ratio [µm/m/J]	% reduction in strain/IE ratio from air to water [%]
Solid	30 cm proctor	Air	14.12	998.92	70.74	-22.76%
		Water	11.856	1029.64	86.85	
	15 cm proctor	Air	7.06	660.60	93.57	-24%
		Water	6.04	701.37	116.12	
Perforated	30 cm proctor	Air	14.12	1006.89	71.3	8%
		Water	11.856	780.5	65.53	
	15 cm proctor	Air	7.06	683.24	96.77	19.76%
		Water	6.04	474.44	77.65	

7.1.1.1.3 Impact Profile for Solid & Perforated Plate in Air vs Water

The topic of impact dynamics is both complex and varied, with a myriad factor that contribute to the impact loading response. To shed light on some factors contributing why solid plate does not seem to gain any effect from being submerged into water, by looking at both solid plate and perforated plate measurements as shown in *Figure 104*.

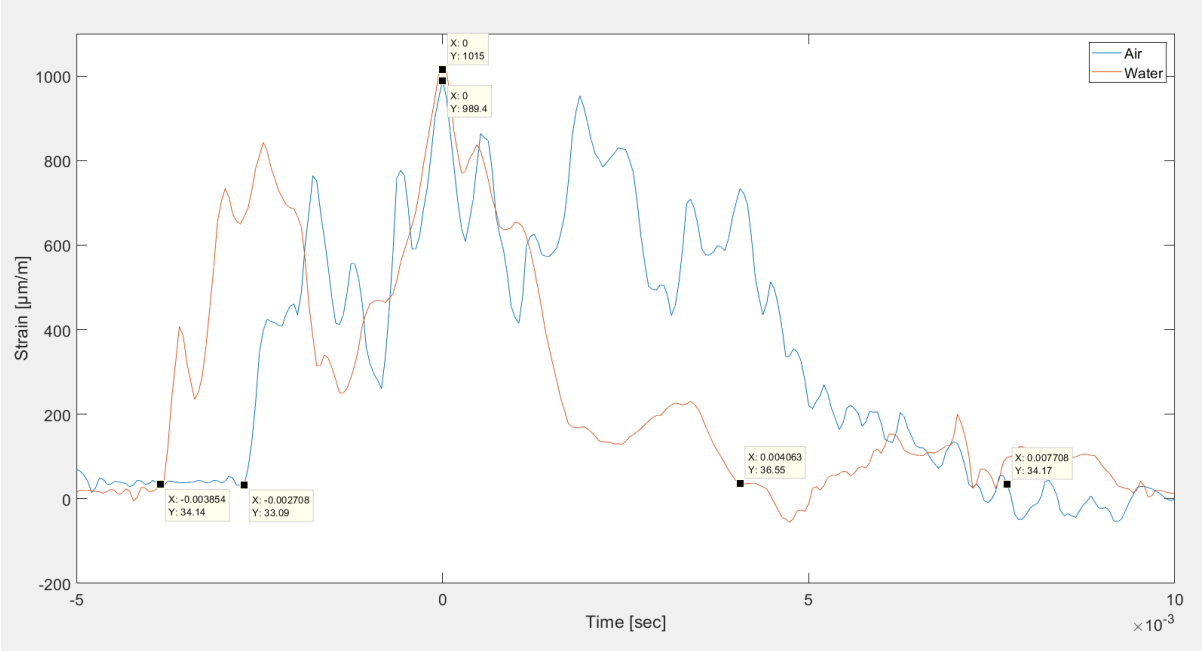

Figure 104: Comparison of the initial peak for solid plate in air vs water (measurement# 3 air and #1 water being used).

Comparing the two peak impact responses from a moment before impact until strain is reduced back to its initial value, it is seen that in air this duration is 10.416 ms compared to 8.46 ms in water. Indicating that the impact duration itself is reduced in water. Additionally, during this longer duration, the material is subjected to higher strain for a longer period, meaning that the average amount of strain per second is higher in air vs water. This is done by evaluating the same time frame being 15 ms interval. However, it is important to note that this calculation is only to give an indication of the difference between these two responses and is not meant to be 100% fair comparison.

Continuing with this approach the strain/second for air and water can be determined to be 6.40e+06 µm/m/s and 5.04e+06 µm/m/s respectively which is a 26.7% larger strain per second on average than for impact response in water. Further analysis of the of the impact profile for air and water with the solid plate is that profile is much more distinct and less jagged, with two distinct sub peaks as compared to multiple.

For perforated plate impact duration measured from impact until strain is reduced to the initial strain is measured to be 9.896 ms 7.916 ms respectively for air and water, illustrated in *Figure 105.* Same as for the solid plate the duration reduced from air to water. Then by calculating the average strain over the time interval of 15 ms. The average strain per second in this case is 6.83e+06 µm/m/s in air and 4.10e+06 µm/m/s in water.

A difference of 66.44% larger strain in air as compared to water, this being a much larger difference than what was observed for the solid plate.

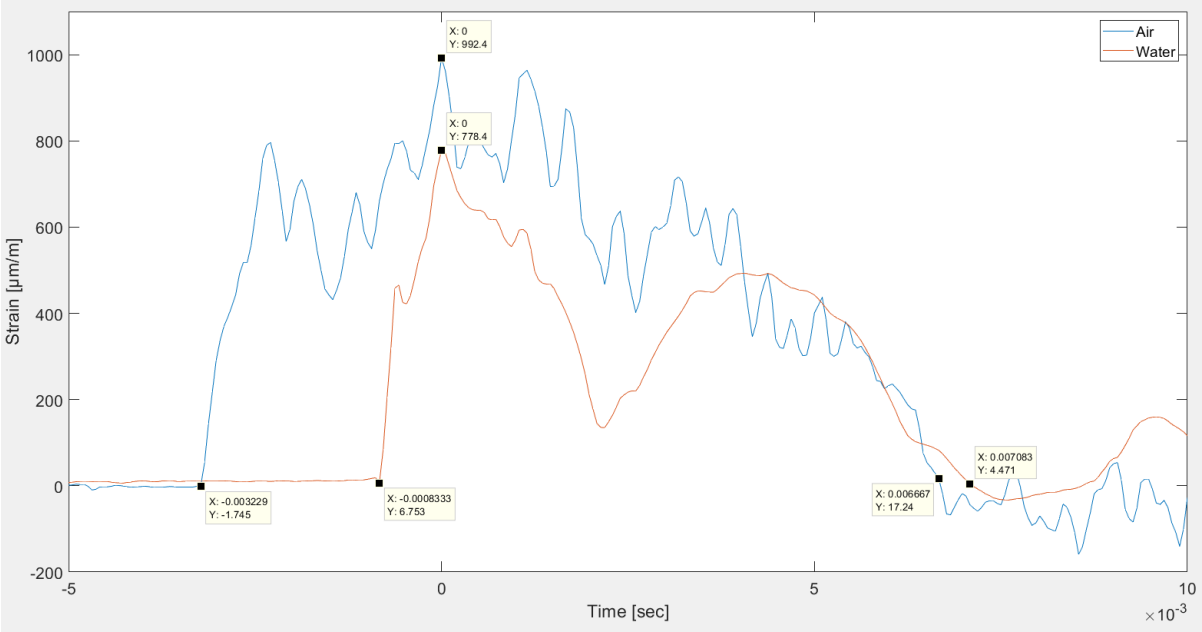

Figure 105: Comparison of the initial peak for perforated plate in air vs water (measurement #10 air and #2 water being used).

The peak profiles itself show very similar traits seen for the solid plate. For peak profile in air for both solid and perforated plate are very jagged, but for the perforated plate see less variation as the maximum peak to valley variation is only 200 µm/m as compared to 400 µm/m for the solid plate. In water the peaks are much more rounded, especially for the second sub peak.

7.1.1.2 Ball Drop Test 2.25 m

For the impact loading measurements done with steel sphere, there was a large degree of variation in the peak maximum as shown in the results ranging from 29.6-37% variation in air and 18-20% in water, with solid plate showing the lowest variation for both air & water. Values displayed in *Table 20.*

Table 20: values for impact energy and corresponding strain averages and standard deviation for ball drop tests in air & water.

Experiment type	Plate type	Fluid medium	Impact energy[J]	Strain [µm/m]	Strain/impact energy ratio [µm/m/J]	% reduction in strain/IE ratio from air to water [%]
Ball drop test 2.25 m	Solid	Air	9.71	1730.769	178.24	-40.73%
		Water	6.52	1778.462	250.84	
	Perforated	Air	9.71	1386.71	142.81	18.69%
		Water	6.52	823.3	116.12	

The trend with regards to dampening seems to persist for the ball drop test as well, further indicating that perforated plate submerged in water have a profound effect on strain produced upon impact. Values regarding the solid plate indicate an even larger increase in strain per unit of joule for the initial impact.

7.1.1.2.1 Strain Variation 2.25m Ball Drop

Problem with the variation in the results being so large, is that such a significant effect on the results. To illustrate this, two additional *Tables 22 & 23* are created with one for the largest recorded values in air combined with the smallest in water and vice versa, using standard deviation from measurements. This sub section should therefore be able to illustrate precision from measurements.

Table 21: values for impact energy and corresponding strain averages and standard deviation for ball drop tests in air & water.

Experiment type	Plate type	Fluid medium	Standard deviation [µm/m]
Ball drop test 2.25 m	Solid	Air	464.12
		Water	235.99
	Perforated	Air	516.31
		Water	161.7

For the minimum strain possible in air combined with the maximum strain in water combined gives the following results as shown in *Table 22*. The strain would then show an increase in strain per unit of impact energy (energy ratio) going from air to water, even the perorated plate is shown to also increase in this scenario.

Table 22 values for impact energy and corresponding strain averages and standard deviation for ball drop tests in air & water (max water, min air).

Experiment type	Plate type	Fluid medium	Impact energy[J]	Strain [µm/m]	Strain/impact energy ratio [µm/m/J]	% reduction in strain/IE ratio from air to water [%]
Ball drop test 2.25 m	Solid	Air	9.71	1266.64	130.44	-136.73%
		Water.	6.52	2014.458	308.96	
	Perforated	Air	9.71	870.4	89.63	-57.31%
		Water	6.52	939.42	144.1	

For the greatest difference in *Table 23* between air and water can be achieved by the same process only vice versa, where maximum possible strain from air is combined with the smallest values possible in water. In this case the strain/impact energy ratio is virtually identical.

Table 23: values for impact energy and corresponding strain averages and standard deviation for ball drop tests in air & water (min water vs max air).

Experiment type	Plate type	Fluid medium	Impact energy[J]	Strain [µm/m]	Strain/impact energy ratio [µm/m/J]	% reduction in strain/IE ratio from air to water [%]
Ball drop test 2.25 m	Solid	Air	9.71	2194.89	226.04	-4.00%
		Water	6.52	1542.496	236.57	
	Perforated	Air	9.71	1903.02	195.98	48.22%
		Water	6.52	661.6	101.47	

Based on the values from these tables, it becomes apparent that there is a significant degree of variation between the individual measurements as the difference between effect from going from air to water can by a factor of over 100%. This being a very strong indication of the degree of local impact variation due to steel sphere which is a much closer approximation to a point load than the proctor used in the other experiments.

7.1.2 Bounce Height vs Impact Loading Response

The measurement of the bounce height was expected to show some degree of correlation to first peak maximum seen in the results. However, based on the measurements a weak correlation between bounce height and impact loading was discovered, especially for ball drop measurements. The possible reasons for this will be highlighted in this section.

Firstly, when considering the physics that was mentioned earlier, is that energy loss in the system is not consistent with the force of the impact. Meaning that a large impact will cause more energy loss as opposed to lesser one. Looking at difference between the 30 cm and 15 cm tests conducted with the proctor shown in *Figure 106*, which showed very consistent values with regards to standard deviation for bounce height. It was shown that the bounce height was roughly (values approximated to closest cm) the same for both tests conducted on the perforated plate. Being 6 cm ± 0.5 for 30 cm tests and 4 cm ± 0.5 for 15 cm tests for both the solid and perforated plate.

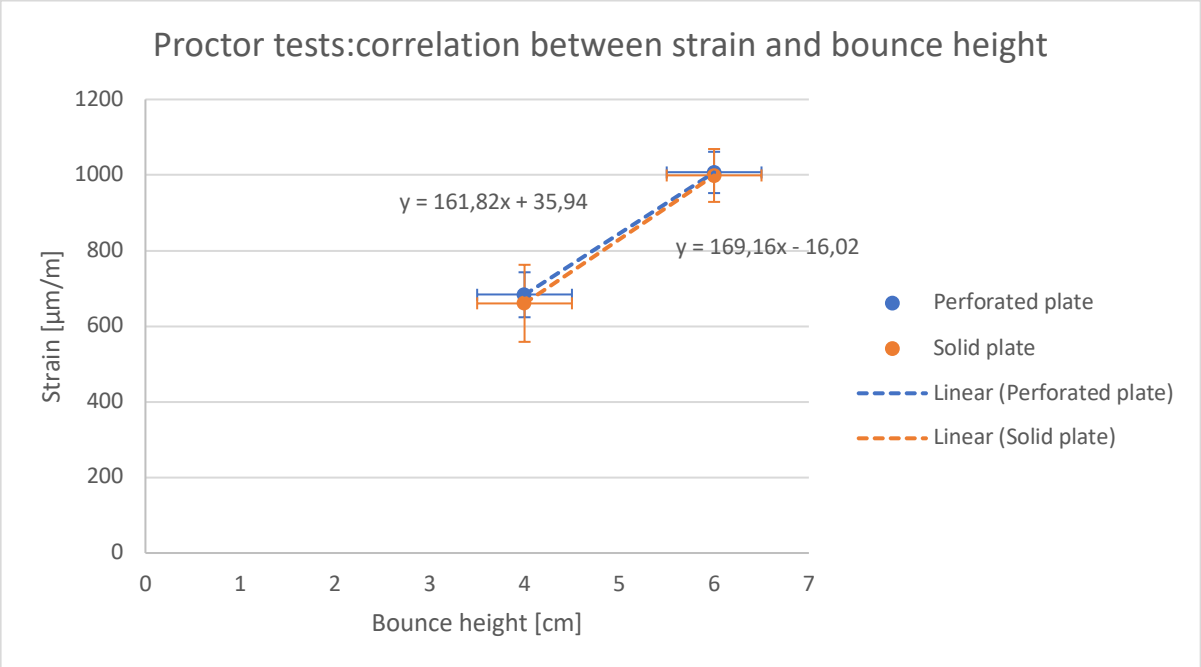

Figure 106: Bounce & strain correlation for proctor tests 30 & 15 cm for solid and perforated plate.

The results based on strain produced on initial impact coupled with the measured bounce height confirm general physics surrounding impact momentum. Solid and perforated plates are shown to overall in this incident as measurement as smallest figure that is possible to accurately measure from the video footage was 0.5 cm. This means that if there was a difference in bounce height for solid and perforated plate smaller than 0.5 cm then it would not be possible to measure it.

If the bounce height could be measured down to a higher degree of accuracy, then the correct degree of correlation between 30 cm and 15 cm tests in air could be determined. Despite this fact, it was still expected to show a positive correlation as shown in *Figure 106* but in this case it is difficult validate the results because of the small variation in bounce height in relation with the standard deviation. The uncertainty pertaining to the bounce height must also be mentioned, because as displayed in the results chapter, the difference between the bounce height for 30 cm and 15 cm was 2 cm for both solid and perforated plate. Even if there is no overlapping bounce height for these two measurements. Uncertainty of 0.5 cm is roughly 16.7% for smallest recorded bounce height and 8.3% for the largest.

Scenario which showed the weakest correlation or at least the smallest amount of correlations was the ball drop tests. Using the plots to analyze the values measured for the tests conducted in air. These results are meant indicate behavioral trends with regards to bounce height after the first impact and is not mean to precisely determine exact relationship. Measurements are presented using error bars which in this case are based on standard error "S_e" (Anon., n.d.) and not standard deviation is based of sample average and not individual measurements. Shown in the equation below.

$$S_e = \frac{S_{n-1}}{\sqrt{n}} \qquad \textit{Equation 20}$$

Then based on this scatterplot of data a linear best fit line is used to indicate trend behavior shown in *Figure 107*. Results from the measurements show that the best fit line indicates a downward trend as opposed to an increasing one for all the tests conducted in air. This being the opposite of the expected relation. Best fit line function shows however that the correlation is extremely weak as the coefficient of determination "R^2", where the value is approximately 0, indicating a very poor fit.

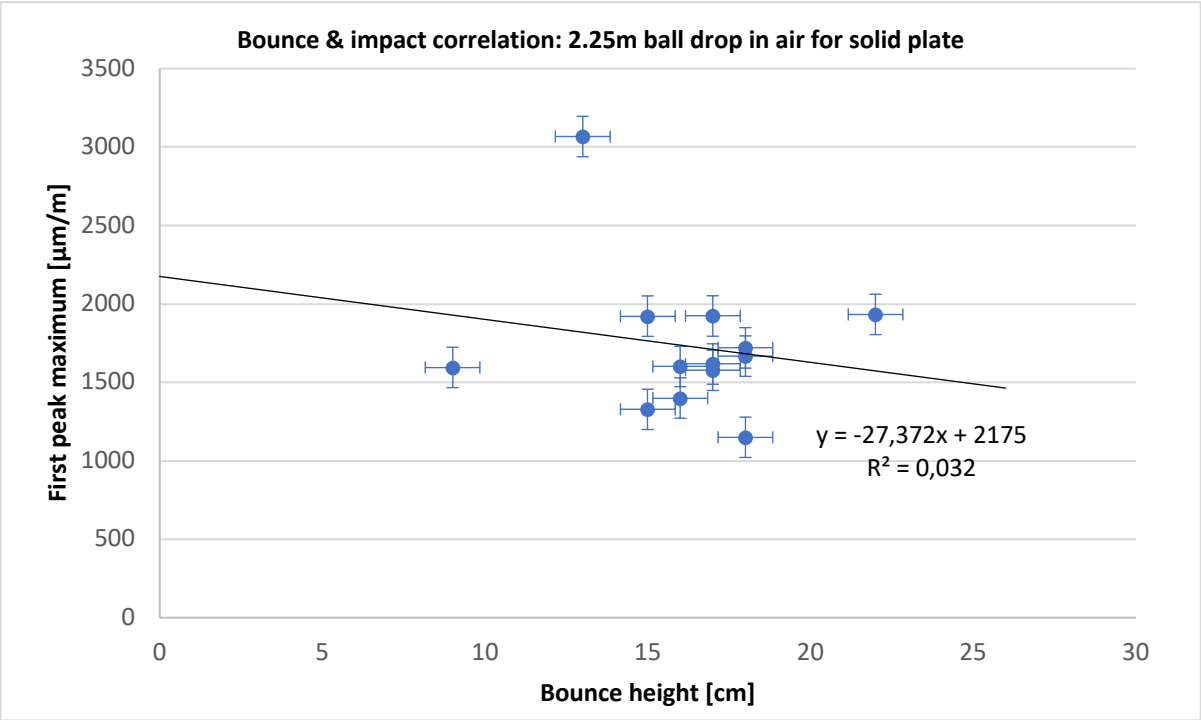

Figure 107: Bounce height & strain correlation for 2.25m ball drop on the solid plate in air.

For the solid plate measurement shown in *Figure 108*, cluster is centered around 15-18 cm spectrum with variation in first peak maximum from 1150 to 1950 µm/m, which all show a very weak correlation. There is also one major outlier with regards to this being 13 cm bounce height, exceeding strain if 3000 µm/m.

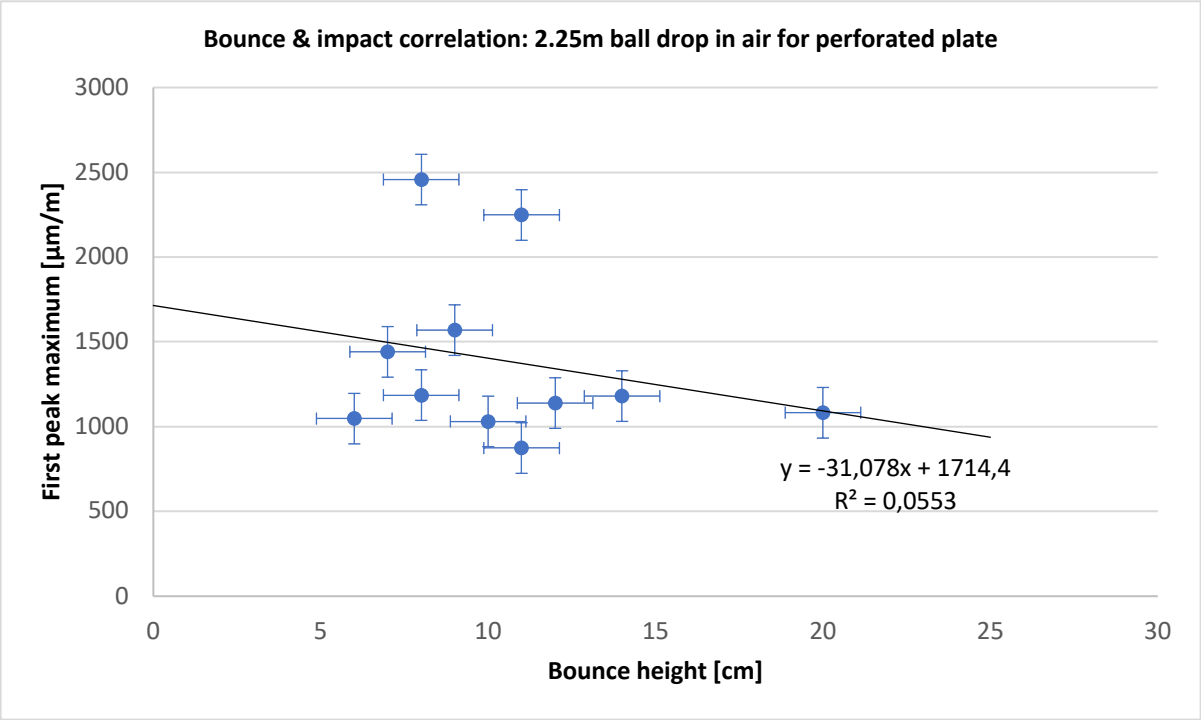

Figure 108: Bounce height & strain correlation for 2.25m ball drop on the perforated plate in air.

For the perforated shown in *Figure 109*, the plate the results were more scattered than for the solid plate, with bounce height varying from 6 cm to 14 cm. However, the best fit line indicates a poor fit for both the solid and perforated plate measurements, with the perforated plate being marginally better.

The tests conducted in water on the other hand overall showed a more consistent result, as the relative standard deviation for tests in air was twice as large as the one conducted in water (37% in air vs 19.6 % in water from perforated plate test). Investigating the correlation based on measurements done in water shows an upwards trend is shown instead, with a much larger coefficient of determination. However, when evaluated by itself the value is still very low indicating poor fit, as a perfect fit would yield $R^2=1$.

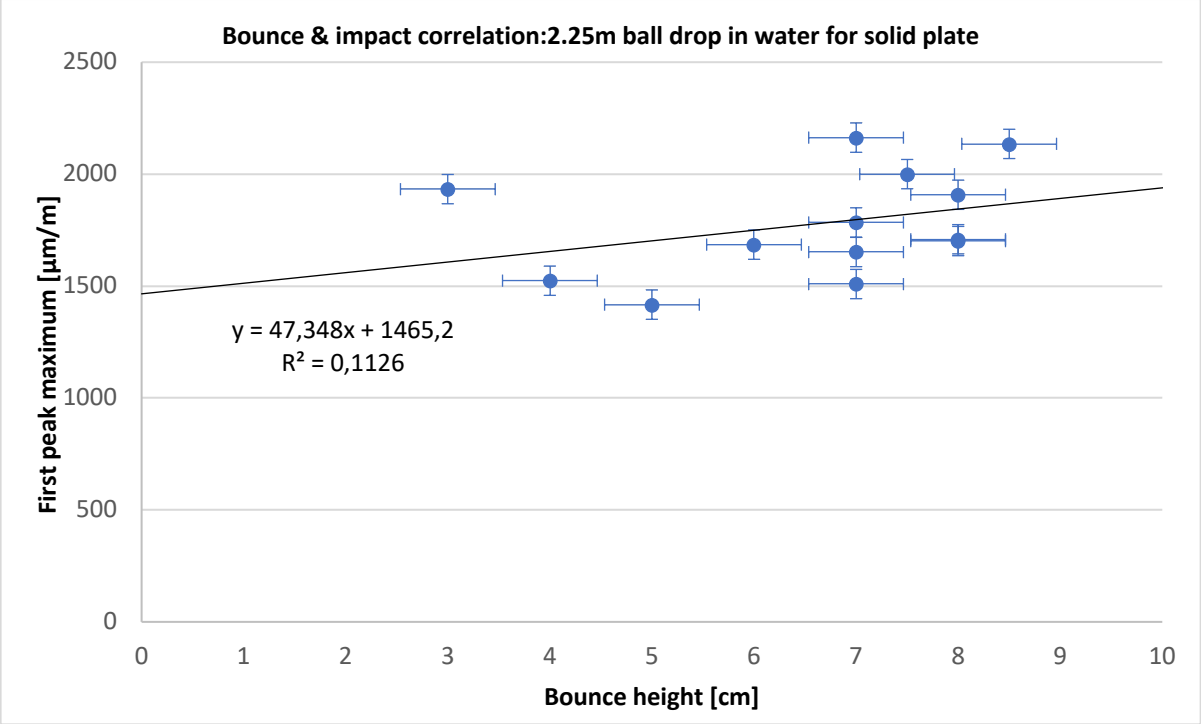

Figure 109: Bounce height & strain correlation for 2.25m ball drop on the solid plate in water.

This goes for both the solid and perforated plate as both have an overall poor fit in the grand scheme of things, but the perforated plate showed the best R^2 of all the results displayed in *Figure 109 & 110.*

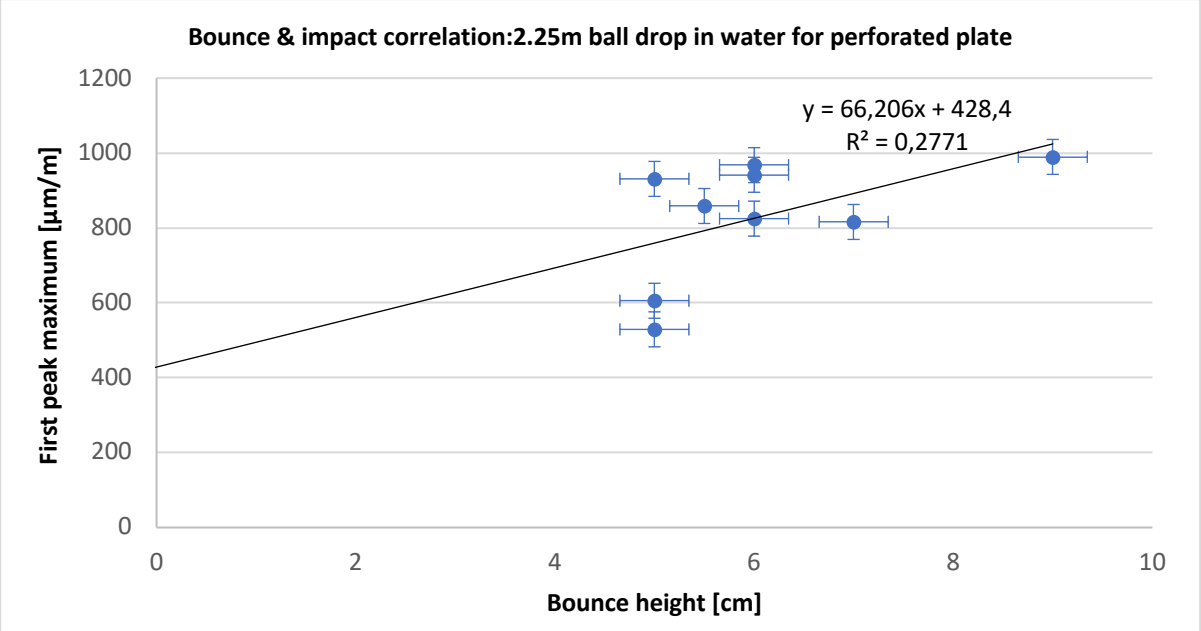

Figure 110: bounce height & strain correlation for 2.25m ball drop on the perforated plate in water.

After inspecting the relationships of bounce height & impact correlation in both air and water for solid and perforated plate, show little indication of an increasing or decreasing correlation, as the issue is seemingly more complex and initially assumed.

There are two major issues contributing to this, one being inconsistent energy transfer between the plate and the steel ball. One possible explanation for this, is that ball drop delivers a very concentrated impact as opposed to the proctor. This means that measurements become much more sensitive to off-centered impacts. The second issue is that in air, the energy amount in combination caused a much larger deviation in the results as compared to tests in water. This is clearly conclusive based on the results which showed that for solid and perforated ball drop tests. Having a large distance for the target to drop meant that there was a larger variation of impacts documented, with many of the ball rebounds showing an angle after impact. These being telltale signs of offset impacts which is portrayed in *Figure 111.*

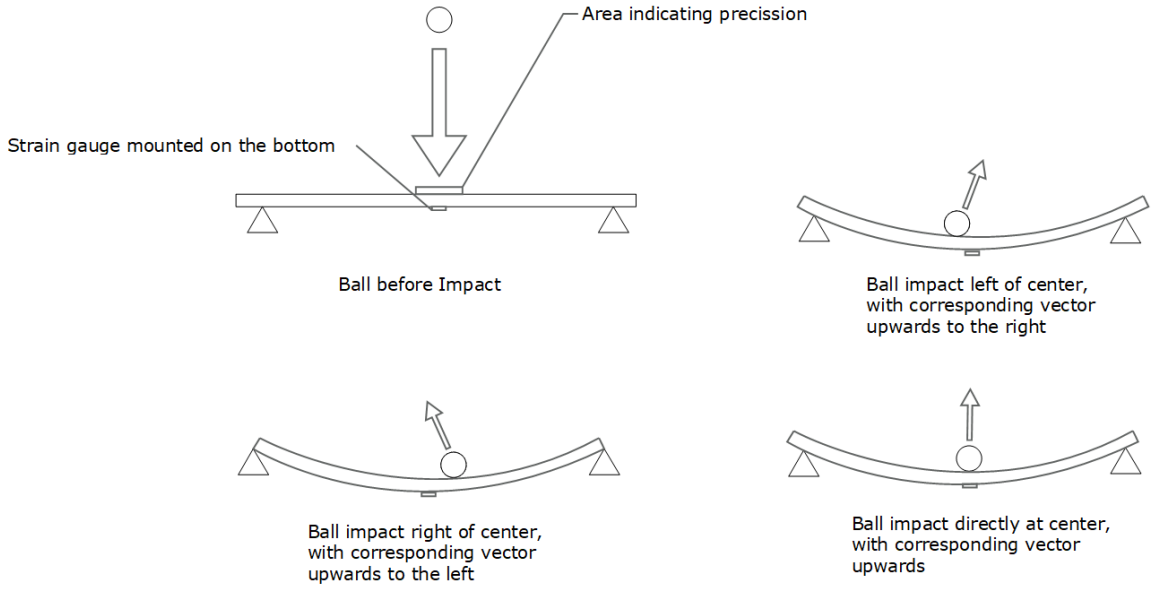

Figure 111: Diagrams illustrating variation in vector direction with regards to momentum/velocity after impact.

The horizontal momentum imparted to the plate is not the issue, but due to the strain gauges sensitivity with regards to impact area. Even as the PVC pipe was kept perfectly vertical and ball was released from the center of the pipe everytime, because the ball is released by hand means that small amount of force may be applied each time it is released causing an ever so slight change in the horizontal direction. Since the ball never touched the walls of the pipe during decent, meant that the maximum possible variation was 1.35 cm of center in any direction. Making the total possible seperation between two impacts 2.7 cm (larger then the length of strain gauge.

7.1.3 Impact Profiles: First & Second Impact

The measurements presented in the results chapter are based on them being closest to the average strain measured from all measurements. The reasoning behind this was that presenting all #1-10 measurements in one plot, would detract the focus from overall impact response. This section aims to sow the overall precision of the measurements performed in this paper. Air tests are not displayed in this section, since impact response was not distinguishable when all measurements are simultaneously displayed (dampening & frequency difference).

7.1.3.1 30 cm Proctor Test on Perforated Plate in Water

Impact response for 30 cm height proctor tests displayed consistent results based on the standard deviation of 47.6 µm/m. This being displayed in *Figure 112*.

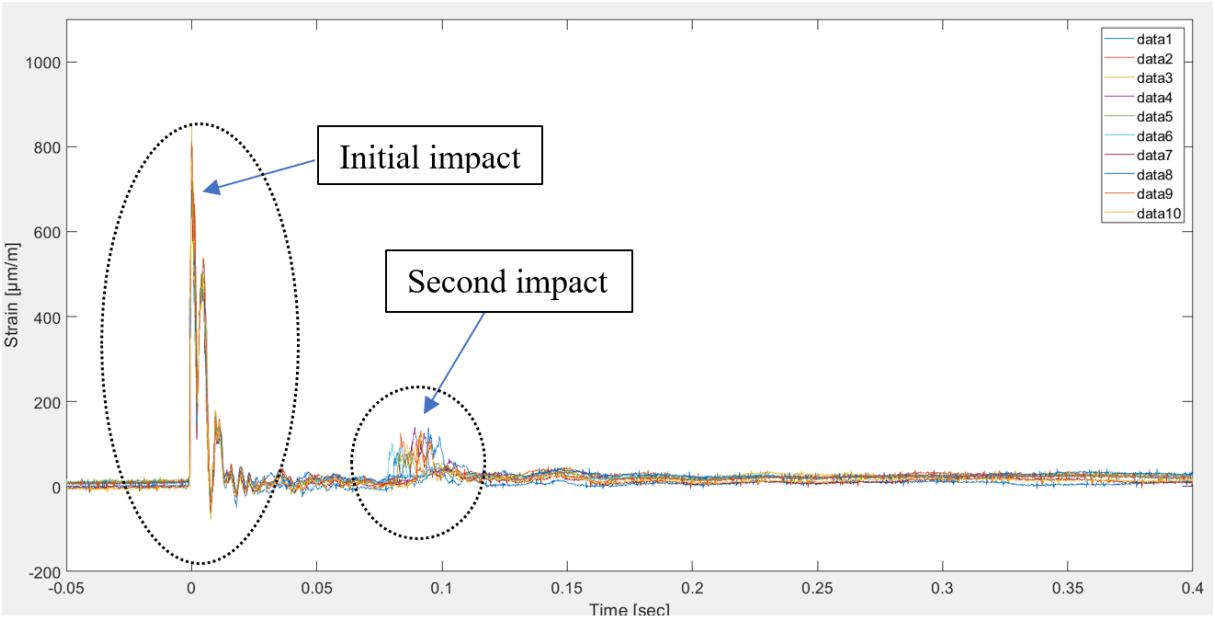

Figure 112: Impact response for 30 cm proctor test in water showing measurements #1-10.

The focus area for the is on the impact response produced on the initial and second impact, with the first impact showing the highest degree of precision(repeatability) relatively to the second impact response.

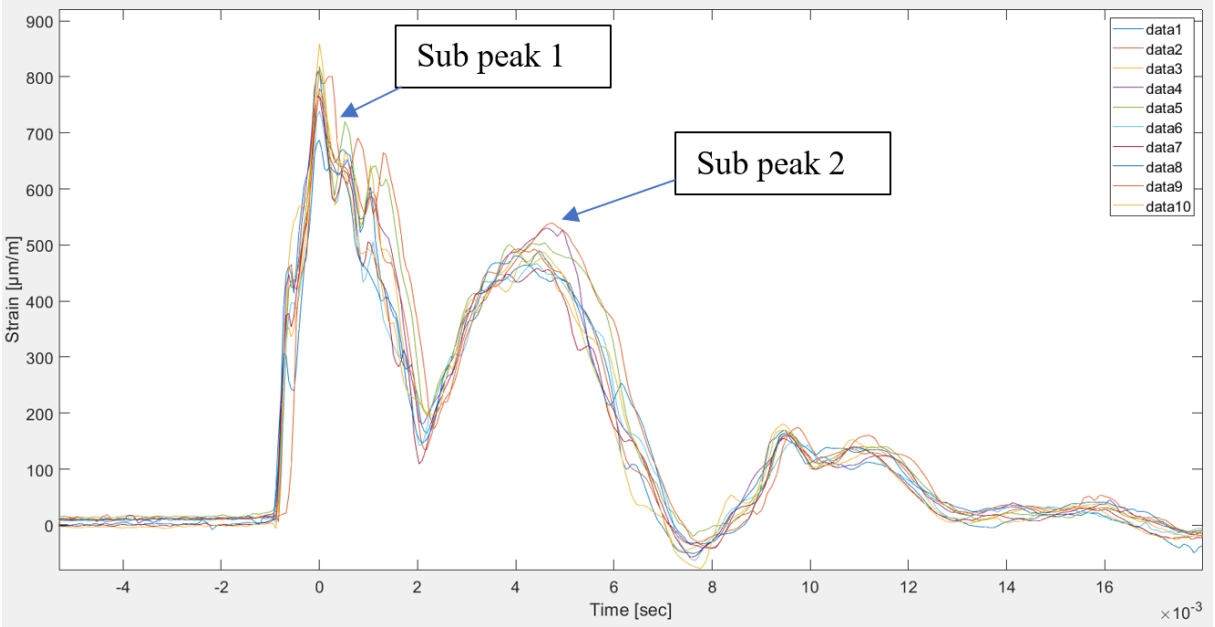

Figure 113: Impact profile from the initial impact, measurements #1-10.

Impact profile produced from initial impact demonstrate very tight and consistent response being produced from the measurements. Variation between the sub peak seen for the first and second is also something to note. The largest difference is 850 and 430 µm/m, a reduction of approximately 50% from first sub peak to the next. Illustrated in *Figure 113*.

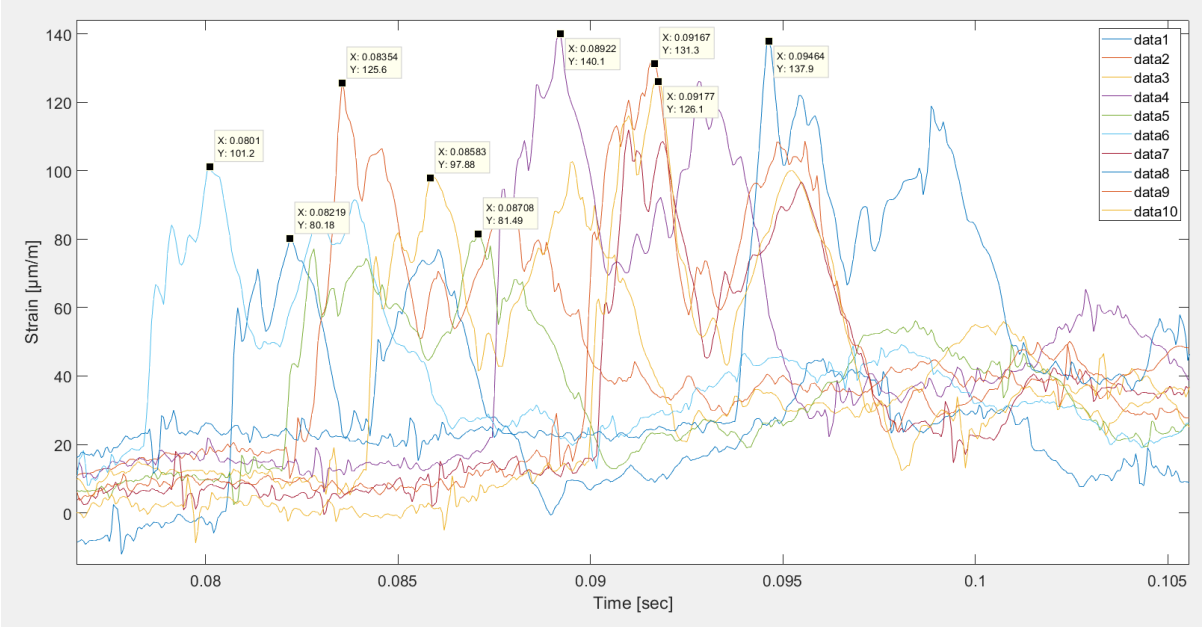

Figure 114: Impact profile from second impact for 30 cm proctor test for measurements #1-10 (data 1-10).

For second impact shown in *Figure 114*, the largest difference in strain between the peaks are 40 µm/m. The variation in bounce height can also be inferred partially from the time difference. For the first and the last maximum from the second impacts in the data set was measured to be 0.015 seconds. This equates to a difference of 15.79 % between them.

7.1.3.2 2.25m Ball Drop on Perforated Plate in Water

For the ball drop tests, it was shown that these tests had the largest variation with regards standard deviation of all the tests conducted. Starting off by looking at the measurements from the perforated plate in water illustrated in *Figure 115*, shows that only measurement #1 (data1) has the characteristics of 3 peaks whilst the majority shows only two distinguishable peaks. This section will therefore focus on the impact loading response profile for first and consecutive impacts, to show similarities and differences between the measurements.

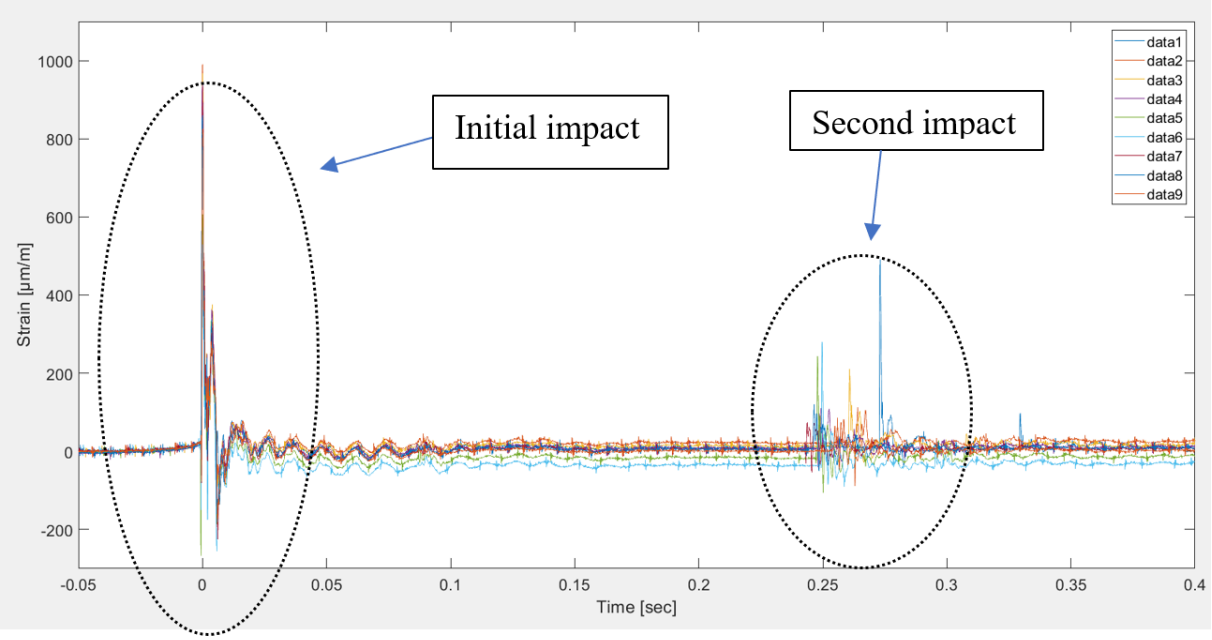

Figure 115: Impact loading response for measurements #1-9 for a perforated plate in water highlighting areas of focus.

First by looking at the ball drop measurements in water for the perforated plate, the variation between each result can be clearly indicated.

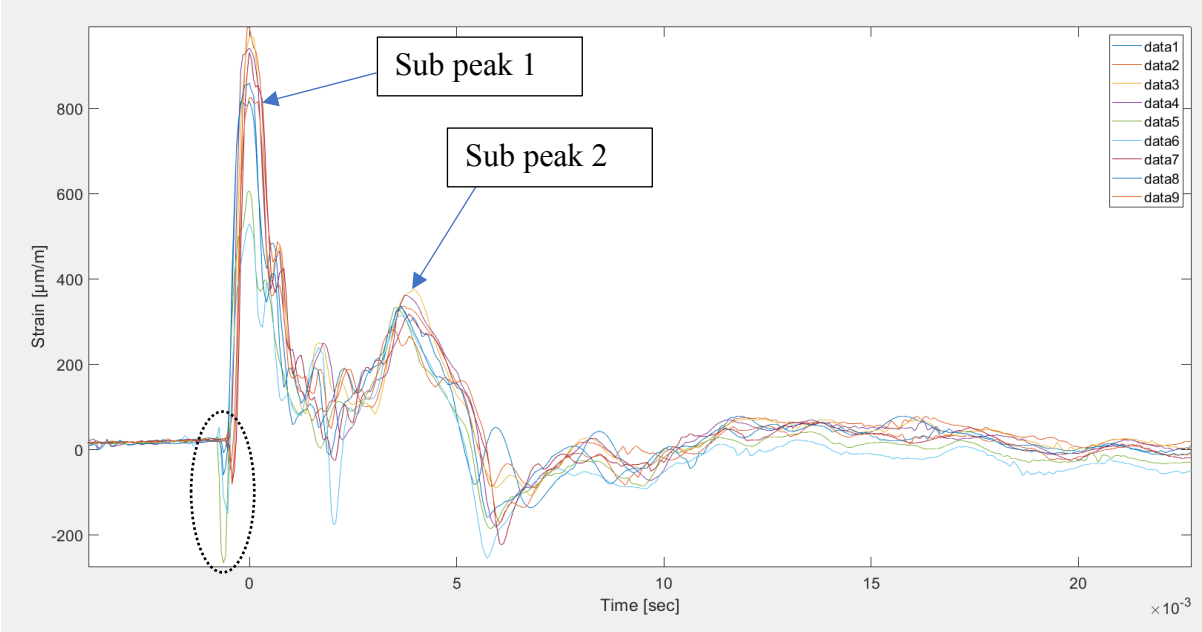

Figure 116: Ffirst peak impact profile for all impact loading measurements #1-9.

Focusing on the initial impact response shown in *Figure 116*, which is a god visualisation of the consitency of the measurements. Overall profile also show great similarities with 30 cm proctor test on the perfate plate. The most notable is that the maximum point of each sub peak's(1&2) distance from each other being the same, clocking in at roughly 4 ms for both.

Variation between the measurments never exceed the calculated standard deviation of 161.7 µm/m. The measurements that show greates variation from the average, behavioral repsonse is data 5 & 6 which showed a first peak maximum of 605 and 529 µm/m respectively. Both also showed a large negative strain before the impact of -220 and -180 µm/m. Looking at the characteristics of the profile for the entire response, it shows a great deal of precision and repeatability.

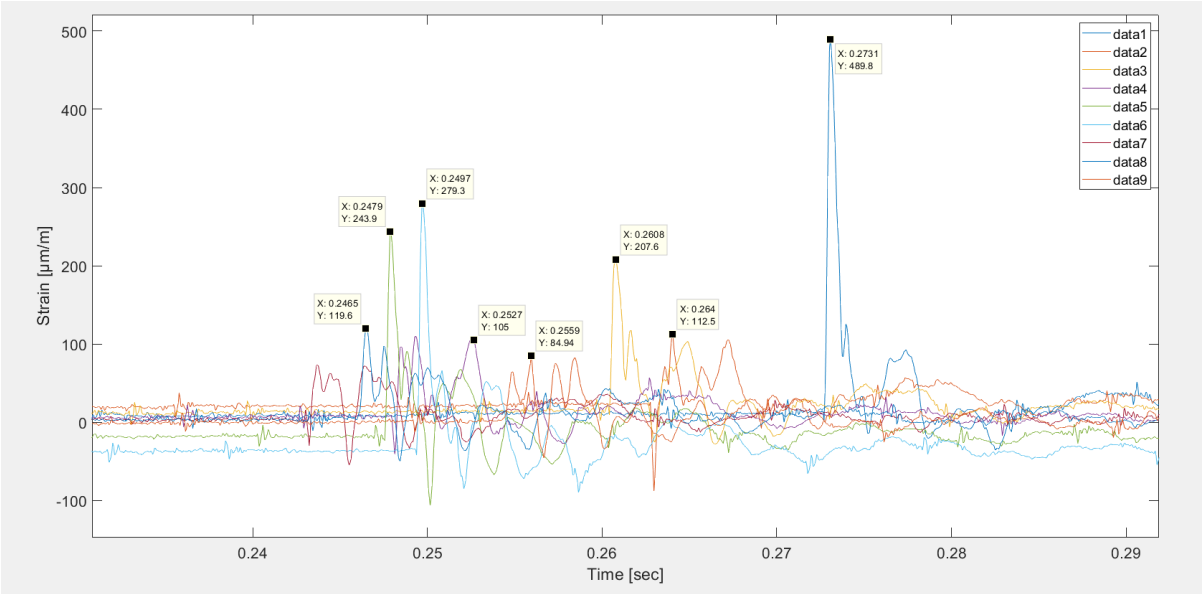

Figure 117: Second impact profile for all measurements #1-9.

For the secondary impact shown in *Figure 117*, the variation is much greater with regards to the overall response as the variation in the second impact location can be seen to be much greater. Results from this being a non-coherent second impact peak for each measurement, which is most likely due to the even larger scatter on impact area. This being due to momentum of the ball not being vertical unless completely centered impact, which was difficult to achieve.

7.2 Relationship Between Approximated Dynamic Strain and Measured Strain for Solid Plate Behavior in Air

This section will look at the relationship between the calculated dynamic strain based on the static equations, to illustrate scales of difference between the two. It was already explicitly said earlier on that static equations cannot be used to accurately determine the strain produced upon dynamic impact. However, the differences should be interesting to highlight as it highlights the behavioral difference/similarities. This is done by using equations which relates force/load "F" to the deflection "$e(max)$". The equation used to approximate impact force is the acceleration required to reduce the velocity of incoming object to zero expressed in as "F_2".

Mass “m” is mass of the plate itself, which is a simplification, as the entirety of the mass is not moved the same distance of "$e(max)$".

$$F_1 = \frac{3(3+v)(1-v^2)D^2 e(\max)}{16\pi E t^3}$$

Equation 21

$$F_2 = \frac{mV^2}{2e(\max)}$$

Equation 22

These can then be combined to express a deflection maximum "$e(max)$"

$$e(\max) = \sqrt{\frac{mV^2 3(3+v)(1-v^2)D^2}{32\pi E t^3}}$$

Equation 23

This deflection can then be used to calculate the strain based on the equation 23, and the strain produced when the mass is assumed as a point load is approximated. The approximated strain compared to dynamic strain is displayed in *Figure 118*.

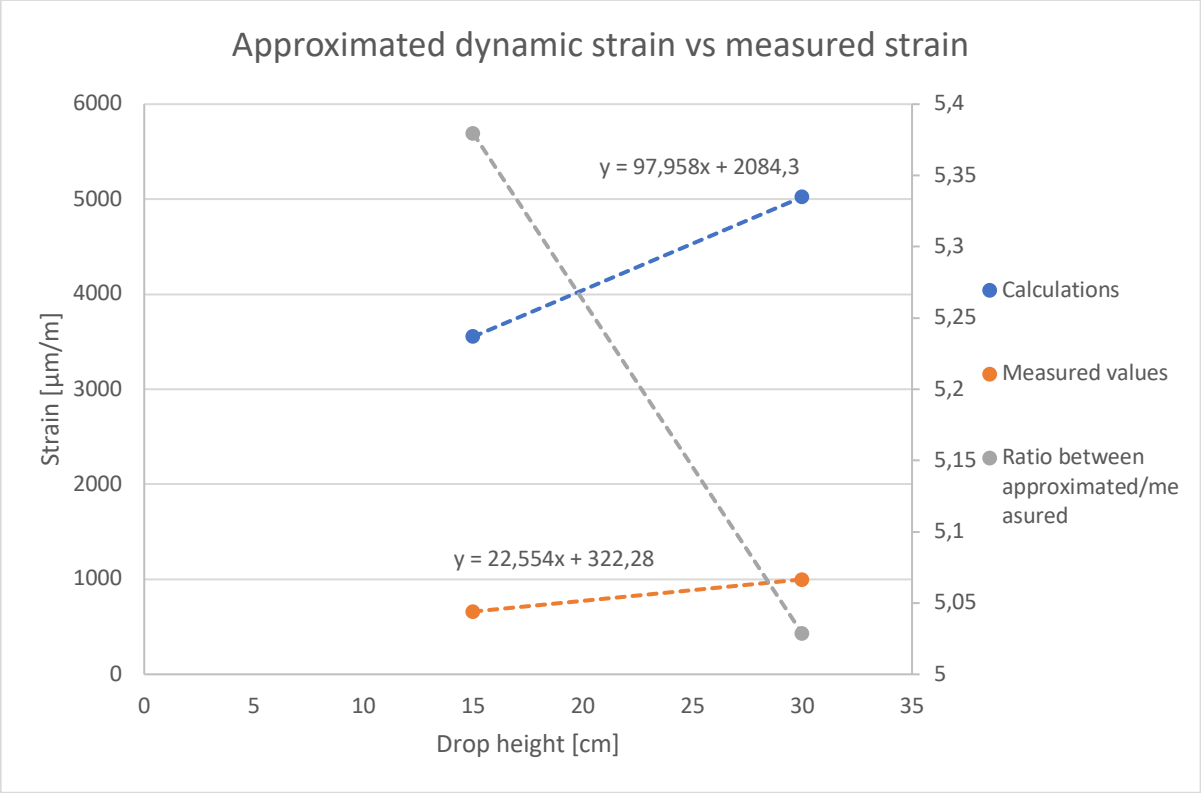

Figure 118: Approximated strain & measured strain comparison for solid plate proctor tests in air.

For the proctor tests the expected strain based on the static equations was 5023 µm/m for 30 cm and 3553.63 µm/m for 15 cm proctor tests in air. Compared to actual dynamic values that was measured from the tests, the order of magnitude of the static based calculation was approximately 5 times larger. The interesting similarities is the reduction in strain from 30 cm to 15 cm. this reduction being 70.7% the original value from the calculations and 66.1 % for the measured data.

For the ball drop method on the solid plate in air the results where the following the expected strain from 440g mass falling 2.25 m would produce 4166.837 µm/m of strain. Comparing this value to what was recorded from the measurements 1730.769 µm/m. This being 2.4 times larger than the measured value being much closer than what was shown for the proctor tests.

7.3 Permanent Deformation of Plate and Dynamic Yield Point.

Due to difficulty with regards to strain gauge measurements for the submerged tests there exists no valuable results obtainable from the perforated plates with regards to strain measurement. Tests were conducted with 4m ball drop on solid plate and perforated plates equal amount of times, to ensure some degree of comparability in the case of plasticity.

In the *Figure 119* shows roughly the deflection cross-section of the solid plate and the perforated plate which was measured with feeler gages.

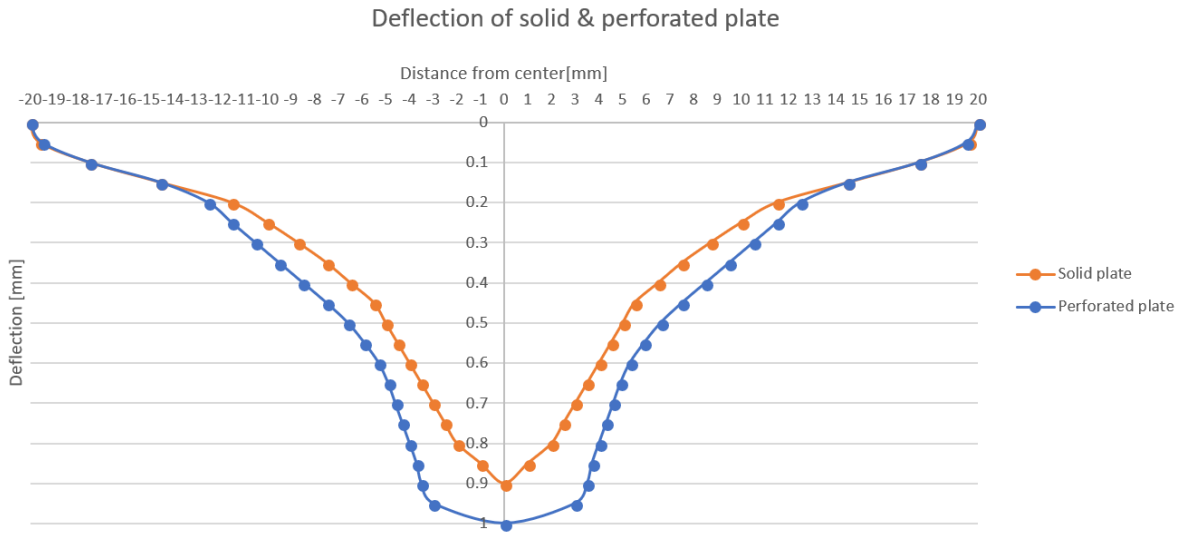

Figure 119: Permanent deflection profile after impact loading tests for solid and perforated plate.

These measurements serve to indicate what the nature of deflection is for both plates. From the Figure its seems that the plate has been significantly deformed due to impact loading as a deflection is 1 mm for the perforated plate and 0.9mm for the solid plate.

It also shows that deflection from the perforated is greater than the solid plate. This is however something that is to be expected as perforated plate has less steel and is subjected to the same amount of impact.

The deflection was not measured when the plates was fresh from the supplier, as it was assumed that the deflection of the plate was zero. However, this would have been the best reference point for the alterations between the original and new deflection profiles.

Based on the deflection measurements it seems that the plates had a natural deflection from the start based of the fact that 1-2 cm region (from the rim) of the plate was supported by the steel disk during the tests. The difference between plastic deformation due to impact loading vs original.

Deflection profile illustrated for the perforated plate seem to indicate significant amount of deflection for both plates. For both plates the effect of chip damage has had little to no effect on the surface and can therefore be considered negligible. Although the deflection seems to be severe, it is not. When based on the entire length of the surface the angle formed is only 0.3°, the deflection is instead much more localized as the steepest angle is found at a distance closer than 5 cm from the center, which in this case would make 1.14° angle with the maximum deflection. It can also be shown that ball remains stationary on the surface, without rolling towards the center, which indicates a very local deformation near the center.

Second method for confirming whether the plates had undergone plastic deformation was to calculate dynamic yield point, as measurement on strain gauge measurements showed strain in the region of 2000-3000 μm/m. Based on the minimum value of the yield strength 355 MPa and the Young's modulus which ranges from 208-215 GPa, the lowest yield point that the plate could have is 1651 μm/m. The time factor involved is approximately 0.2 ms for specimen to go from unstrained equilibrium to its maximum strain. This is very important when estimating whether plasticity has occurred, since the impact loading tests conducted showed large strain rates. An important property of steel is that yield stress changes depending on the strain rate (Anon., n.d.), which important aspect of dynamic loads with regards to plasticity.

This effect can be illustrated using the empirical equation by Rolfe & Barsom(1977)

$$\sigma_{yd} = \sigma_{ys} + \frac{6.665 * 10^5}{Tlog(2 + 10^{10}t)} - 190$$ *Equation 24*

Equation describes the behavior of dynamic yield strength σ_{yd} based on the static yield strength of the material σ_{ys} and the temperature T and the time t . As the equation follows and inverse log behavior means that dynamic yield strength increases exponentially as loading duration is reduced.

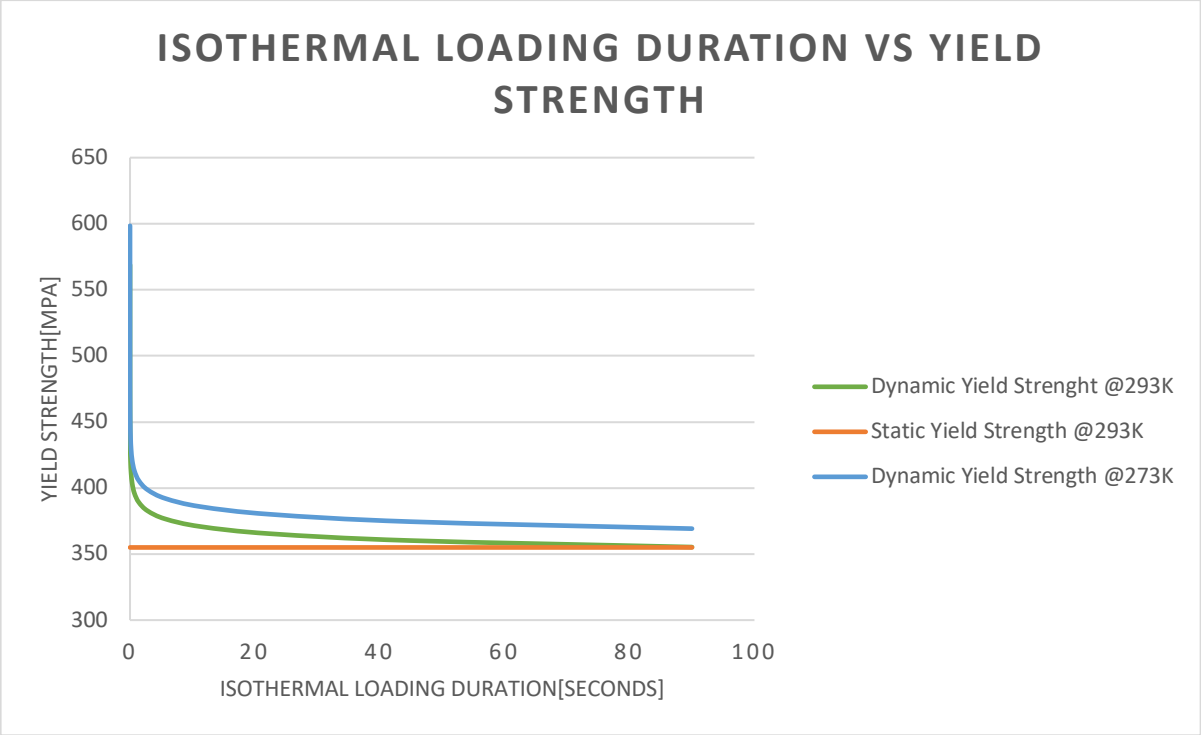

Figure 120: Relationship between dynamic yield strength and strain rate.

This relationship is clearly demonstrated in *Figure 120*, the dramatic increase in yield strength for very small loading intervals, meaning the bigger the "shock" the more the dynamic yield strength will increase. Calculated values for dynamic yield show that the maximum strain rates that the plates can handle are approximately 2631 µm/m for the strain rates shown in the measurements. This value is exceeded in the 4m ball drop tests by at least 280 µm/m, and it is also important to note that this formula is for iso-thermal loading. In a real-life scenario there will always be some heat generated by the bending of the plate, and as such the aforementioned value is a slight overestimation of the actual plates maximum limit. This would therefore confirm that the plate has been plastically deformed by both feeler gauge measurement and dynamic yield point calculation.

However, velocity of dropped object is a huge factor with regards to strain rate of the material, meaning heavy objects with slow velocity will not see little of this beneficial behavior.

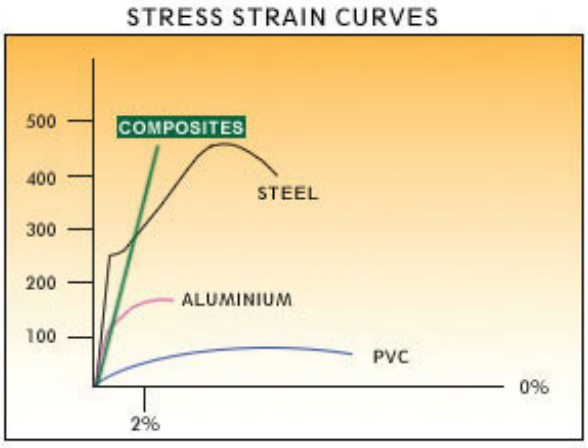

Figure 121: Stress-Strain curve with composites highlighting (Anon., n.d.).

However, this behavioral phenomenon is not present in material as fiberglass (GRP), which behaves like a linear elastic until fracture as shown in *Figure 121*.

7.3.1 Strain Hardening

Does measurements show indications of strain hardening and at what extent has it impacted the measurements If that is so then. Results identical after 4m and 2m drops for proctor tests? This was the question that was asked after the permanent deflection was discovered. This section will investigate the behavior of the impact loading tests conducted after the permanent deflection was discovered. If so, then the material should have undergone so called strain hardening due to the plastic deformation. This phenomenon is caused by dislocation entanglement, which is the increase in material strength for any subsequent loading, requiring a large amount energy to deform that granular structure (Gedeon, 2010). Behavior is illustrated using *Figure 122 & 123.*

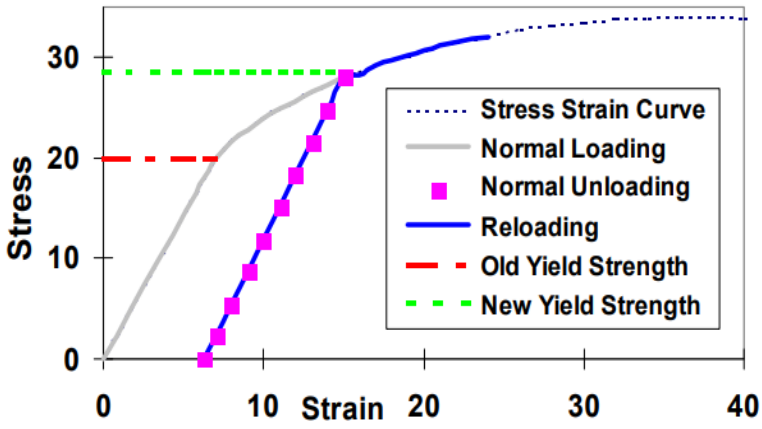

Figure 122: Strain hardening behavior for arbitrary ductile metal (Gedeon, 2010).

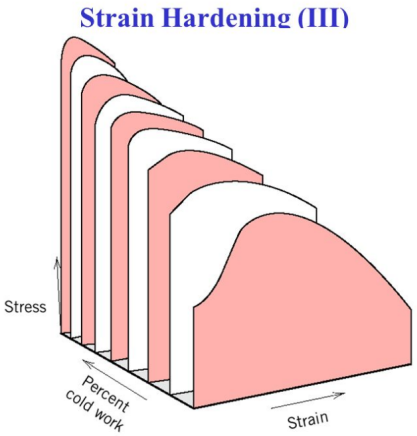

Figure 123: Illustration of the variation between the different degrees of strain hardening (Anon., n.d.).

The change in material property is only pertaining to the yield strength of the material and as such the results conducted after permanent deformation of the plate has occurred should yield similar result. Tests conducted to investigate this was the proctor measurement in air for 30 cm mass height. Like previously represented data, the results are chosen based on them being the most representative data, based on their closest proximity to the average peak value.

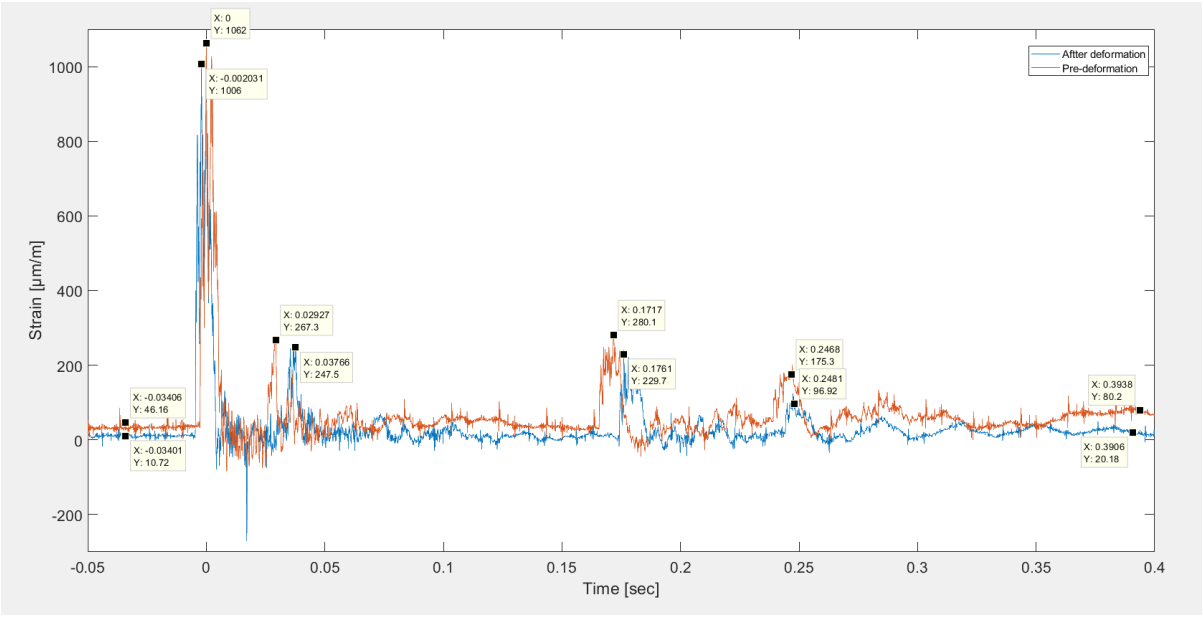

Figure 124: Comparison of before and after test conducted on the deformed solid plate.

The results from *Figure 124* show little variation between the values of the peaks, when not considering the horizontal shift. Even as these results where expected, it is interesting to demonstrate that the material response is more or less unaltered as long as the strain is within the elastic region.

7.3.2 Fatigue Limit

Material fatigue is always a prevalent topic with regards to any process that involves subjecting a specimen cyclic load. The number of tests conducted in this paper for measuring impact loads on solid and perforated plates (Boardman, n.d.). Fatigue pertains to issue regarding accurate determination of when the plates were permanently deformed. Material behavior is displayed in *Figure 125.*

The key to all engineering applications is to remain below the so-called endurance limit of the material in question as below this point an infinite number of cyclic loads can be applied without fatiguing the material. This value is usually roughly 50% of the materials tensile strength which is then 245 MPa which is 69% of the yield strength of steel plates.

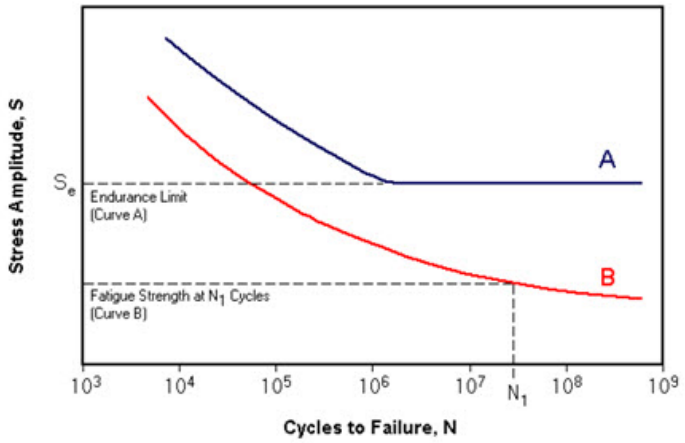

Figure 125: Fatigue of material illustrated by Stress amplitude vs cycle (Anon., 2018).

If the plate suffered some degree of fatigue from the several 100s of tests, then material might have become plastically deformed before the final stress test of 4.2m ball drop which was intentionally meant to cause permanent deformation of the plate.

7.4 Solidworks and Measurements Comparison

The comparison between the Solidworks simulations and measurements are interesting not only with regards to comparing the most valid approximation possible between theory and reality. This segment will look at proctor test in air only for solid and perforated plate. Important difference between the simulation and measured values being that simulation recreates a perfect pulse load. Additionally, it was discovered that the duration of the impact response was approximately 1 ms as opposed to the 10 ms shown from the measured values.

The comparison is therefore based on the interval 0-1ms for. Measured data selected to compare with each simulation are the same as the ones used in *chapter 6*.

7.4.1 Perforated Plate

The impact response based on the simulation results indicate *Figure 126*, the maximum strain produced for simulated 30 cm proctor test to be 1130 µm/m as compared to the measured average 1006.89 µm/m. Simulated values being 12.2% larger than measured value which is very close to real measurement, when considering variation in measured data of 5.9%. In the response interval, the measured data reaches a maximum of 792.2 µm/m compared to response maximum of 989.4 µm/m in measurement #10.

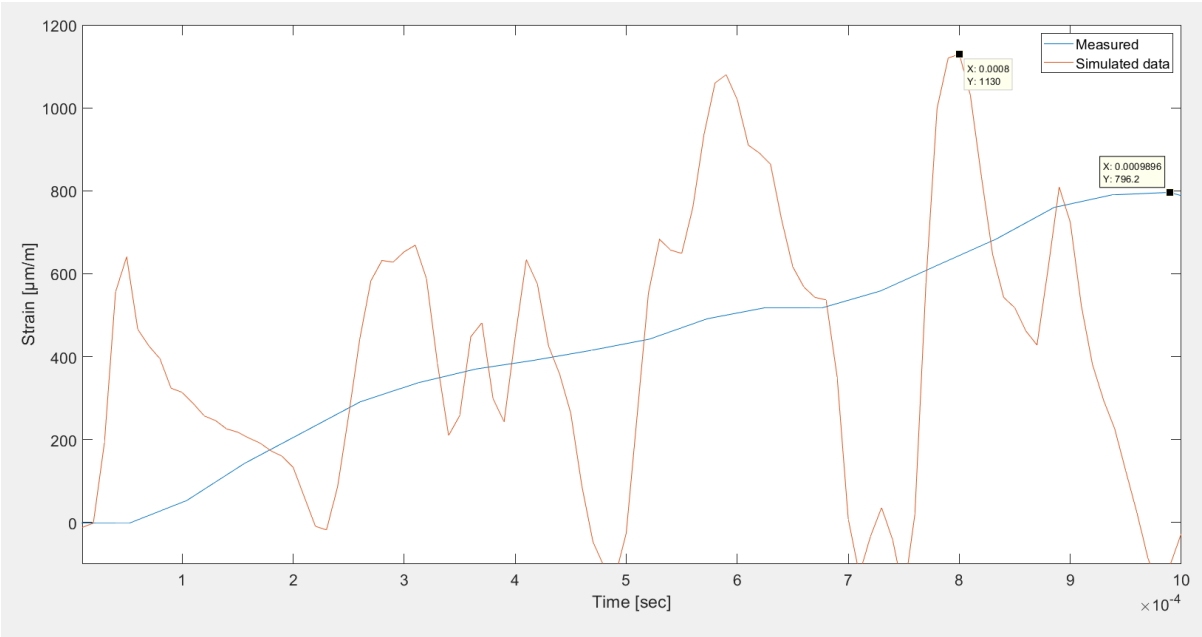

Figure 126: Comparison between simulated data and measured data (measurement #10) for 30 cm proctor test in air on perforated plate.

When evaluating the simulation of 15 cm proctor test in *Figure 127*, the maximum strain for perforated plate from simulated data was roughly 747 µm/m compared to the measured average 683.24 µm/m from the data set, which is a difference of roughly 8.5%. This being a relatively small difference considering the standard deviation being 10.6%. The response interval shows how the measured data reaches strain value of 553 µm/m, compared to the recorded maximum of 690.5 µm/m for measurement #6.

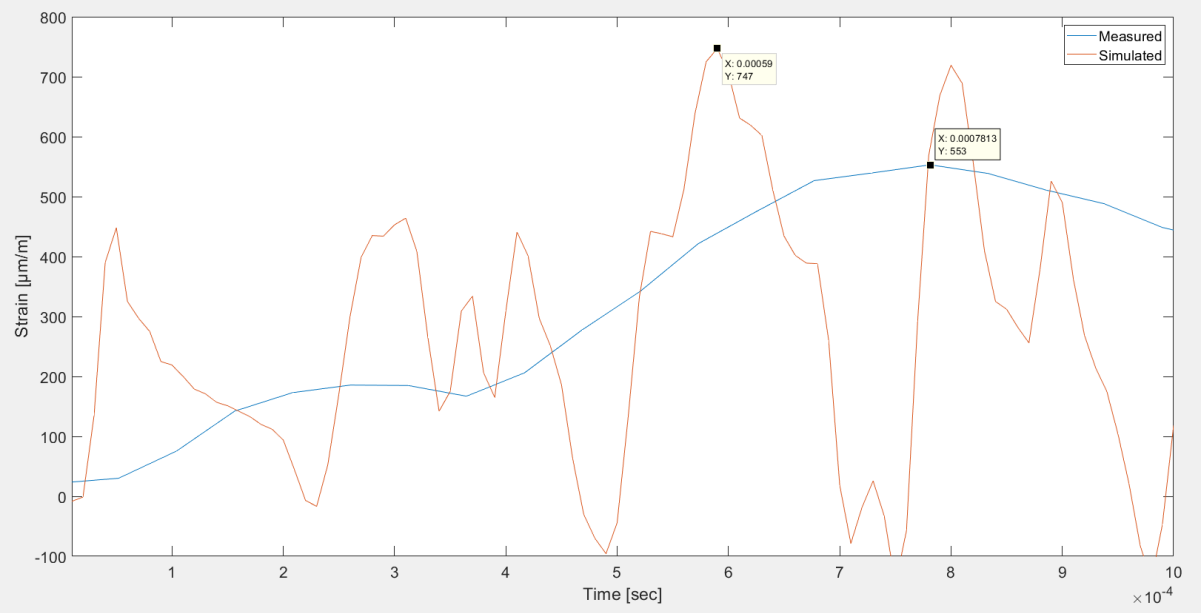

Figure 127: Comparison between simulated data and measured data (measurement #6) for 15 cm proctor test in air on perforated plate.

Reasoning behind why the simulations show consistently larger values, might be twofold. Firstly, measured data shows how perforated plate is lifted of its supports after the initial impact, in addition to how not all the energy is transferred energy is absorbed into the plate, since the mass receives a partial amount of the energy in return (bounce height). Even when the simulations calculate results with a better contact area, which in turn distributes the force more evenly. The balance however, might predominantly cause the results to produce larger strain.

Lastly with regards to impact profile, the difference is very significant, as the simulated data show oscillations of ± 600 whilst the measured data show an increasing trend throughout the interval. A Possible cause for this is most likely due to the damping effect of the proctor resting on top of the plate after impact, whereas the simulations recreate a perfect impact pulse. This would then result in the measured data has a lower frequency (function of damping coefficient), as compared to the simulated data which would have a closer value to the natural frequency. Which might explain why the results are so different.

7.4.2 Solid Plate

The solid plate simulations for the 30 cm proctor drop showed a maximum strain of 940 µm/m which was 5.9% smaller than the average measured value of 998.92 µm/m for the same scenario shown in *Figure 128*. Additionally, the values for the simulated solid plate are smaller than the measured data as opposed to the perforated plate where it was shown be larger. For the given interval the maximum strain for the measured data is 763.6 µm/m out of the actual 989.4 µm/m.

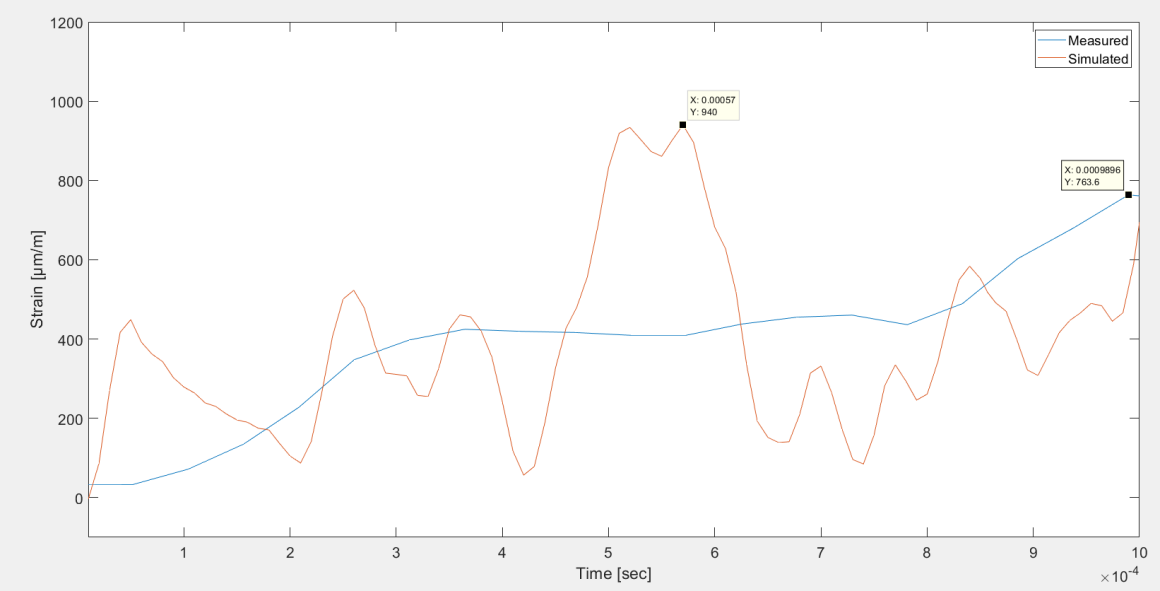

Figure 128: Comparison between simulated data and measured data (measurement #3) for 30 cm proctor test in air on solid plate.

Last scenario being 15 cm proctor test in *Figure 129* showed the strain 657 µm/m, compared to the measured average of 660.6 µm/m, which is 0.54% smaller than the measured maximum.

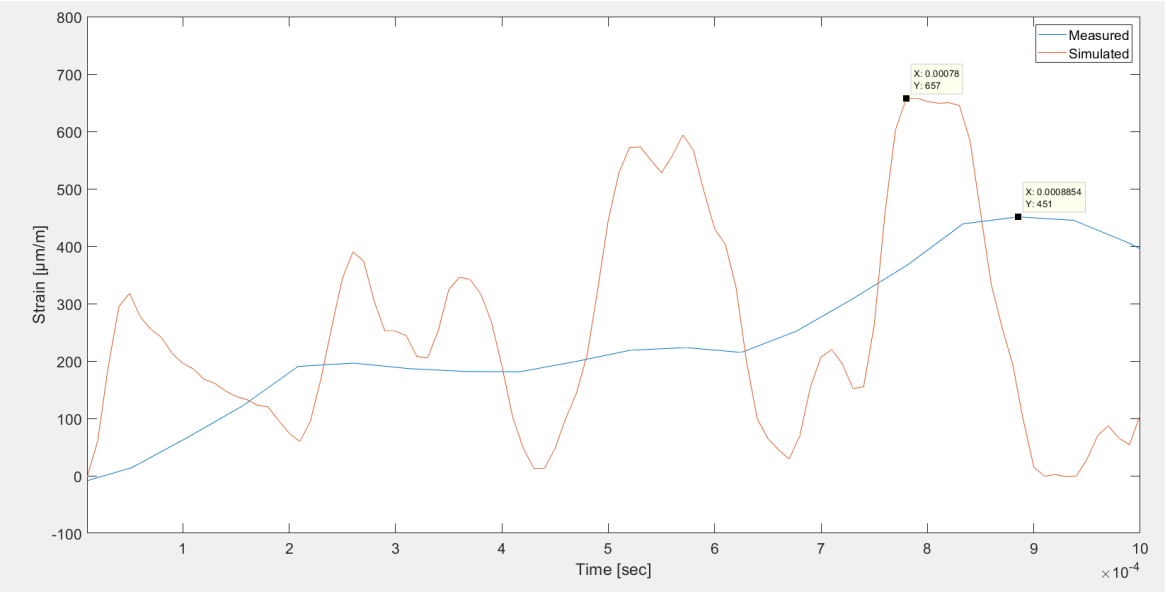

Figure 129: Comparison between simulated data and measured data (measurement #10) for 15 cm proctor test in air on solid plate.

The comparison of the simulated and measured data for the solid plate in *Figure 129* show that the simulated to be smaller than the measured values, which contrasts the trend discovered for the perforated plate. Reason behind why the solid plate shows smaller maximum strain as compared to the perforated plate is interesting, as both plates are suspended fully/partially in the air after the impact.

The only noticeable difference from the measurements is the duration of which the plate is freely suspended and impacts with the support rim, which is an indication of the transmitted force/energy. It is also plausible that the answer is related to how the software treats boundary conditions of freely supported plate.

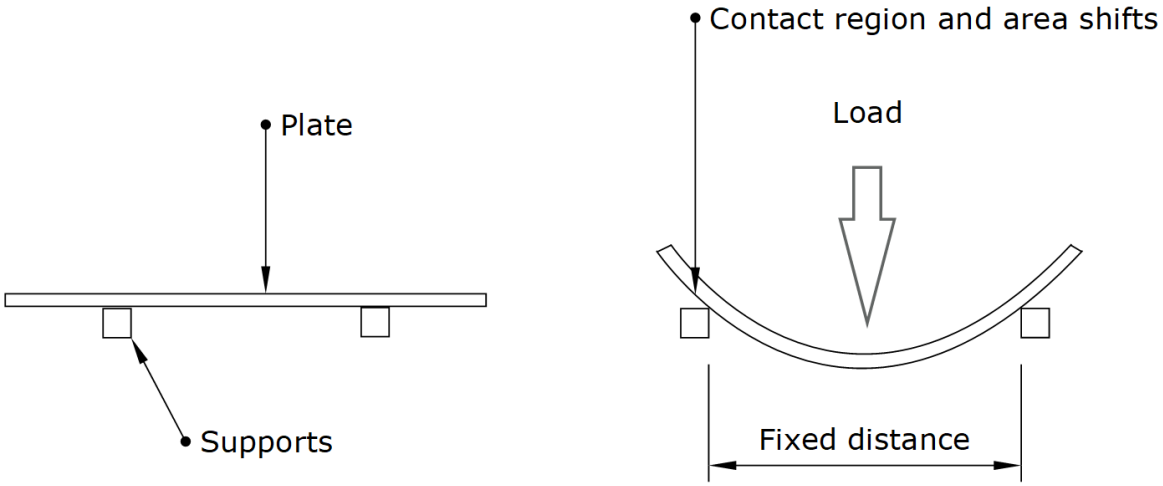

Figure 130: Illustrations of freely supported plate subjected to large load, which affects contact points and area of the support regions.

As the distance of between the supports have a fixed distance that means plate is pushed down in between supports as edges of the plate are retain less contact area. This effect being presented in *Figure 130.*

7.4.3 Perforated Plate Strain Variation from Center

The focus in this paper is based around the strain produced at the center of the plate, as this is region that experiences the highest amount of strain in addition to mass impact is also at center. However, the perforated plate was mounted with a total of 6 different strain gauges to determine variation from center. Strain gauges "SG" was marked from 1-6 in order to correctly correlate the measurement to the appropriate strain gauge.

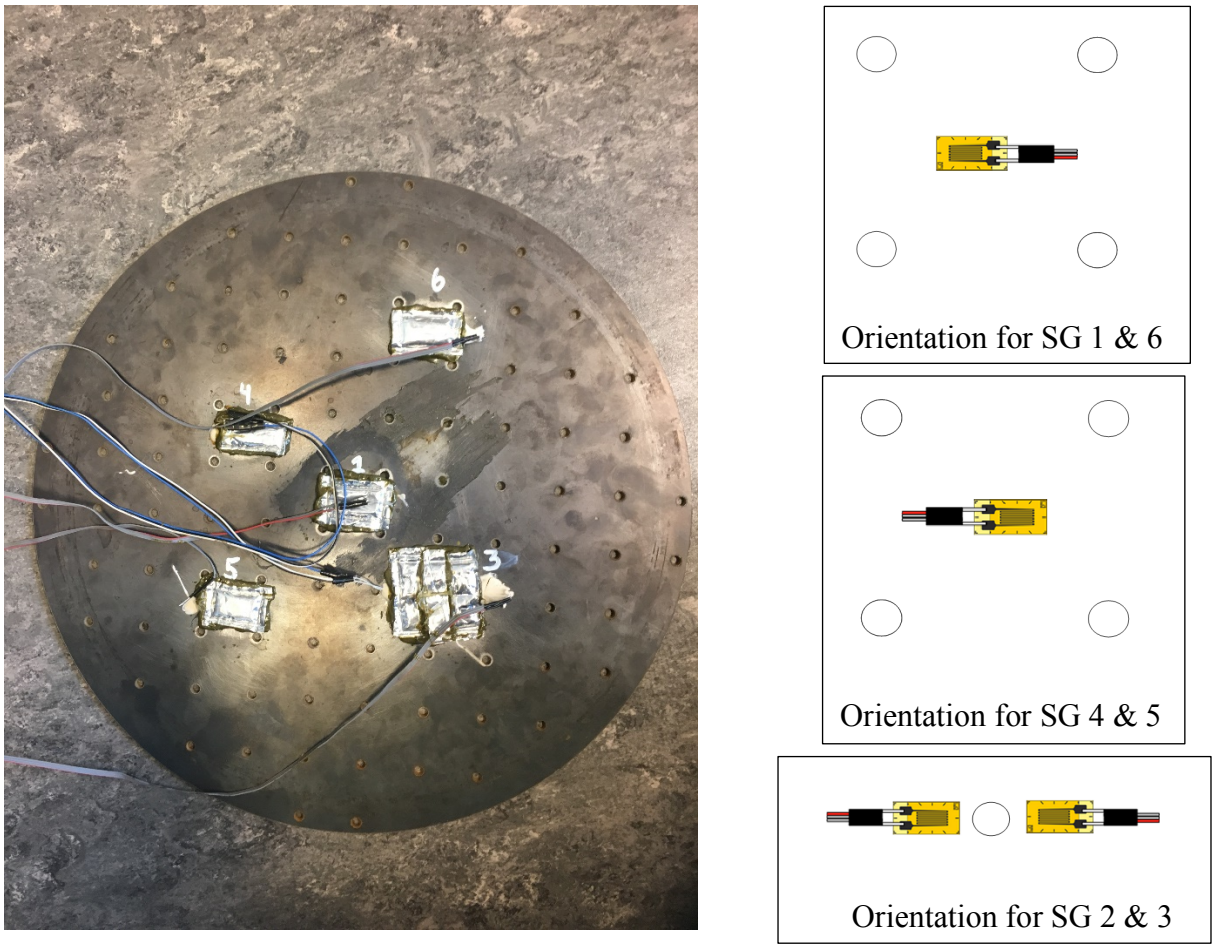

Figure 131: Illustration of the perforated plate and the placement & orientation of strain gauges 1-6.

For the tests done in water there was issues with sealing for SG 2, meaning water measurements for this particular strain gauge was not properly recorded, but this sealing issue did not damage the strain gauge itself. SG 4 also seem to have some issue with noise related disturbance, as the background noise for SG 4 showed a max/min variation of ± 75 µm/m at idle conditions, which compared to the SG 1,3,5,6 was only ± 14 µm/m (further discussed in uncertainty *chapter 4.6*).

The radial distance from center is as shown in *Table 24:*

Table 24: Strain and radial distance for strain gauges mounted on the perforated plate.

Strain gauge nr#	Radial distance from center [cm]
1	0
2	8.48
3	8.48
4	8.94
5	11.31
6	12.64

To highlight the values recorded from the other strain gauges, these values are therefore tabulated to compress all these values as much as possible.

Table 25: mean and standard deviation for strain gauges 1-6 for proctor test on perforated plate in air.

Plate type	Fluid medium	Experiment type	Strain gauge nr#	Mean [µm/m]	Standard deviation [µm/m]
Perforated	Air	Proctor 30cm	1	1006.89	59.52
			2	278.34	41.50
			3	224.96	29.47
			4	442.52	63.87
			5	343.94	51.35
			6	298.26	40.97
		Proctor 15cm	1	683.24	54.60
			2	531.20	344.84
			3	446.51	416.34
			4	641.53	414.48
			5	852.86	905.36
			6	488.84	448.26

Looking at results from proctor tests in air show overall good and consistent results for 30cm proctor tests with acceptable values of standard deviation. This cannot be said for 15 cm proctor test as all SG in this scenario except for center strain gauge have standard deviation values close to or greater than their mean. The exact cause for this is most likely due to overflow which caused the maximum to be much larger than the average, causing a higher than normal degree of standard deviation.

Then the for the proctor tests in water on the perforated plate is presented in the same fashion, with the strain gauges who were affected by poor water sealing is marked in red. This being presented in *Table 26:*

Table 26: mean and standard deviation for strain gauges 1-6 for proctor test on perforated plate in air.

Plate type	Fluid medium	Experiment type	Strain gauge nr#	Mean [µm/m]	Standard deviation [µm/m]
Perforated	water	Proctor 30cm	1	780.50	47.60
			2	420.76	90.14
			3	188.55	20.43
			4	284.04	22.46
			5	261.27	20.04
			6	221.30	10.29
		Proctor 15cm	1	474.44	56.74
			2	396.03	35.36
			3	161.49	14.71
			4	207.60	27.99
			5	171.23	27.05
			6	181.39	14.69

Lastly the combination of data can be used to illustrate the strain vs distance from center, considering excluding strain gauges 2 & 3 as these are not center aligned. This was done for both air and water but serves as a representation of the data that indicates localization of strain.

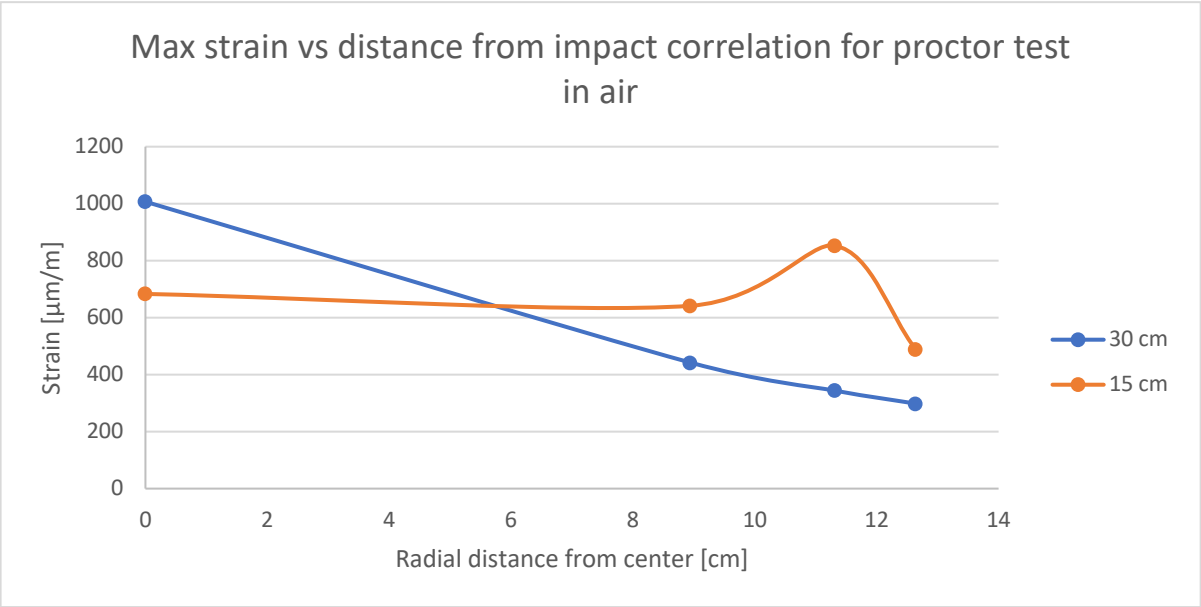

Figure 132: Localization of strain based on strain vs distance correlation for proctor tests in air on perforated plate.

Figure 132 representing the reduction in strain based on radial distance as seen in air from center, show 50% reduction in strain for the 30 cm proctor test at distance of roughly 8 cm from the center. In the diagram the standard deviation being much poorer for 15 cm test in air shows little to no reduction in comparison, in addition to an increase in strain seen at 11.31 cm from strain gauge 5.

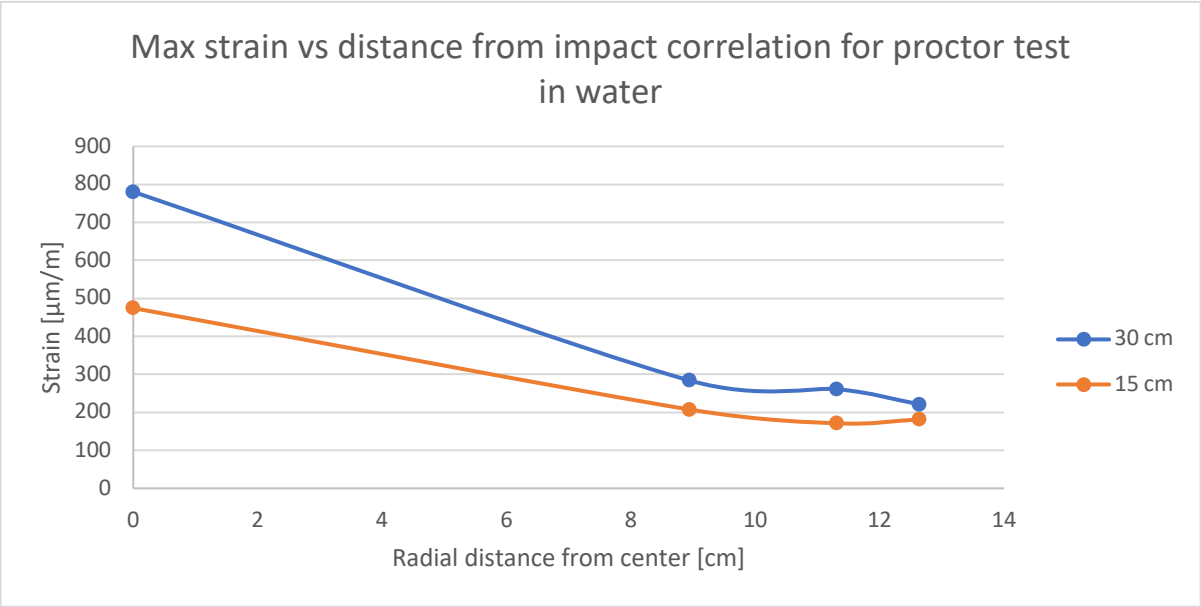

Figure: 133: Localization of strain based on strain vs distance correlation for proctor tests in water on perforated plate.

For the correlation in water shown in *Figure 133* the results show that at a distance of 7 cm for 30 cm proctor test and 8.5 cm for the 15 cm proctor test is required for the strain to be reduced below 50% of its maximum value seen at the center point.

7.5 Energy Dissipation Perforated vs Solid Plate

Having investigated that perforated plate has a visible reduction in strain due to dynamic load. This section will discuss some of the observed behavior for these two types of plates, with the focus being on the measurements conducted in water, and proctor tests. This is because difference in the fluid behavior after impact was only visible in water and the proctor tests showed the highest degree of consistency.

Starting with the perforated plate, the effect of the impact causes a large amount of water jet streams to be produced through the perforations with some droplets reaching well over 1m. In starch contrast to air both the rheology and compressibility contribute to these jet streams. As the energy being transferred into the plate must be used for displacing the water due to its compressibility. As water is displaced by the deflection of the plate, the water is forced upwards in a vertical direction.

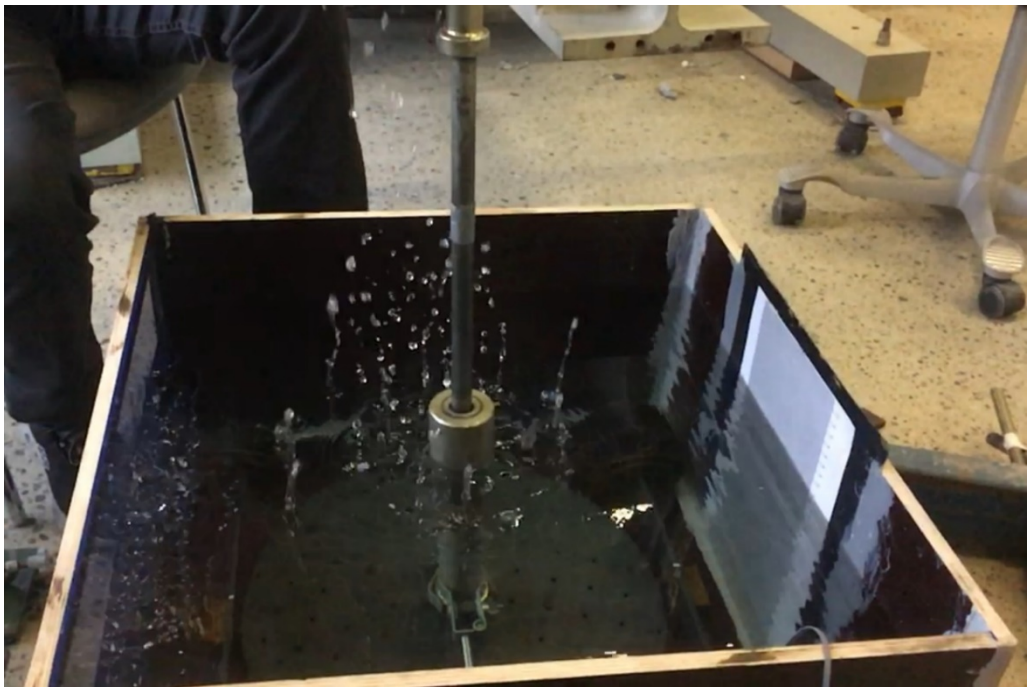

Figure 134: Image of the water Jet stream caused by impact on perforated plate.

Another interesting aspect of the is how the height of droplet is reduced away from the center of impact. Tallest droplets/streams are seen closest to the proctor at approximately 1 m tall, with the furthest noticeable streams only at 5 cm or less. However, this distribution is not symmetrical as indicated by *Figure 134*. The cause is not certain but two possible explanations is that the perforated plate does not vibrate symmetrically around its center meaning that some areas will have positive deflection, whilst others will have negative deflection.

Second factor affecting is perhaps the wire openings created by grinding away areas of the support ring. Where these creates additional areas for which the water can be evacuated. Illustration of jet streams is shown in *Figure 135*.

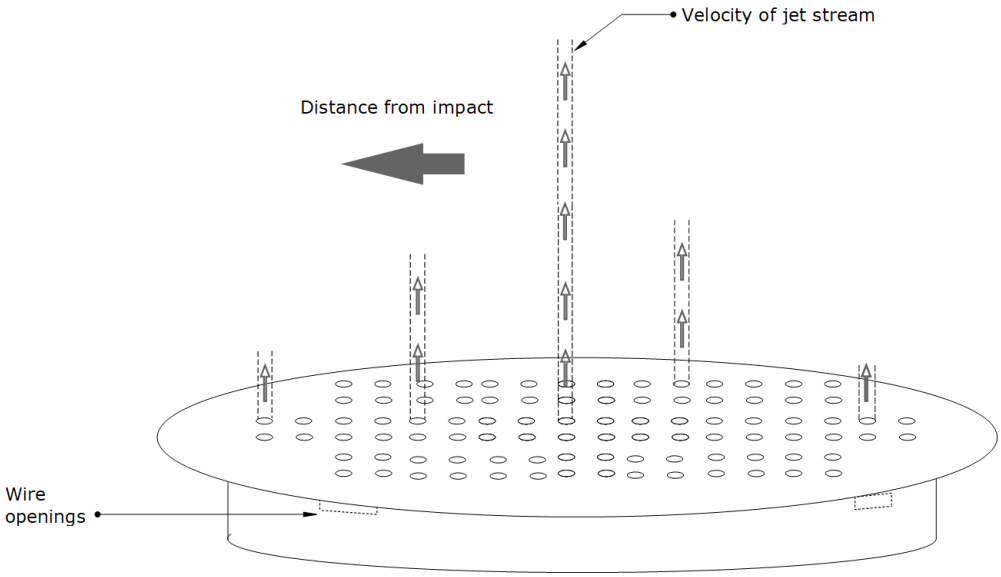

Figure 135: Illustration of jet stream velocity moving away from center of impact.

For the solid plate shown in *Figure 136* there is of course no jet streams produced due to the lack of perforations, but the surface disturbance was apparently larger. This was however difficult to illustrate due lack of visible difference. The gist of it is that due to lack of ways for water to be evacuated more resistance is met due to water being forced through the wire openings. Which in turn results in a larger horizontal wave motion being produced. In summary, the observable surface difference between the solid and perforated plate in water was that more of energy was transferred into wave motion.

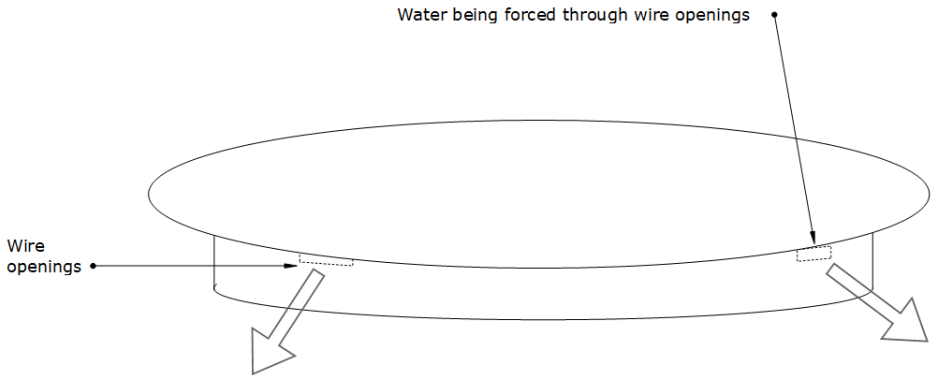

Figure 136: Illustration of water being channeled through the narrow wire openings.

Taking into strong consideration that these are not measured differences but an observable difference from the conducted tests the surface.

7.6 Uncertainty

This final sub chapter will highlight some of the uncertainties with regards to experimental method and equipment used to measure the impact loading response for solid and perforated plate in air and water.

7.6.1 Proportionality with Regards to Thale's Theorem

Bounce height is read from as distance behind test object which was roughly 3-5 cm from the steel and the measurement chart was placed at 5 cm behind the steel frame, making the total distance between the camera and the measurement board 52 cm, whilst the distance to the measurement tape on proctor being 26 cm (Agricola, 2008). The aspect ratio with regards to distance is shown in *Figure 137*.

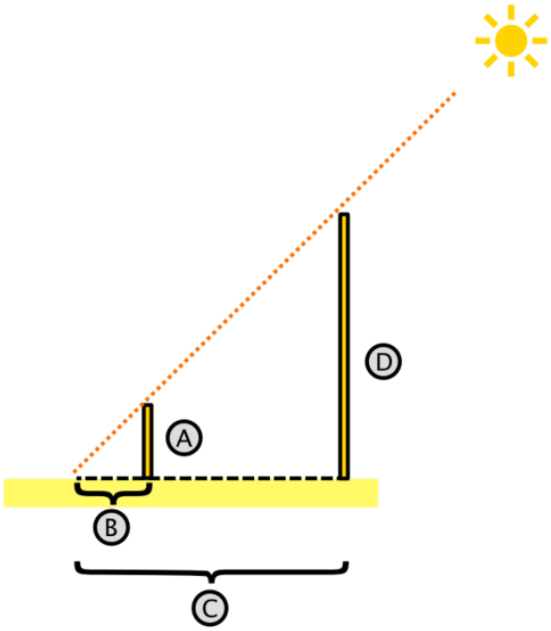

Figure 137: Illustration of the principle of Thale's Theorem (Anon., n.d.).

But since the distance from the frame was not constant for the measurement board and the tripod for the camera, means that some degree of uncertainty exists in the comparison between the individual measurements. Even if this was known before the start of the experiments, it serves as an additional element of uncertainty.

7.6.2 Background Noise

The background noise is always something that exists in these type of measurements, and the noise generated is not only due to surrounding electrical noise, but insulation of strain gauge and wiring. This became clear for the six strain gauges that was mounted on the perforated plate. Measured background noise was measured for reference to the precision of the measurements. Noise itself was measured by running strain sampling for 15 seconds on the plates freely resting on the support ring, with all measurements being zeroed beforehand. This was done for air & water for both plates. The values for the background noise are tabulated in *Table 27.*

Table 27: Values for background noise for mounted strain gauges on solid & perforated plate in air & water.

Plate type	Fluid medium	Strain gauge nr#	Max [µm/m]	Min [µm/m]	Mean [µm/m]	Standard deviation [µm/m]
solid	air	1	38.82	-42.18	-2.30	4.44
	water		-110	104.50	-3.53	11.87
Perforated	air	1	26.74	-30.41	-1.83	3.29
		2	38.17	-45.63	-4.27	4.78
		3	22.46	-23.43	-0.78	2.60
		4	37.77	-37.09	0.60	4.24
		5	37.48	-38.74	0.35	4.34
		6	23.33	-25.22	-1.18	2.76
	water	1	14.66	-13.82	0.61	1.69
		2	335.5	-338.50	-0.98	38.12
		3	11.47	-12.03	0.03	1.43
		4	75.51	-77.9	-1.08	8.49
		5	13.48	-12.20	0.3324	1.58
		6	9.833	-11.17	-0.2841	1.26

Based on the recorded measurements there was little consistency with regards to change in noise when going from air to water. This is since for the solid plate, noise increases when the plate is submerged into water, whilst it decreases in water for the perforated plate.

The actual values seen from the noise measurements show that for the solid plate the max/min variation was ±40.5 μm/m in air as compared to ±107 μm/m in water. Showing that noise variation in air was only 37.8% of what was measured in water. Meaning noise increased by 164% in water. This as mentioned earlier might have contributed to making water measurements larger than air for strain & impact energy, as noise levels are different.For perforated plate in the water, noise is reduced by 51.1-56.8% based on all the strain gauges (excluding SG 2 & 4 due to complications in water).

8 Conclusion

Having evaluated the process and procedures of the experiment in addition to evaluating the results, to determine behavioral differences with regards to solid and perforated plate in air and submerged in water, within the elastic range of the material. The major goal with regards to the thesis was to document the difference in observed behavior for these plates based from dynamic impacts or impact loading, as impact in water was expected to be smaller than what seen in air due to dampening difference between the fluids. With perforated plate being in focus with regards to protection covers used for the CAP-X also having perforated surface on the top sections. The results were then compared on basis of impact energy in relation to maximum produced strain from the impact, and the correlation was displayed for both perforated and solid plate and the behavior in air and submerged in water. The solid plate showed unexpected results, which indicated larger strain in water than in air for all the proctor tests and ball drop tests. Even when considering the zero loss of impact energy the results in water would show an overlap with the results in air. On the other hand, it was discovered that perforated plate showed a consistent reduction in impact strain based on the measurements, for all the proctor tests and ball drop tests this trend stayed the same. Even when considering the statistical variation in data the was still a difference of 1.5-8.8% between the strain in air compared to ones submerged in water. It is can therefore be said with large degree of certainty that there is indeed a reduction in strain due a dampening effect due to grating/perforation on a surface, which causes the maximum strain to be smaller in water as compared to air for the same value of impact energy. However due to relatively small difference between air and water compared uncertainties in the measurements, this difference cannot be accurately quantified in addition to impact energy being conservatively calculated as stated previously, means that actual difference between strain in water vs air can be anything from larger (most likely) to smaller. Based on this further investigation on this topic would be strongly encouraged to accurately determine the reduction in dynamic strain when submerging a perforated plate in water.

9 Future Work

Having conducted impact loading measurements and analyzed the data, the elements that could be improved became more apparent. In this final segment some ideas will be put forth to better enhance future experiments conducted on the topic of elastic behavior of plates in air vs submerged. The proctor setup used for the measurements is shown in *Figure 138.*

Firstly, by looking at the improvements that could be made to the setup used for the proctor tests where the camera setup and measurement chart was not fixed installations which means errors with regards to distance and alignment became a prevalent issue. Even if the distance between frame and the camera setup & measurement chart was checked, like in the procedure for experiments conducted. It was however believed to be the best solution at the time as fixing the setup and the measurement chart to the steel frame as one solid rigid structure would most likely result in unusable footage due to camera shake.

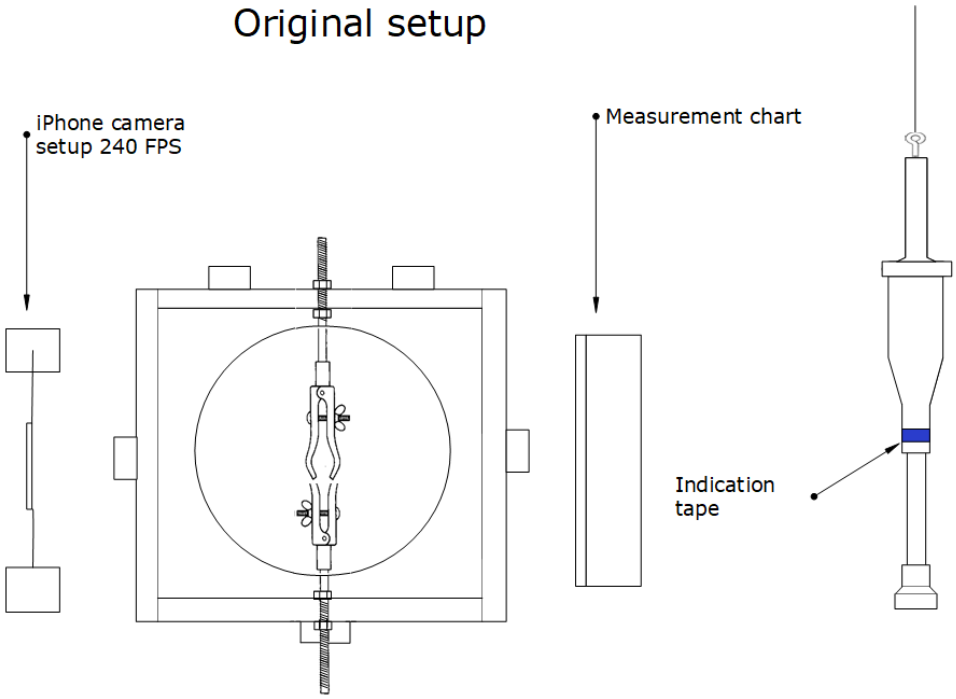

Figure 138: Setup used for measurements in the paper for proctor tests in air.

The second major issue pertains to the lack of high speed (high cost) camera available for the measurements, but due to limited budget and lack of available cameras, a 240 FPS @720P camera was used instead. Not having the ability to accurately determine the velocity before impact and correlate this to the impact energy was a major crux for the data evaluation. Meaning that the one should ideally have a high-speed camera capable of 1400 FPS+ @480P or better, if using the approach as shown in this paper. It is also important to not have a large distance measurement indicator and moving object, to improve accuracy of the measurements. The suggested improved setup for conducting improved experiments is illustrated in *Figure 139*.

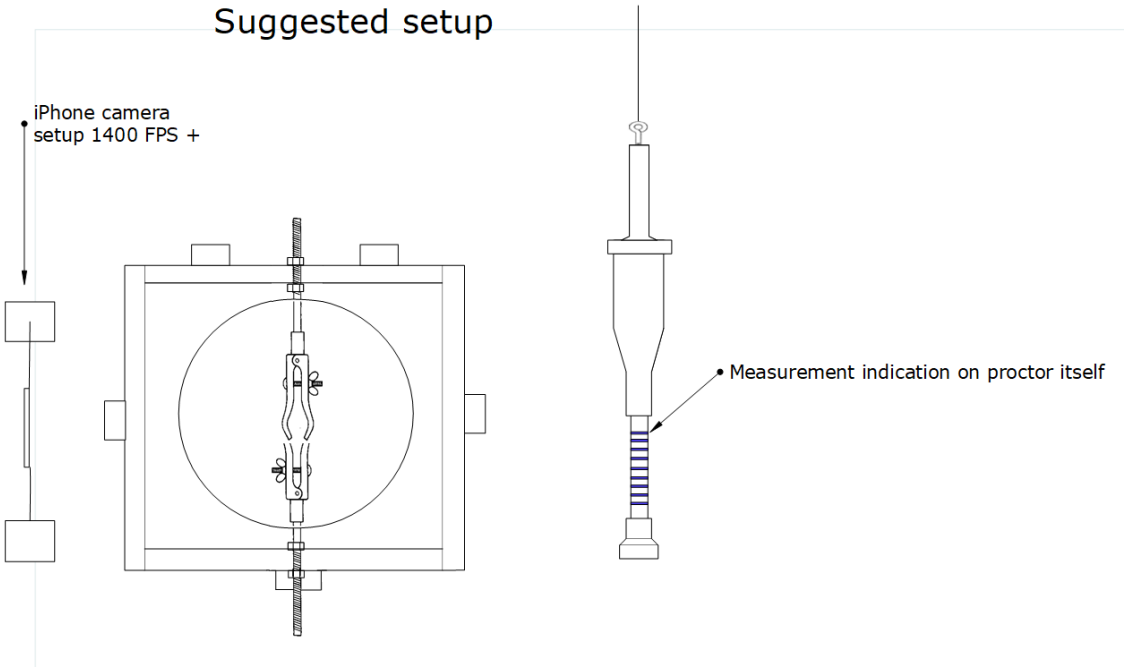

Figure 139: Suggested setup for improved precision & accuracy for impact loading measurements.

The major change for the proctor test would be the removal of the measurement chart/table used for the proctor tests, as height measurement could be read using of the base shaft of the proctor. This could be a viable option as the this increases accuracy of the measurements as Thale's theorem effect is no longer an issue when object is adjacent to the new measurement chart. Camera setup would remain unchanged as making the camera rig part of the steel frame as mentioned to avoid camera shake.

These suggestion deal with conducting measurements on material within its elastic range, in addition to these experiments focusing on the plate effect itself. Therefore, with regards to testing the CAP-X protection covers, a full structural test should be conducted to encapsulate the effect of the covers themselves. This is because there are such a multitude of factors that could affect these protection covers either negatively/positively. The stress distribution for a structure for example is heavy effected by how it is supported, and since the CAP-X protection covers uses hinges combined with interaction between the two halves of the protection covers.

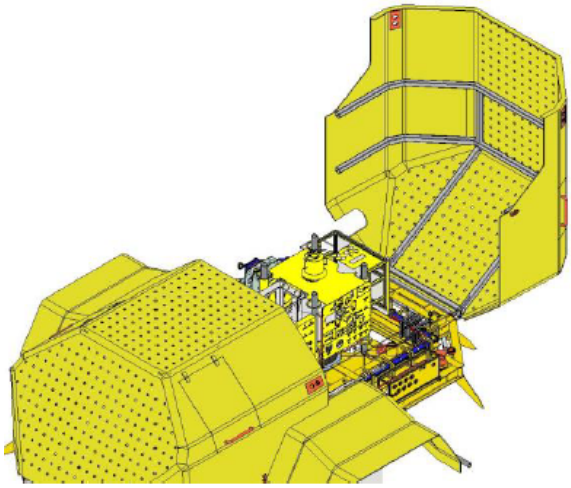

Figure 140: Image of protection covers from CAP-X technology by Statoil ASA (Anon., 14.12.2016).

These dynamics can only be captured when applied to entirety of the structure as opposed to the focus area in this paper, which was centered around a two test subjects with fixed geometry and supports with different surface structures.

Last point for future work does not pertain to experimental procedure but how the difference in behavior for a perforated plate in water vs air can be quantified. In addition to using strain & impact energy correlation it would also be good to compare the amount of energy the plate is subjected to by using the relationship between strain and stress.

10 Bibliography

Agonafir, M. B., 2015. *Introduction to PET 525, Advanced Drilling Engineering and Technology.* Stavanger: Univertitetet i Stavanger.

Agricola, I., 2008. *Elementary Geometry.* s.l.:s.n.

Andersen, I., 2016. CAP-X: Denne Statoil-utviklede teknologien skal gjøre Barentshavet lønnsomt.. *Teknisk Ukeblad*, 19 April, pp. https://www.tu.no/artikler/denne-statoil-utviklede-teknologien-skal-gjore-barentshavet-lonnsomt/346459 .

Anon., 14.12.2016. *Snilehorn dual Cap-X foundation and manifold,* s.l.: Statoil ASA.

Anon., 2009. *hyperphysics.* [Online] Available at: http://hyperphysics.phy-astr.gsu.edu/hbase/flobi.html

Anon., 2018. *Total Materia.* [Online] Available at: https://www.totalmateria.com/page.aspx?ID=CheckArticle&site=kts&NM=282

Anon., 2018. *WolframMathworld.* [Online] Available at: http://mathworld.wolfram.com

Anon., n.d. Chapter 7 Strengthening. In: *Introduction to material science.* s.l.:s.n.

Anon., n.d. *docsity.* [Online] Available at: https://www.docsity.com/en/strain-hardening-science-and-engineering-of-materials-lecture-slides/285224/

Anon., n.d. *General Composites PVT.LTD..* [Online] Available at: http://www.generalcomposites.in/structural.htm

Anon., n.d. *radford.edu.* [Online] Available at: https://www.radford.edu/~biol-web/stats/standarderrorcalc.pdf

Anon., n.d. *Slideplayer.* [Online] Available at: http://slideplayer.com/slide/1486649/

Anon., n.d. *twi-global.com.* [Online] Available at: https://www.twi-global.com/technical-knowledge/faqs/faq-what-is-the-effect-of-elevated-dynamic-loading-rate-on-tensile-properties-in-steel/

Anon., n.d. *wikipedia.* [Online]
Available at: https://en.wikipedia.org/wiki/Intercept_theorem

Çengel, Y. A. M. C., 2006. *FLUID MECHANICS.* McGrawhill: s.n.

Bethany, 2017. *A Brief History Of SolidWorks.* [Online]
Available at: https://www.scan2cad.com/cad/solidworks-history/
[Accessed 2018].

Boardman, B., n.d. *Fatigue Resistance of Steels,* s.l.: Deere and Company.

Cârstea, D., n.d. *Numerical simulation of the large power cables using the finite element method.* [Online]
[Accessed 2 5 2018].

Day, R. M., 2001. *Soil Testing Manual: Procedures, Classification Data, and Sampling Practices.* Michigan: McGraw-Hill.

Dimitrios.G.Pavlou, 2018. *Meeting* [Interview] 2018.

Dimitrious.G.Pavlou, 2011. *Elastodynamic analysis of a thin layer bonded on a visco-elastic medium under combined in-plane and lateral pulse loads.* [Online]
Available at: https://www.sciencedirect.com/science/article/pii/S0093641311001455

DohrenWend, C. M., 1944. Transverse impact transients. *Exp. Stress Analysis*.

Einstein, A., n.d. *Ordtak - Enkelhet.* [Online]
Available at: www.ordtak.no/sitat.php?id=8601
[Accessed 2 Mai 2018].

Ellingesen, K. E., 2016. *Subops.no.* [Online]
Available at: www.subops.no/content/uploads/2016/05/Kjell-Einar-Ellingsen.pdf
[Accessed 2018].

Ellingsen, K. E., 2017. *Statoil utvikler egen subseateknologi for å åpne markedet for nye leverandører* [Interview] (6 Februar 2017).

Figari, P., 2015. *Steps To Analyzing a Material's Properties From Its Stress/Strain Curve.* [Online]
Available at: http://www.instructables.com/id/Steps-to-Analyzing-a-Materials-Properties-

from-its/
[Accessed 2018].

Fracture Mechanics, n.d. *Stress Concentrations at Holes.* [Online] Available at: www.fracturemechanics.org/hole.html
[Accessed 31 5 2018].

Gambhir, M., 2009. *Fundamentals of Solid Mechanics - A Treatise on Strength of Materials.* New Delhi: PHI Learning .

Gedeon, M., 2010. Strain hardening & Strength. *Tecnical Tidbits*.

HBM, 2018. *Instructions for use - ABM75.* [Online] Available at: https://www.hbm.com/fileadmin/mediapool/hbmdoc/technical/a1665.pdf

HBM, n.d. *A Covering Material Applied from the Tube.* [Online] Available at: https://www.hbm.com/en/3082/sg250-a-transparent-single-component-silicon-rubber/
[Accessed 27 February 2018].

HBM, n.d. *A Practical Foil That Protects the Measuring Point.* [Online] Available at: https://www.hbm.com/en/3078/strain-gauge-protective-coatings-abm75/#addsearch=cellophane
[Accessed 27 February 2018].

HBM, n.d. *catman DAQ Software: Visualize - Save - Automate - Analyse.* [Online] Available at: https://www.hbm.com/en/2290/catman-data-acquisition-software/
[Accessed 5 April 2018].

HBM, n.d. *Cleanly Installed Strain Gauges.* [Online] Available at: https://www.hbm.com/en/4628/strain-gauge-cleaning-material/
[Accessed 2 2018].

HBM, n.d. *LY Linear Strain Gauges with 1 Measuring Grid.* [Online] Available at: https://www.hbm.com/en/4561/ly-linear-strain-gauges-with-1-measurement-grid/
[Accessed 22 Februar 2018].

HBM, n.d. *Polyimide Tape.* [Online] Available at: https://www.hbm.com/en/3093/strain-gauge-solder-material-polyimide-tape/ [Accessed 27 2 2018].

HBM, n.d. *Quantum X MX840B and MX440B.* [Online] Available at: https://www.hbm.com/en/2129/quantumx-mx840b-8-channel-universal-amplifier/
[Accessed 5 April 2018].

HBM, n.d. *QuantumX Accessories.* [Online] Available at: https://www.hbm.com/en/3784/quantumx-accessories/ [Accessed 5 April 2018].

HBM, n.d. *Strain Gauge Accessories.* [Online] Available at: https://www.hbm.com/en/0400/strain-gauge-accessories/ [Accessed 2 2018].

HBM, n.d. *Super-Fast Curing Time for Strain Gauge Installation.* [Online] [Accessed 2 2018].

HBM, n.d. *The Proven Superglue for Strain Gauges.* [Online] Available at: https://www.hbm.com/en/2961/x60-2-component-fast-curing-adhesive/ [Accessed 27 February 2018].

Hibbeler, R. C., 2010. *Mechanics Of Materials.* s.l.:Pearson Education Center.

Hoffmann, K., 1973-1978. *Fundamentals of the Strain Gauge Technique.* Darmstadt: Hottinger Baldwin Messtechnik.

Kirsch, E., 1898. "Die Theorie der Elastizität und die Bedürfnisse der Festigkeitslehre,". *Zeitschrift des Vereines deutscher Ingenieure, .*

Kurowski, P. M., 2015. *Engineering Analysis with SOLIDWORKS Simulations 2015.* [Online] Available at: https://www.sdcpublications.com/Textbooks/Engineering-Analysis-SOLIDWORKS-Simulation-2015/ISBN/978-1-58503-933-3/
[Accessed 2018].

Michael Moran, H. S. D. B. M. B., 2014. *Fundamentals of Engineering Thermodynamics.* s.l.:Wailey.

MIT, 2014. *Ten-node tetrahedal element.* [Online] Available at: http://web.mit.edu/calculix_v2.7/CalculiX/ccx_2.7/doc/ccx/node33.html [Accessed 2018].

National Instruments, 2016. *Measuring Strain with Strain Gages.* [Online] Available at: http://www.ni.com/white-paper/3642/en/#toc3

OMEGA, n.d. *Strain Gauge Installation.* [Online] Available at: https://www.omega.co.uk/techref/pdf/Strain-gauge-application-info/how-to-position-strain-gauges.pdf
[Accessed 25 Februar 2018].

Paul A. Tipler, G. M., 2008. *PHYSICS for scientists and engineers.* New York: W.H. Freeman and Company.

Pavlou, D., 2011. Elastodynamic analysis of a thin layer bonded on a visco-elastic medium under combined in-plane and lateral pulse loads. *Mechanics Research Communications*.

R.L Hannah, S. R., 1992. *Strain Gage Users' Handbook.* London: Chapman & Hall.

SIEMENS, n.d. *Finite Element Analysis (FEA).* [Online] Available at: https://www.plm.automation.siemens.com/global/en/our-story/glossary/finite-element-analysis-fea/13173
[Accessed 1 5 2018].

SimScale, n.d. *Finite Element Analysis - What is von Mises Stress.* [Online] Available at: https://www.simscale.com/docs/content/simwiki/fea/what-is-von-mises-stress.html
[Accessed 2 5 2018].

SSAB, n.d. *SSAB Domex 355MC.* [Online] Available at: https://www.ssab.com/products/brands/ssab-domex-structural-steel/products/ssab-domex-355mc
[Accessed 2nd June 2018].

Standards, N., 2005. NORSOK Standards ISO 13628-1:2005 Dropped Objects.

Statoil, 2016. *Statoil lanserer nytt undervannskonsept.* [Online] Available at: https://www.statoil.com/no/news/statoil-launches-new-subsea-concept.html

Vegvesen, S., 1996. *Modifisert Proktor,* s.l.: s.n.

Wheatstone, C., 1843. An account of several new instruments and processes for determining the constant of a voltaic circuit. In: London: Philosophical Transactions of the Royal Society of London.

Woinowsky-Krieger, T. a., 1959. *Theory of plates and shells 2nd edition.* s.l.:McGraw-Hill Book Company.

YR, 2018. *Datosøk, Ullandhaug, Stavanger (Rogaland).* [Online] Available at: https://www.yr.no/sted/Norge/Rogaland/Stavanger/Ullandhaug~2784502/almanakk.html?dato=2018-03-01

Appendix A

```
ClearAll["Global`*"]
q0=-5000;
r0=0.38;
rho=7850;
h=3*10^-3;
Ey=209*10^9;
vp=0.28;
k=0.01;
c=10;
qr=2;
Df=(Ey*h^3)/(12*(1-vp^2));
lambda2=(rho*h)/(Df);
lambda1=c/Df;
lambda0=k/Df;
mew=(lambda1/lambda2);
cw=(x^4-qr*x^2+lambda0)/(lambda2);
rho1=(-mew+Sqrt[(mew^2)-4*cw])/(2);
rho2=(-mew-Sqrt[(mew^2)-4*cw])/(2);
t=0.01;
f=((E^(rho1*t)-E^(rho2*t))/(rho1-rho2));
w=((q0*r0)/(lambda2*Df))*NIntegrate[BesselJ[1,r0*x]*BesselJ[0,r*x]*f,{x,0,1000}]
a=2;
b=-2;
Plot[w,{r,b,a}]
RevolutionPlot3D[w,{r,b,a},RevolutionAxis->"Z",BoxRatios->{1,1,.5}]
```

Appendix B

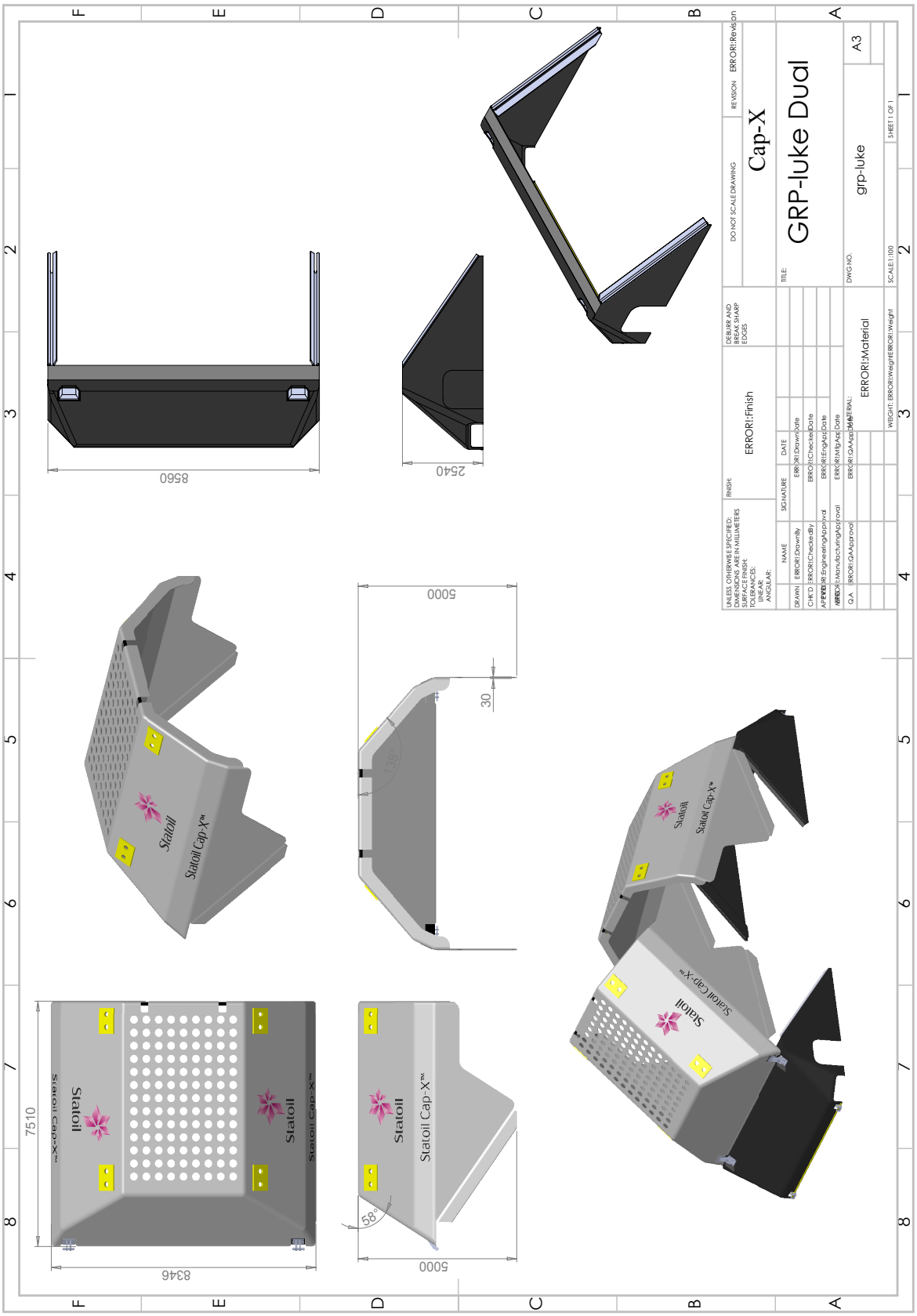
GRP-luke Dual
Cap-X
grp-luke
A3
ERROR!:Material
ERROR!:Finish
DO NOT SCALE DRAWING
8560
2540
5000
30
7510
8346
Statoil
Statoil Cap-X™

Appendix C

CO #	Item #	Del #	Heat	Lot	Your art #	Qty	Description
20170623-Phong	100	RP2504 38	21-2110			10	VV PL DX/S355MC 3,00 X 1500 X 3000 MM

This document is electronically reproduced and is identical to the original.

NORSK STÅL

SSAB

Page 1 (1)

SSAB EMEA AB, SE-781 84 BORLÄNGE, Sweden A01

Inspection certificate A02	Issuing department A05	Purchaser order no A07	Our order no A08	Invoice no A19	Certificate no and date A03
EN 10 204 - 3.1	Quality inspection	P10000774	130415-1	2880169	16629424 2017-06-01

Purchaser A11
45280
NORSK STÅL AS
BOX 123
NO-1378 NESBRU
NORGE

Product B01
Hot rolled sheets

Marking B06
Manufacturer, MATERIAL ID

Customer marks B15

Quantity B08
252

Dimensions [mm] B09-B11
T 3 W 1500 L 3000

Weight [kg] B12
26910

Deliv. Cond. B04

Internal code B16

Consignee A06
NORSK STÅL AS BOX 123 NO-1378 NESBRU NORGE

Standard/rules B02
SSAB
Steel grade SSAB Domex 355MC E

MATERIAL ID B07
21-2110-173279-01 , 21-2110-173279-02 , 21-2110-173279-03 , 21-2110-173279-04 , 21-2110-173279-05 , 21-2110-173279-06 , 21-2110-173279-07 , 21-2110-173279-08 , 21-2110-173279-09 , 21-2110-173279-10 , 21-2110-173279-11 , 21-2110-173279-12 , 21-2110-173279-13 , 21-2110-173279-15

Chemical composition C71-C92

Heat no	C	Si	Mn	P	S	Cr	Ni	Mo	V	Ti	Cu	Al	Nb	B	N	Cekv
21-2110	.059	.01	.57	.009	.003	.02	.04	.00	.00	.00	.02	.060	.023	.0000	.002	.16

Carbon equivalent etc C93-C99
Cekv = C + Mn/6 + (Ni + Cu)/15 + (Cr + Mo + V)/5

100

Testtype C04	Millcode C00	Specimen position C01	Direc-tion C02	Treat-ment B05	Specimen type C10	Temp [degr C] C03	Test results		
Tensile test	DGK109	Top end	Longitudinal	Delivery condition	Rectangular 380x40		C11 Reh [MPa] 405	C12 Rm [MPa] 478	C13 A5 [%] 40.5
Tensile test	DGK110	Top end	Transvers	Delivery condition	Rectangular 380x40		C11 Reh [MPa] 473	C12 Rm [MPa] 485	C13 A5 [%] 38.5
Bend test	DGK111	Top end	Transvers	Delivery condition	Rectangular 300x25		C50 The_test_is satisfactory -		

Production time: 2017-06-01

Customer article no: 29924

	This certificate is produced with EDP and valid without signature Material Testing/ H Leu / M Eriksson / V Esbelani Z02		It is hereby certified that the material described above complies with the requirements of the order. Z01	A22	A04

PROV 1.0 (45280)